81-3-138

DEUTSCHES ELEKTRONEN-SYNCHROTRON DESY

DESY 80/129
December 1980

e^+e^- COLLIDING BEAM EXPERIMENTS

by

B. H. Wiik

NOTKESTRASSE 85 · 2 HAMBURG 52

DESY behält sich alle Rechte für den Fall der Schutzrechtserteilung und für die wirtschaftliche Verwertung der in diesem Bericht enthaltenen Informationen vor.

DESY reserves all rights for commercial use of information included in this report, especially in case of apply for or grant of patents.

To be sure that your preprints are promptly included in the HIGH ENERGY PHYSICS INDEX , send them to the following address (if possible by air mail) :

DESY
Bibliothek
Notkestrasse 85
2 Hamburg 52
Germany

DESY 80/129
December 1980

e^+e^- COLLIDING BEAM EXPERIMENTS

B.H.Wiik

Deutsches Elektronen-Synchrotron DESY, Hamburg, Germany.

1.
INTRODUCTION

Electron-positron colliding rings were first proposed[1] in 1957 and they have grown in the short time span of some 20 years from small table top devices[2] into large machines several kilometers in circumference. Indeed LEP - the proposed electron-positron colliding beam machine at CERN with its circumference of 30.4 km - will cover more real estate than any other accelerator in the world. This growth has of course been fueled by the physics results obtained[3] at these machines and it might be useful to revisit the recent past before reviewing the results obtained in the past few years.

The motivation behind the first e^+e^- machines was the desire to test QED in a clean environment free from strong interaction effects. The first result, a measurement of the cross section for Möller scattering $e^-e^- \to e^-e^-$, was published[4] in 1966 by a Princeton-Stanford Collaboration and it confirmed the QED theory down to distances of about 10^{-14} cm. However, soon hadron production via the one photon annihilation channel became of primary interst. Unlike hadron-hadron collisions the annihilation channel leads to a well defined intermediate state with the quantum numbers of the photon - i.e. the timelike photon couples directly to resonances with these

quantum numbers. The storage rings at Orsay and Novosibirsk found that the annihilation cross section up to 1 GeV is dominated by the production of the ρ, ω and ϕ vector mesons. A wealth of information[5] on various decay modes and coupling constants has come from this work. The total cross section measurements were extended to higher energies at Adone. They found[6] a rather large cross section decreasing as $1/s$ where s is the c.m. energy squared. These features could be understood if the photon couples directly to the pointlike constituents observed in deep inelastic electron-proton collisions. However, scattered data points obtained at CEA[7] and at SPEAR[8] at still higher energies showed a surprisingly weak energy dependence - in fact the data were consistent with a constant cross section.

The first step towards the solution of this problem was the discovery at BNL[9] and at SPEAR[10] of the J/ψ, a new narrow 1^{--} state with a mass of 3.1 GeV. Within a few months related 1^{--} states were discovered[11] and the total cross section was found to exhibit a step with a complex structure around 4 GeV. Related states with the quantum numbers different from those of a photon were found at DORIS[12] and at SPEAR[13] in the radiative decays of the ψ'.

These observations could be explained by introducing a new heavy quark Q and interpreting the new states as bound $Q\bar{Q}$ states[14]. The most natural choice for Q is to identify it with the charmed quark c, originally proposed[15] to achieve symmetry between leptons and quarks and later to explain[16] the absence of strangeness changing neutral currents. Verification of the charm model required the existence of states with open charm i.e. $c\bar{q}$ ($\bar{c}q$) states resulting from combining a charm quark with a light quark. The $D^0(c\bar{u})$ and $D^+(c\bar{d})$ states were found at SPEAR[17] while DORIS[18] has produced evidence for the $F^+(c\bar{s})$ state.

In 1975 a new generation of fermions was introduced by the discovery[19] at SPEAR of a new lepton, the τ with a mass around 1.8 GeV. Like the electron and the muon, the tau seems to have its own lepton number and its own neutrino. A doublet of new quarks therefore was needed to restore the lepton quark symmetry. The first evidence for a new quark came from FNAL. They observed[20] narrow states - the T states - in the e^+e^- mass spectrum produced in proton nucleus collisions. The DORIS energy was subsequently increased such that the two first T states could be

observed[21]. These and further data[22] showed that the new states were 1^{--} states made of a new quark b of charge 1/3 e. The total cross section data were extended[23] to higher energies at the Cornell storage ring CESR. They observed two additional $T(1^{--})$ states and found the heaviest of these states to be above $b\bar{b}$ threshold. Perhaps the most exciting aspects of the T family is the opportunity it offers to study the strong forces acting between two quarks. At present we believe these forces to be mediated by gluons, the quanta of quantum chromodynamics[24] (QCD). Indeed, the hadronic decays of the T observed at DORIS[25] are consistent with the 3 gluon intermediate states as predicted in QCD. The level spacing, the electronic widths of the $c\bar{c}$ and the $b\bar{b}$ states can be reproduced[26] with the wave functions computed from simple flavour independent potentials.

Hadron production[27-30] in e^+e^- annihilation proceeds in the naive quark-parton model by quark pairproduction resulting in two collinear jets of hadrons with small and maybe constant momentum transverse and large and growing momenta along the jet axis. First evidence for a jet-like behaviour[31] was found at SPEAR and the jets are directly visible at PETRA energies. In any field theory of strong interactions including QCD the produced quark will radiate gluons which are expected to materialize as a jet of hadrons in the final state. In a fraction of the events the gluon will be radiated at an angle which is large compared to the angular spread of the hadrons in a jet leading to planar events with three well separated hadron jets. Such events have been observed[33-36] at PETRA at a rate which is much above the rate expected from statistical fluctuations of two jet events. Detailed measurements have shown that the properties of these events, including the spin one nature of the gluon jet, are consistent with the QCD predictions.

2.
ELECTROWEAK REACTIONS

The Feynman graphs for Bhabha scattering, lepton pair production and two photon annihilation are shown in Fig. 1. Effects caused by the interference of the weak and the electromagnetic currents start to become visible at the highest energies now available at PETRA and we will re-

turn to these effects after a brief discussion on the experimental QED limits.

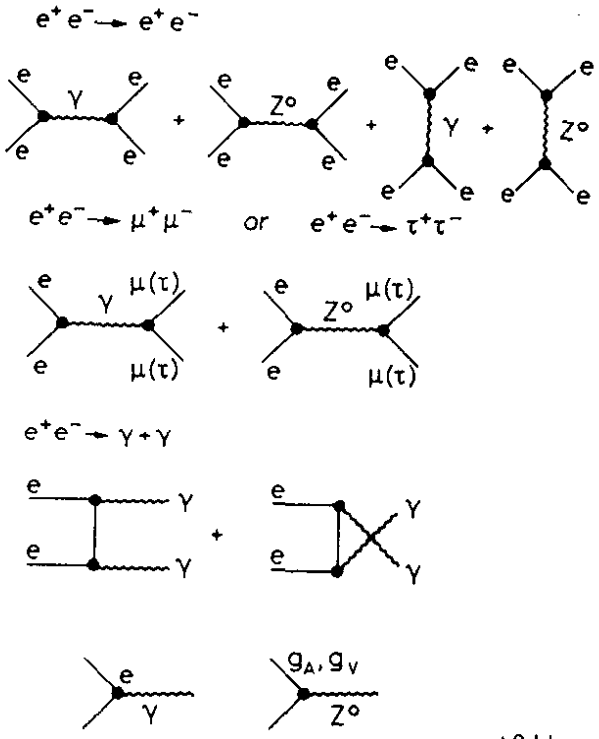

Fig. 1
Feynman graphs for
a) $e^+e^- \rightarrow e^+e^-$
b) $e^+e^- \rightarrow \mu^+\mu^-$ $(\tau^+\tau^-)$
c) $e^+e^- \rightarrow \gamma\gamma$

2.1 Test of QED

The QED predictions are based on the validity of the Maxwell equations and on the assumption that leptons are pointlike objects without excited states. The reactions above make it possible to test these assumptions at very small distances in a clean environment with only small corrections due to strong interactions.

The standard procedure used to compare data with the QED predictions can be summarized as follows:

1) Weak effects are neglected.

2) The measured cross section $d\sigma_o/d\Omega$ is corrected[37] for radiative effects δ_R and effects due to the hadronic vacuum polarization δ_H.

$$\frac{d\sigma_c}{d\Omega} = \frac{d\sigma_o}{d\Omega}\,(1 + \delta_R + \delta_H). \qquad (1)$$

3) The corrected cross section is compared to the QED predicted cross section and deviations are parametrized[38] in terms of form factors. The formfactors used for Bhabha scattering and lepton pair production can be written as:

e^+e^- COLLIDING BEAM EXPERIMENTS

$$F_s(q^2) = 1 \pm \frac{q^2}{q^2 - \Lambda_{s\pm}^2} \qquad F_t(s) = 1 \pm \frac{s}{s - \Lambda_{t\pm}^2} \tag{2}$$

where F_s and F_t are respectively the formfactors for spacelike and timelike momentum transfer squared.

The reaction $e^+e^- \to \gamma\gamma$ is modified by a form factor[39] of the type

$$F(q^2) \sim 1 \pm q^4/\Lambda^4 \tag{3}$$

Exchange of a heavy electronlike lepton would modify[40] the cross sections as

$$F(s) \sim 1 + (s^2/2\Lambda^4) \sin^2\theta \tag{4}$$

where Λ is the mass of the heavy lepton.

All groups working at PETRA have data[41,42] on these reactions and some typical results are shown in Figs. 2 - 5.

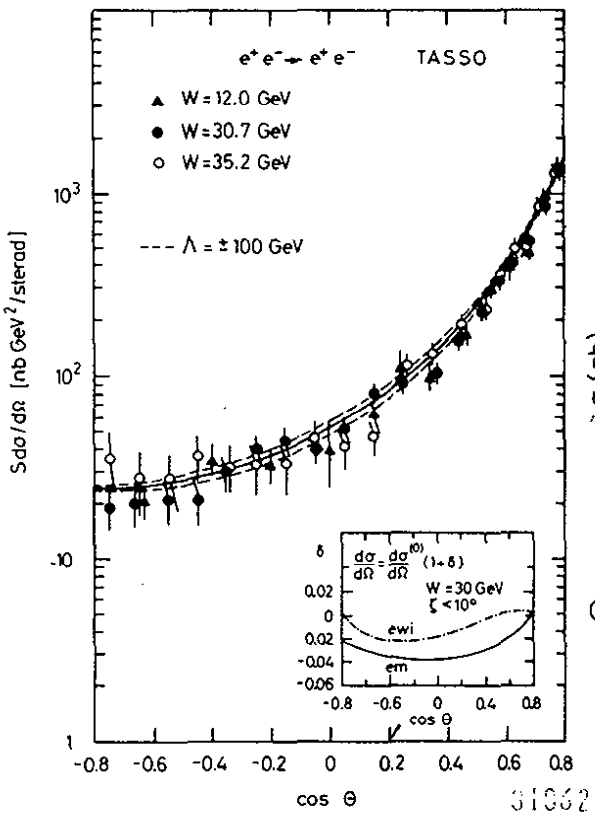

Fig. 2
The cross section $s \cdot d\sigma/d\Omega$ for $e^+e^- \to e^+e^-$ measured by TASSO between 12.0 and 35.2 GeV in c.m.

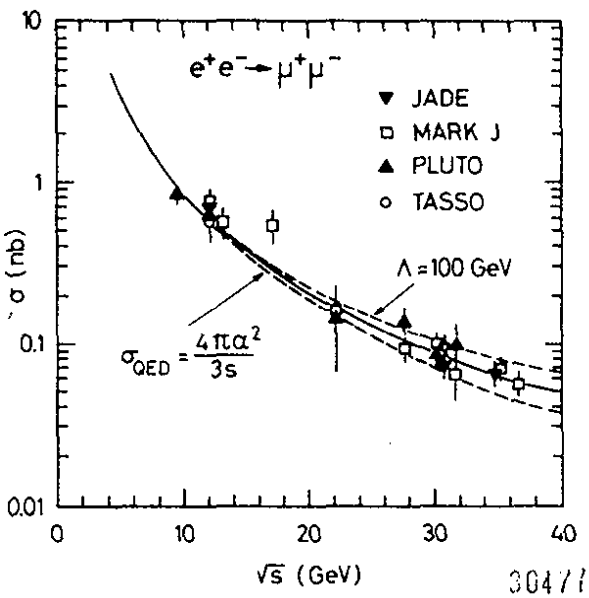

Fig. 3
The total cross section for $e^+e^- \to \mu^+\mu^-$ measured by JADE, MARK J, PLUTO and TASSO plotted versus c.m. energy.

The cross section s $d\sigma/d\Omega(e^+e^- \to e^+e^-)$ measured by the TASSO Collaboration for c.m. energies between 12 and 35.2 GeV is plotted in Fig.2 versus scattering angle Θ. The data scatter around the QED prediction shown as the solid curve, the dotted curve indicates the limits corresponding to a cut off parameter Λ = 100 GeV.

The total cross section for $e^+e^- \to \mu^+\mu^-$ measured by JADE, MARK J, PLUTO and TASSO is plotted in Fig. 3 versus c.m. energy. The data agree well with the QED prediction shown as the solid curve and they are in general within the dotted curves corresponding to a cutoff parameter Λ of 100 GeV.

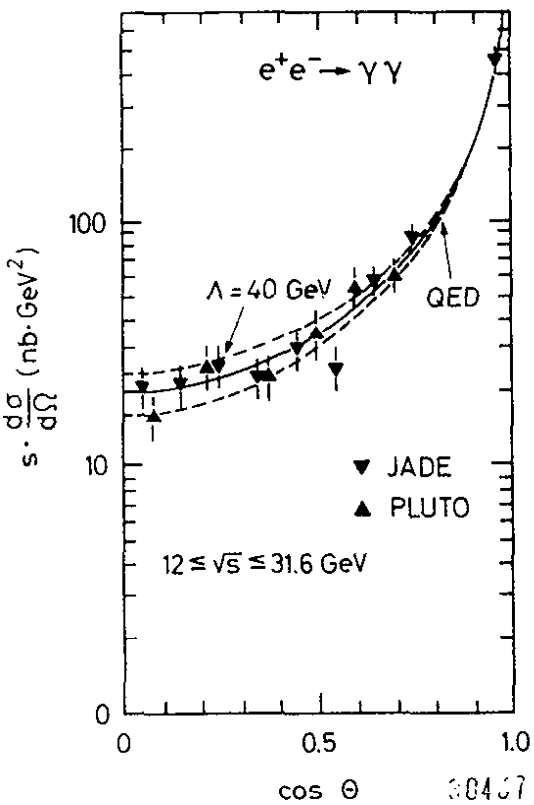

Fig. 5
The cross section s $d\sigma/d\Omega$ for $e^+e^- \to \gamma\gamma$ measured by JADE and PLUTO plotted versus cosθ.

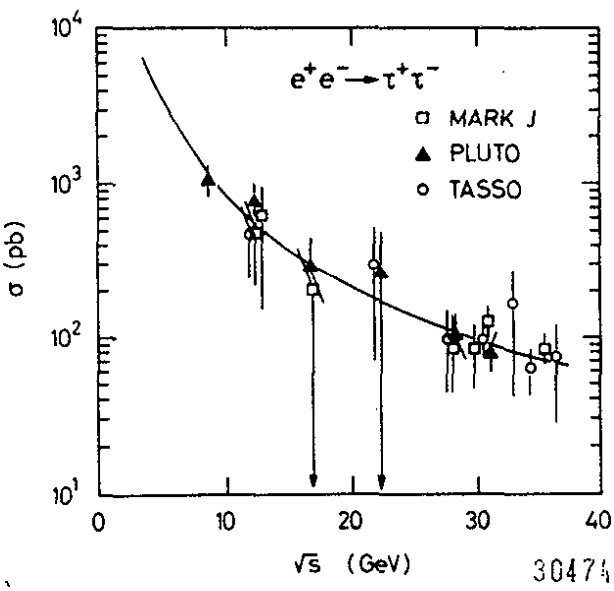

Fig. 4
The total cross section for $e^+e^- \to \tau^+\tau^-$ measured by MARK J, PLUTO and TASSO plotted versus c.m. energy.

The total cross section for $e^+e^- \to \tau^+\tau^-$, measured by MARK J, PLUTO and TASSO, is plotted in Fig.4 versus c.m. energy. This reaction has a very distinct signature at high energies and is easily separated from multihadron reactions. Again the data are in good agreement with the

QED prediction shown as the solid curve.

The angular distribution for s $d\sigma/d\Omega$ ($e^+e^- \to \gamma\gamma$) measured by the JADE and PLUTO Collaborations is plotted in Fig. 5 for c.m. energies between 12 and 31.6 GeV. The data are in good agreement with the QED prediction, the deviation corresponding to a cutoff parameter Λ = 40 GeV is shown as the dotted curve.

All data are in agreement with QED and the limits on Λ are summarized in Table 1.

From this table we conclude the leptons are indeed pointlike down to distances of about 2×10^{-16} cm. Furthermore there is no evidence for a charged electronlike lepton.

Table 1 - Limits on $\Lambda_\pm$ in GeV

		JADE	MARK J	PLUTO	TASSO
$e^+e^- \to e^+e^-$					
	Λ_+	112	91	80	150
	Λ_-	106	142	234	135
$e^+e^- \to \mu^+\mu^-$					
	Λ_+	137	123	116	80
	Λ_-	96	142	101	118
$e^+e^- \to \tau^+\tau^-$					
	Λ_+	-	76	74	115
	Λ_-	-	154	65	76
$e^+e^- \to \gamma\gamma$	$F(q^2) = 1 \pm q^4/\Lambda_\pm^4$				
	Λ_+	-	44	46	-
	Λ_-	-	34	36	-
	heavy electron Λ^*				
	Λ_+	47	55	46	34
	Λ_-	44	38	-	42

2.2 Electroweak effects

The interference between the electromagnetic and the neutral weak current[43] will change the normalized QED cross section for muon and tau pair production by ΔR and lead to a forward-backward asymmetry A in the angular distribution of the leptons in the final state. At pre-

sent PETRA and PEP energies these effects can be written[44] as:

$$\Delta R = \left(\frac{G_F}{2\cdot\sqrt{2}\cdot\pi\alpha}\right)\frac{2s\cdot g_V^2}{(s/m_z^2-1)} + \left(\frac{G_F}{2\cdot\sqrt{2}\cdot\pi\alpha}\right)^2\frac{s^2(g_V^2+g_A^2)^2}{(s/m_z^2-1)^2} \qquad (5)$$

$$A_{\mu\mu} = \frac{F-B}{F+B} = \frac{3}{4}\frac{G_F}{\sqrt{2}\cdot\pi\cdot\alpha}\frac{s\cdot m_z^2}{s-m_z^2}g_A^2 \simeq 2.7\times 10^{-4}\frac{m_z^2\cdot s}{s-m_z^2}g_A^2 \qquad (6)$$

Here F and B denotes the number of negative muons (taus) in the forward, respectively in the backward hemisphere. In the standard model[43] with $\sin^2\theta_W = 0.23$, $m_z = 89$ GeV, $g_V = -1/2(1-4\sin^2\theta_W) = -0.04$ and $g_A = -1/2$ where g_V and g_A denote the vector and the axial vector coupling of the neutral current to a pair of charged leptons. At $s = 1000$ GeV^2 this leads to $\Delta R = 0.002$ and $A_{\mu\mu} = -0.076$.

The change in ΔR cannot be observed at present energies whereas a measurement of the asymmetry is within reach.

The asymmetry data[41] obtained by the various PETRA groups are listed below:

Group	JADE	MARK J	PLUTO	TASSO
$A_{\mu\mu}$(%)	-8 ± 9	0 ± 9	7 ± 10	1 ± 12

The systematic uncertainties are quite small and the data from the various groups can therefore be combined. The combined angular distribution is plotted in Fig. 6 and it yields $\langle A_{\mu\mu}\rangle = -(0.9 \pm 4.9)\%$ to be compared to the predicted value of -6% including acceptance corrections.

The 95% upper confidence limit is $|A_{\mu\mu}| < 9\%$ i.e. $g_A^e \cdot g_A^\mu < 0.375$ compared to the standard model value of 0.25.

The relative deviation[45] of the Bhabha cross section due to weak effects, is plotted in Fig. 7 versus scattering angle for various vales of m_z. Also indicated are the deviations expected for a cut off parameter Λ of 250 GeV. It is clear that weak effects in $e^+e^- \to e^+e^-$ cannot be parametrized in terms of Λ and they should be included in the theoretical cross section before extracting a value for Λ.

e^+e^- COLLIDING BEAM EXPERIMENTS

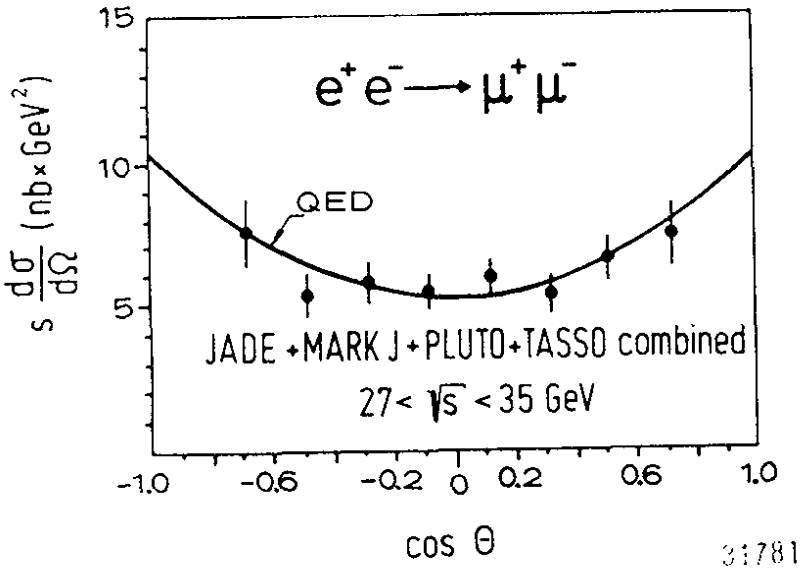

Fig. 6
The combined angular distribution of $s\, d\sigma/d\Omega$ for $e^+e^- \rightarrow \mu^+\mu^-$ at c.m. energies between 27 and 35 GeV.

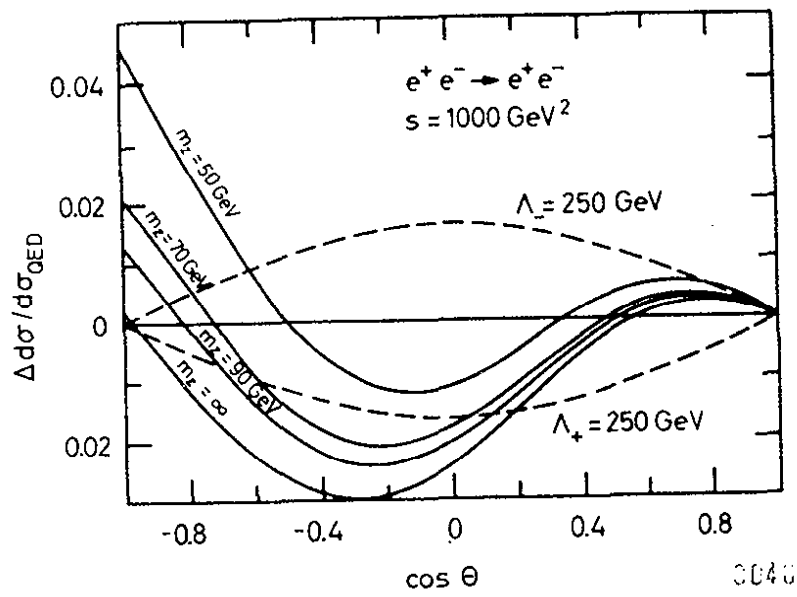

Fig. 7
Relative deviation of Bhabha cross section from the QED prediction plotted versus the scattering angle for various values of m_z. The dashed curves show the deviations expected for a cut off parameter of 250 GeV.

The deviation of Bhabha scattering from the lowest order QED prediction as measured by MARK J[46] from c.m. energies between 29.9 and 35.8 GeV is plotted in Fig. 8 and compared to various predictions of the standard model with $\sin^2\theta_W = 0.25$, 0.01 and 0.55 respectively. Only the cross section between 0° and 90° is measured since they do not determine charge. The data favours $\sin^2\theta_W = 0.25$, however, better data at higher energies are needed to set stringent limits on $\sin^2\theta_W$ from this reaction.

Using the standard model the data on $e^+e^- \rightarrow e^+e^-$, $e^+e^- \rightarrow \mu^+\mu^-$ have been used to extract values on $\sin^2\theta_W$. The results are listed in Table 2.

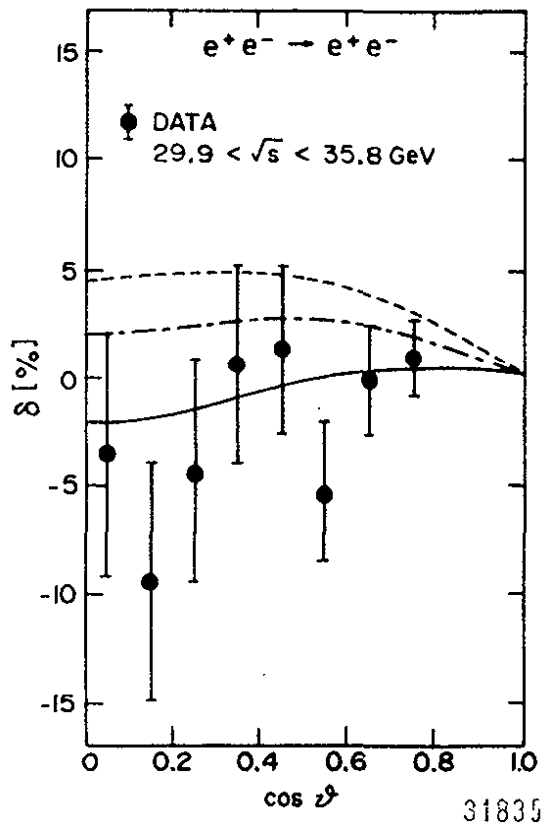

Fig. 8
The difference between the measured cross section for $e^+e^- \to e^+e^-$ and the QED prediction plotted versus the scattering angle θ. Predictions based on the standard model with $\sin^2\theta_W$ = 0.55, 0.01 and 0.25 are shown in the dashed, the dashed-dotted and the solid curve respectively. The data are from MARK J.

Table 2 – Results on $\sin^2\theta_W$

Group	Limits on $\sin^2\theta_W$		
	lower	upper	$\sin^2\theta_W$
MARK J	0.07	0.42	0.24 ± 0.11
JADE	-	0.55	0.25 ± 0.18
PLUTO	-	0.57	0.23 ± 0.17
TASSO	-	0.52	-

It is clear that the present data from e^+e^- interactions on neutral currents do not yet compete with the values obtained in neutrino interactions. However, they are the only data which test the theory at high values of Q^2 and they are also the only data which yield information on the neutral weak coupling to muons and taus.

It is possible[47,48] to construct gauge models which reproduce the low energy data but have a richer spectrum of vector bosons. In such models $g_V^2 = 1/4\ (1-4\ \sin^2\theta_W)^2 + 4\ C$ and $g_V \cdot g_A$ and g_A^2 remain unchanged.

e^+e^- COLLIDING BEAM EXPERIMENTS

JADE and MARK J have determined[41,46,49] the limits on C from measurements of Bhabha scattering and muon pair production. They find with 95% confidence:

JADE	-0.059	$<$	C	$<$ 0.033
MARK J	-0.097	$<$	C	$<$ 0.027 .

There are various ways to realize such models. For example SU(2) x U(1) x U'(1)[50] will have only one charged but two neutral vector bosons. In this case

$$C = \cos^4\theta_W \, (m_z^2/m_1^2 - 1) \, (1 - m_z^2/m_2^2) \qquad (7)$$

here m_z is the mass of the z^o in SU(2) x U(1) and m_1 and m_2 are the masses of two neutral bosons in the extended model.

It is also possible to construct a model with SU(2) x SU'(2) x U(1)[51]. Such a model will have two charged and two neutral vector bosons, and in this case the $\cos^4\theta_W$ factor is replaced by $\sin^4\theta_W$.

The limit on C can therefore be translated into limits on m_1 and m_2 using the expressions given above. The results are plotted in Fig. 9.

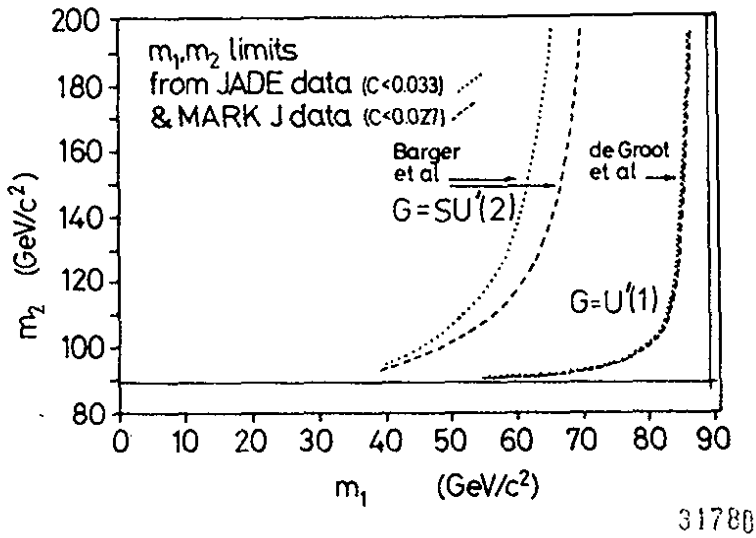

Fig. 9
Limits on the mass of neutral vector bosons.

3. THE TAU AND SEARCH FOR NEW LEPTONS

3.1 The tau

Leptons are pair produced with the point crosssection

$$\sigma = \frac{4\pi\,\alpha^2}{s} \, \frac{\beta(3 - \beta^2)}{2} \quad , \qquad \beta = p_L/E \qquad (8)$$

and decay either leptonically $L \to \nu_L \ell\nu_\ell$ or semihadronically $L \to \nu_L$ · hadrons. This leads to rather distinct final states like:
a) $e^+e^- \to e^{\mp} \mu^{\pm}$ + neutrinos. The muon and the electron are in general acollinear and the total energy visible in the event is much less than the available c.m. energy.

b) $e^+e^- \to e^{\mp}$ $(\mu^{\mp})$ + $(\text{hadrons})^{\pm}$ + neutrinos. In this final state the electron (muon) is recoiling against a low multiplicity hadron jet.The electron (muon) and the jet axis are in general acollinear and some of the available energy is carried off by neutrinos.

The first evidence for a new lepton, presented by M.Perl and his Collaborators[19], was based on the observation of $e^+e^- \to e^{\mp}\mu^{\pm}$ + nothing. This discovery was confirmed by many groups, in particular the DASP Collaboration[52] observed τ-production below charm threshold excluding charm as the source for the τ signal.

A recent measurement[53] by the DELCO group of $e^+e^- \to \tau^+\tau^-$ near threshold is shown in Fig. 10. Plotted is

$$R_{ex}^{2p}(\text{all}) = \frac{\sigma(e^+e^- \to e^{\pm} + x^{\mp} + \geq 0 \text{ photons})}{\sigma_{\mu\mu}}$$

as a function of energy in the threshold region together with the theoretical cross section for point particles with J = 1/2, 1 and 3/2. Only J = 1/2 curve fits the data, i.e. a lepton is defined by the production cross section - the rapid rise near threshold is characteristic for pair-production of a fermion, the 1/s dependence of the cross section at high energies shows that the particle is pointlike and the magnitude of the cross section si proportional to the charge squared.The rapid rise of the

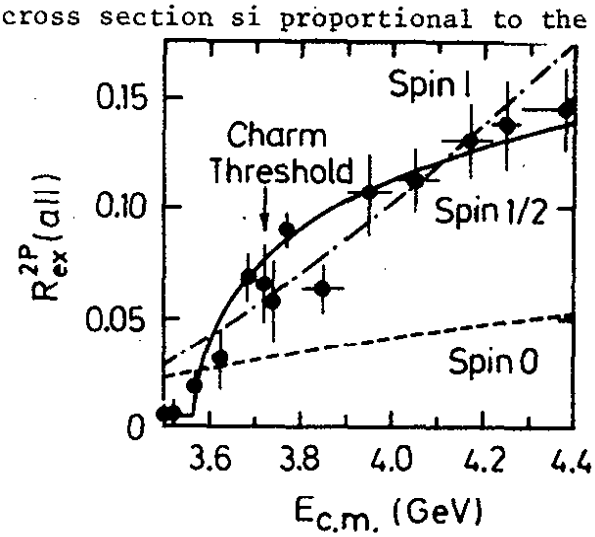

Fig. 10
The ratio $R_{ex}^{2p} = \sigma(e^+e^- \to e^{\pm}x^{\mp}, x \neq e)/\sigma_{\mu\mu}$ *as measured by the DELCO Collaboration.*

cross section near threshold can be used to determine the mass of the τ. The most precise determination, based on the data shown in Fig. 10 yield $m_\tau = 1782\ ^{+3}_{-4}$ MeV/c^2 in agreement with earlier data from DORIS.

The lepton spectrum in the leptonic decays of the τ can be used to determine the space time structure of the current. If only vector (V) and axialvector (A) type couplings are considered, then the Hamiltonian for $\tau \to \nu_\tau e\bar{\nu}_e$ is of the form[54]

$$\mathcal{H}_{int} = \frac{G_F}{\sqrt{2}} (\bar{\psi}_e \gamma_\mu(1-\gamma_5)\psi_e) (\bar{\psi} g_+ \gamma_\mu(1+\gamma_5) + g_- \gamma_\mu(1-\gamma_5) \cdot \bar{\psi}\nu_\tau) \qquad (9)$$

where g_+ (g_-) are the coupling strengths for V+A (V-A) coupling. In the τ rest system the shape of the lepton spectrum can be expressed in terms of the lepton momentum p and energy E and the maximum energy E_{max} as:

$$\frac{dN(z)}{dz} \sim z^2\{ 9 (1-z) + 2\rho (4z - 3)\} \qquad (10)$$

with $z = E/E_{max}$. Radiative corrections and terms of order m_e/m_τ have been neglected. The shape of the spectrum is then determined by the Michel parameter ρ defined as:

$$\rho = \frac{3}{4} \frac{g_-^2}{g_+^2 + g_-^2} \qquad (11)$$

The electron momentum spectrum for $\tau \to \nu_\tau e^- \bar{\nu}_e$ measured by the DELCO group[55] is plotted in Fig. 11. The dotted curve represents a V+A spectrum, the V-A spectrum is shown by the solid curve. A fit to the data as-

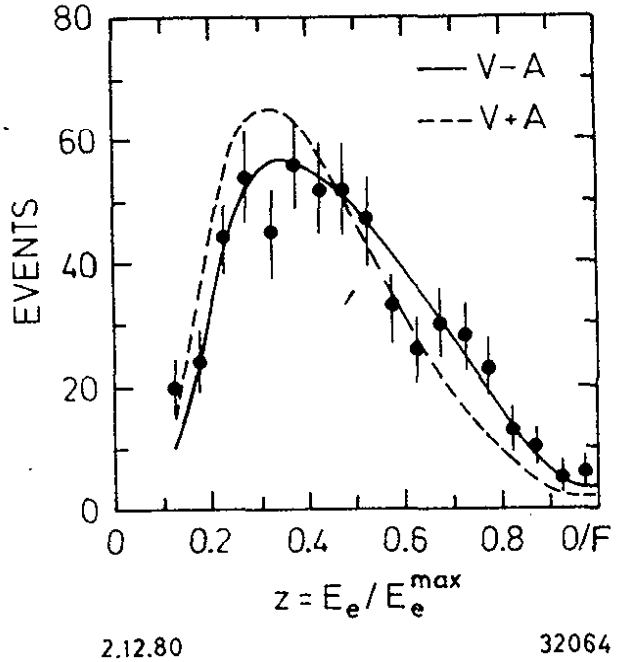

Fig. 11
Electron momentum spectrum from $\tau \to \nu_\tau e\bar{\nu}_e$ *in* $e^+e^- \to \tau^+\tau^-$ *candidate events as measured by the DELCO Collaboration. The solid and dashed curves represent the spectra expected for V-A and V+A couplings at the* $\nu_\tau\tau$ *vertex.*

suming a massless neutrino gave $\rho = 0.72 \pm 0.10$ compared to $\rho = 0.75$ for V-A and $\rho = 0$ for V+A. Pure vector or axial vector coupling gives $\rho = 3/8$. A V+A interaction is thus excluded and a pure A or V interaction is rather unlikely. An upper limit of $m_{\nu_\tau} < 250$ MeV is obtained from a V-A fit to the spectrum.

The tau decay modes are shown schematically in Fig. 12a and b. The theoretical branching ratios[56] and data are listed in Table 3 for some selected decay modes.

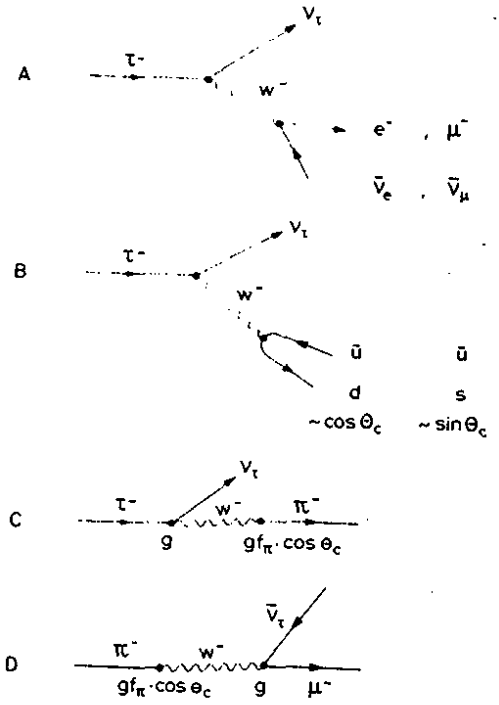

Fig. 12

a,b) The graphs for leptonic and semihadronic decays of a heavy sequential lepton

c,d) The relationship between $\pi^- \bar{\nu}_{\mu\mu}$ *and* $\tau^- \to \bar{\nu}_\tau \pi^-$.

The leptonic decay modes of the τ can, within the standard model, be unambigously predicted

$$\Gamma_e(\tau \to \nu_\tau e\bar{\nu}_e) = 0.973\, \Gamma_\mu(\tau \to \nu_\tau \mu\bar{\nu}_\mu) = \frac{G_F^2 \cdot m_\tau^5}{192\, \pi^3} \qquad (12)$$

with $G_F = 10^{-5}/m_p^2(\mathrm{GeV}^2)$.

In the conventional theory, semihadronic decays will yield final states of low multiplicity and a small ratio of strange to non strange particles. Some of the decay widths can be predicted with little ambiguity. The decay $\tau \to \nu_\tau \pi$ tests the axial current and is directly related to $\pi \to \bar{\nu}_\mu \mu$ as shown in Fig. 12c, d. Similarily $\tau \to \nu_\tau K$ is directly related to $K \to \bar{\nu}_\mu \mu$. The decay $\tau \to \nu_\tau \rho$ tests the vector current and is

related to $e^+e^- \to \rho^0$ using CVC. Indeed this hypothesis relates all decay modes $\tau \to \nu_\tau$ $(n\pi)$ to $e^+e^- \to n\pi$ where n is an even number. The branching ratio of some of these modes are listed in Table 3 and compared to the predicted values. The agreement is very good.

In the conventional model the decay into final states containing strange particles should be supressed. The DASP group found[57] the ratio

$$\frac{\sigma(e^+e^- \to \tau^+\tau^- \to e^\pm K^\pm + \geq 0 \text{ photons})}{\sigma(e^+e^- \to \tau^+\tau^- \to e^\pm \pi^\mp + \geq 0 \text{ photons})} = 0.07 \pm 0.06$$

consistent with this prediction. The MARK II Collaboration has measured this suppression factor directly by comparing $\tau \to \nu_\tau K^*(890)$ with $\tau \to \nu_\tau \rho$. According to the standard model

$$\frac{B(\tau \to \nu_\tau K^*(890))}{B(\tau \to \nu_\tau \rho)} = 0.93 \ tg^2\theta_c \approx 0.05$$

where 0.93 is a small phase space correction factor and θ_c the Cabbibo angle.

Data on $\tau \to \nu_\tau \rho$ have been reported by the DASP group[58] and by the MARK II[59] Collaboration. The $\pi^\pm\pi^0$ invariant mass spectrum measured by the MARK II Collaboration in $e^+e^- \to \tau^+\tau^-$ candidate events is shown in Fig. 13. This yield $B(\tau \to \nu_\tau\rho) = 21.6 \pm 1.8 \pm 3.2\%$ consistent with the old DASP value $B(\tau \to \nu_\tau\rho) = 24 \pm 9\%$.

The MARK II Collaboration has measured[60] $\tau \to \nu_L K^*(890)$ using the decay sequence $e^+e^- \to \tau^+\tau^- \to e^\pm(\mu^\pm) + (K^0_s + \pi^\mp)$ + neutrinos, where the

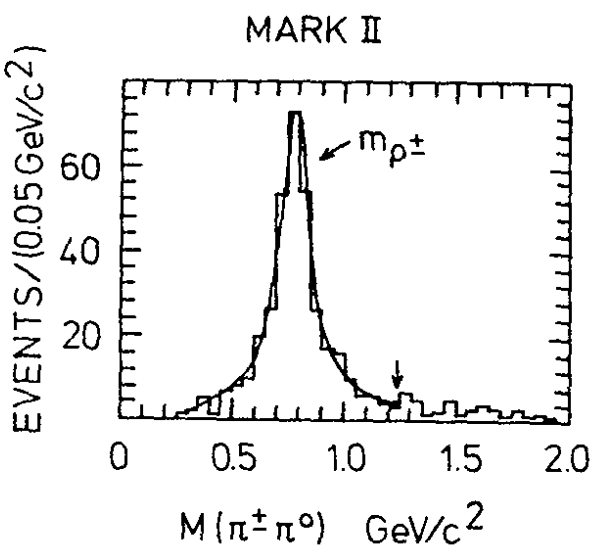

Fig. 13
The $\pi^\pm\pi^0$ mass spectrum in $e^+e^- \to \tau^+\tau^-$ candidate events measured by the MARK II Collaboration.

K^o_s state is reconstructed from $K^o_s \to \pi^+\pi^-$. The $K^o_s\pi^\pm$ mass spectrum from the candidate events plotted in Fig. 14 shows a clear peak at the mass of the $K^*(890)$. The branching ratio after corrections is $B(\tau \to \nu_\tau K^*(890)) = 1.7 \pm 0.7\%$. This yields

$$\frac{B(\tau \to \nu_\tau K^*(890))}{B(\tau \to \nu_\tau \rho)} = 0.085 \pm 0.038$$

in agreement with the predicted value of 0.05.

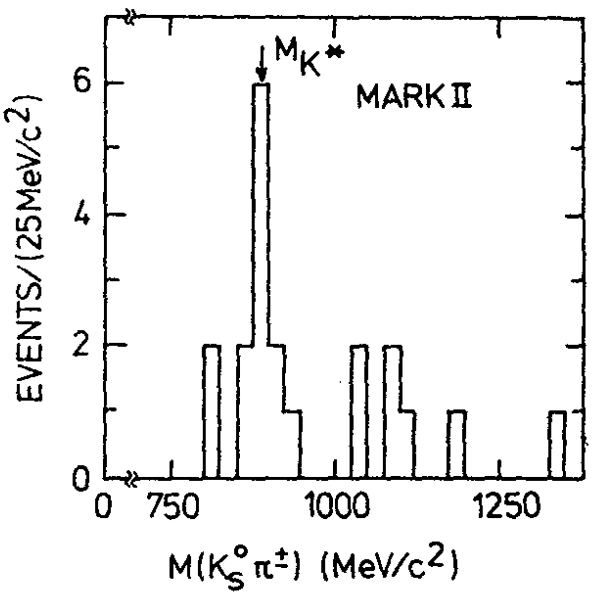

Fig. 14
The $K^o_s\pi^\pm$ mass spectrum in $e^+e^- \to \tau^+\tau^-$ candidate events measured by the MARK II Collaboration.

Table 3 – Selected decay modes

Decay mode	Theoretical B.R. %	Experimental [61] B.R. %
$\nu_\tau + e^- + \bar{\nu}$	17.6	(17.5 ± 1.2)
$\nu_\tau + \mu + \bar{\nu}_\mu$	17.2	(17.1 ± 1.2)
$\nu_\tau\ \pi^-$	10.5	(9.1 ± 1.1)
$\nu_\tau\ K^-$	0.66	< 1.6
$\nu_\tau\ \rho^-$	21.5	(21.6 ± 1.8 ± 3.2)
$\nu\ K^*(890)$	1.46	(1.7 ± 0.7)
$\nu\ A_1^-$	8.7	(10.4 ± 0.03)

The τ lifetime in the standard model is given by:

$$\tau_\tau = B_e \left(\frac{m_\mu}{m_\tau}\right)^5 \tau_\mu \simeq (2.8 \pm 0.2) \times 10^{-13}\ s \qquad (13)$$

The TASSO Collaboration [62] has extracted an upper limit on the τ life-

time from a limit on the τ decay length. The find $\tau_\tau < 14 \times 10^{-13}$ s with 95% confidence. The weak interaction responsible for τ decays is at least 46% of full strength.

So far we have treated the tau as a new sequential lepton arranged in a weak doublet with its own neutrino like the electron and the muon. Indeed the data are all consistent with this assumption. If the τ^- has the same lepton number as the e^+ or the μ^+ then the branching ratios for the leptonic decays of the tau into electrons or muons would differ by a factor of two. This is excluded experimentally. It has been found[63] that the $(\nu_\mu - \tau)$ coupling strength is less than 0.025 of the $(\nu_\mu - \mu)$ coupling strength excluding that the τ^- has the lepton number of the μ^-. It remains to be shown that the τ^- has not the e^- lepton number.

3.2 Search for new leptons

It seems reasonable to expect that the charged lepton in a new generation of elementary fermions is lighter than the quarks. Leptons are pairproduced with a known cross section and decay either leptonically $L \to \ell\, \bar{\nu}_\ell\, \nu_L$ or semihadronically $L \to \nu_L$ hadrons. All the groups working at PETRA have searched[41,64] for new leptons. No evidence was found, and the resulting mass limits are summarized in Table 4.

Table 4 – Mass limits on new leptons in GeV

Group	PLUTO	MARK J	TASSO	JADE
Sequential lepton	14.5	16.0	15.5	17.0
Scalar lepton	13.0	16.0	–	16.0

PLUTO and MARK J have searched by selecting events in which a single high energy muon was recoiling against many hadrons. PLUTO demanded that the visible energy of the event should be greater than 3.0 GeV and the missing momentum greater than 2.5 GeV/c. Furthermore the thrust should be less than 0.95. MARK J required that the visible energy should be greater than 10% but less than 50% of the c.m. energy. The acoplanarity should be greater than 30°. The acoplanarity is defined as the absolute value of $(180^\circ - \delta\phi)$, where $\delta\phi$ is the angle between the muon momentum vector and the total energy flow vector (see below) of the hadrons $\vec{E}_H$ projected on a plane perpendicular to the beam line. The energy de-

posited in the outer calorimeter should be 0.2 E_{vis}. The event should contain more than two charged tracks and the polar angle between the beam line and the energy flow vector should be between 30^{o} and 150^{o}.

TASSO selected events in which a single isolated charged particle with momentum greater than 1.5 GeV/c was separated by at least 90^{o} from any other charged track. The event should contain at least 5 charged tracks and the charged energy should be greater than 8.0 GeV (9.3 GeV) at 30 GeV (35 GeV) in c.m. A similar search was also made requiring the track to be a lepton.

JADE considered events with a visible energy between 11 GeV and 32 GeV produced at 35 GeV in c.m. They searched for non coplanar events as follows: They defined two planes, the first plane was defined by the thrust of one of the "jets" and the e^{+} direction, the second plane by the momentum of the remaining particles. The opening angle between the two planes should be greater than 45^{o}, and the angle between the thrust axis and the e^{+} direction should be at least 45^{o}.

In SU(5) the charged lepton and the charge 1/3 quark within the same generation are degenerate in mass at the unification energy of 10^{15} GeV. This has been used[65] to compute the mass of the s quark from the muon mass and to predict the mass of the b quark from the tau mass. If the same relationship is also valid for the next generation then, from the present limit on a new lepton, the charge 1/3 quark must have a mass greater than 50 GeV.

In the present phenemenology[66] of supersymmetric[67] theories all particles will have partners which differ in spin by half a unit. Thus there will be scalar electrons (muons) which can be pairproduced in $e^{+}e^{-}$ annihilation and which may decay into electrons (muons) and undetectable particles (photinos, goldstinos) leading to acoplanar two prong electron (muon) events. No evidence[41,64] was found resulting in the limits on the mass of a scalar lepton listed above in Table 4.

4.
QUARKONIA

A $Q\bar{Q}$ system of heavy quarks bound in a steeply rising potential will lead to the level scheme shown in Fig. 15. The levels are labeled by

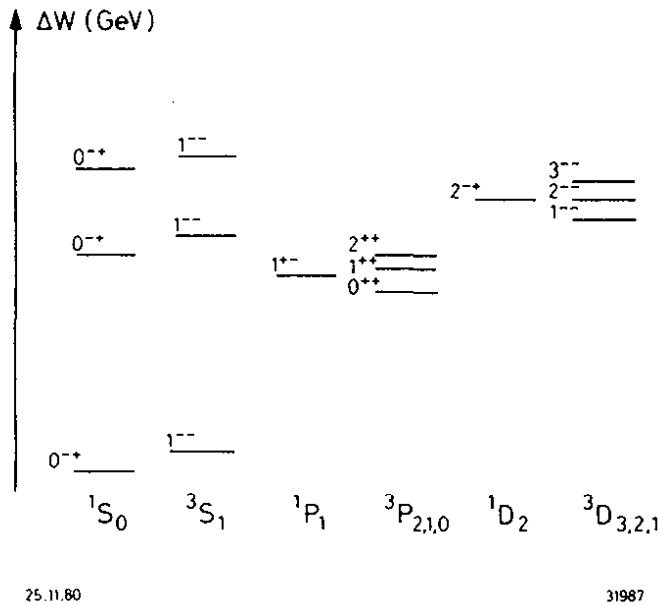

Fig. 15
The level scheme of two heavy quarks $Q\bar{Q}$ bound in a steeply rising potential.

J^{PC} with $P = (-1)^{L+1}$ and $C = (-1)^{L+S}$. For each value of L there are two bands of radial excitations with opposite charge conjugation depending whether S = 0 or 1. The spectroscopic notation $n^{2S+1}L_J$, where n-1 is the number of radial modes, is used to label the levels. The P levels will split into one $^1P_1$ level with odd and three states $^3P_{2,1,0}$ with even charge conjugation. In a pure coulombic potential the first set of P levels will be degenerate with the 2^3S_1 level. The addition of a confining potential pushes the mass of the 1P levels below the mass of the 2^3S_1 level.

The D levels will split into one state $^2D_1$ with even and three states $^3D_{3,2,1}$ with odd charge conjugation. The 1^3D_1 state has the quantum number of a photon. The wave function of this state may acquire a finite value at the origin by mixing with the nearby 2^3S_1 state and can be produced directly in e^+e^- collision.

The number and quantum numbers of the predicted levels are mainly a reflection of the spin 1/2 nature of the quark. The level spacing and the level widths on the other hand are strongly model dependent and can be used to test the theory.

The $^3S_1$ state decays to lowest order into hadrons via a 3 gluon intermediate state (one gluon forbidden because of colour, two gluons because of charge conjugation). The hadronic width is given[68] by

$$\Gamma(^3S_1 \to ggg \to \text{hadrons}) = \frac{160}{81}(\pi^2 - 9)\,\alpha_s^3\,\frac{^3S_1(0)}{M^2} \qquad (14)$$

M is the mass of the quark, $^3S_1(0)$ the wave function at the origin. The strong interaction constant $\alpha_s = 12\pi/(33-2N_f)\ln(q^2/\Lambda^2)$, where N_f is the number of flavours and Λ the characteristic strong interaction mass. The width for the decay into a pair of leptons given[69] by:

$$\Gamma(^3S_1 \to e^+e^-) = 16\pi\alpha^2 e_q^2 \frac{|^3S_1(0)|}{M^2} \qquad (15)$$

A richer level structure than the one predicted by a simple $Q\bar{Q}$ model might of course exist. Quark pairs may bind to form quark molecules[70] ($c\bar{q}\,\bar{c}q$) with a complex level scheme. The gluon field in a heavy $Q\bar{Q}$ system may have vibrational excitations[71] which may couple weakly to photons. So far there is no evidence for such states.

4.1 $c\bar{c}$ - states

The parameters of the $c\bar{c}$ vector states observed[9-11,72] in e^+e^- annihilation between 3.0 GeV and 4.5 GeV in c.m. are listed in Table 5. The Novosibirsk group[73] reports a very precise value of the J/ψ and the ψ' mass by using a spin depolarizing machine resonance to calibrate the beam energy. The J/ψ, ψ' and ψ'' can be identified with the 1^3S, 2^3S, and 1^3D_1 levels respectively and there is general agreement on the resonance parameters of these states. The situation above the ψ'', however, is still not settled. There are indications of a step in the cross section around 3.95 GeV, the DASP group observe two separate states at 4.04 GeV and 4.16 GeV whereas there is general agreement on the existence of a state near 4.41 GeV.

New preliminary data on the total cross section between 3.6 GeV and 4.5 GeV in c.m. by the Crystal Ball Collaboration are shown in Fig. 16. Plotted is the total annihilation cross section normalized to the point cross section. The data are corrected for τ-production but not for radiative effects. The radiative correction will enhance the peak structure. The data confirm the existence of the states around 4.03 GeV and 4.16 GeV and indicate structure in the cross section below 4.0 GeV.

e^+e^- COLLIDING BEAM EXPERIMENTS

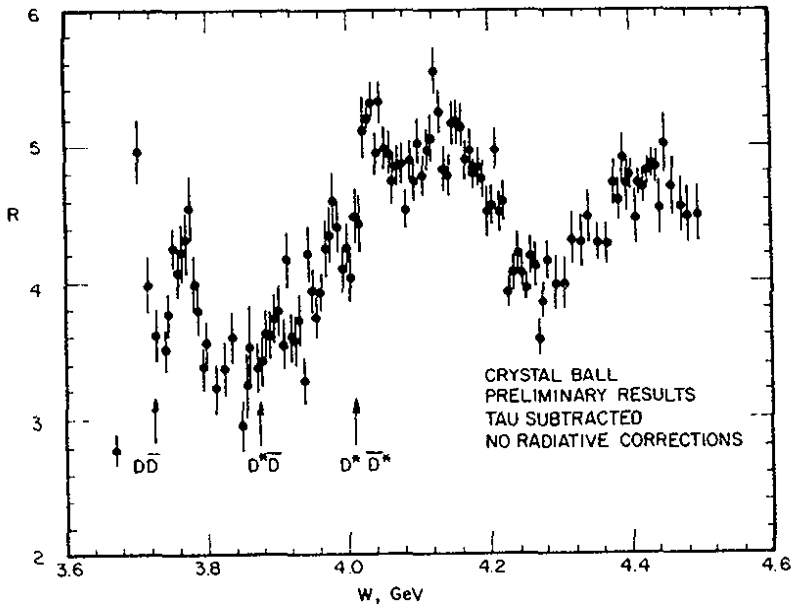

Fig. 16
The cross section for $e^+e^- \to$ hadrons as measured by the Crystal Ball Collaboration normalized to the point cross section.

Table 5 - Resonance parameters of $c\bar{c}$ vector states

State	Mass (MeV)	(MeV)	(MeV)
J/ψ	3096.93 ± 0.09	0.063 ± 0.009	4.8 ± 0.6
ψ'	3686.00 ± 0.15	0.215 ± 0.040	0.19 ± 0.2
ψ''	3768 ± 5	26 ± 5	0.27 ± 0.06
$\psi(4.030)$	4030 ± 5	52 ± 10	0.75 ± 0.10
$\psi(4160)$	4159 ± 20	78 ± 20	0.78 ± 0.31
$\psi(4415)$	4415 ± 6	43 ± 20	0.43 ± 0.13

Several C = +1 states have been observed in the decays J/ψ or ψ' into final states of γ + anything. The states found[12,13] at 3.41 GeV, 3.51 GeV and 3.55 GeV can be associated rather naturally with the $^3P_0$, $^3P_1$ and the $^3P_2$ levels whereas the states seen at 2.82 GeV[74], 3.45 GeV[75] and 3.59[76] were not easily fit into the $Q\bar{Q}$ scheme.

The Crystal Ball detector, designed to measure photons with a good energy resolution in a large solid angle, has produced a wealth of new data on the C = +1 states. Their main findings are summarized below.

a) They find no evidence[77] for the states at 2.82 GeV, 3.45 GeV and 3.59 GeV with a sensitivity much higher than the sensitivity reached in the original experiments.

b) They have observed[77] the decays $\psi' \to \gamma^3P \to \gamma\gamma\ J/\psi$ with much

higher statistics than previous experiments.

The inclusive photon spectrum observed in the ψ' decays is plotted in Fig. 17. The spectrum is rich and the connection between the ob-

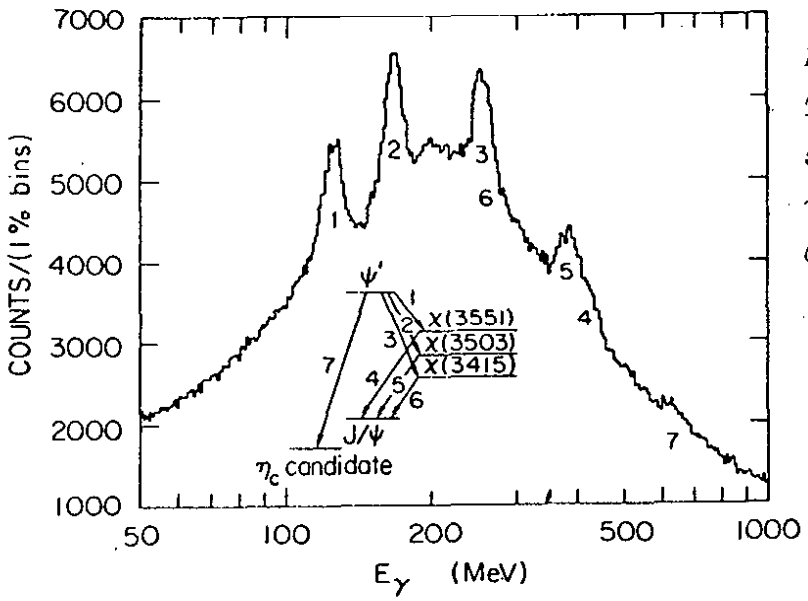

Fig. 17
The inclusive photon spectrum observed in ψ' decays by the Crystal Ball group.

served spectrum and the level scheme is shown in the insert. Evidence for the cascade decay $\psi' \to \gamma\ ^3P \to \gamma\gamma\ J/\psi$ are clearly seen. A more detailed study identifying the J/ψ via its leptonic decay mode $J/\psi \to e^+e^-$ ($\mu^+\mu^-$) has yielded the data summarized in Table 6.

Table 6 – Parameters for the charmonium P states

State	Mass MeV	$B(\psi' \to \gamma P)$ %	$B(\psi' \to \gamma P) \cdot B(P \to \gamma J/\psi)$ %
2^{++}	3553.9 ± 0.5 ± 4	7.02 ± 2.3	1.26 ± 0.09 ± 0.2
1^{++}	3508.4 ± 0.4 ± 4	7.1 ± 2.0	2.38 ± 0.12 ± 0.38
0^{++}	2413 ± 5	7.2 ± 2.0	0.059 ± 0.015 ± 0.004

These Crystal Ball results are in excellent agreement with the earlier[3] data. From the angular correlations in the cascade decays the Crystal Ball Collaboration finds that the $P_c/\chi(3.51)$ state has spin 1 and the $\chi(3.55)$ state has spin 2 in agreement with earlier assignment.

An interesting byproduct of this measurement is the observation[77] of the isospin forbidden decay $\psi' \to \pi^o\ J/\psi$. The find $B(\psi' \to \pi^o\ J/\psi) = (0.09 \pm 0.02 \pm 0.01)\%$ consistent with the value $B(\psi' \to \pi^o\ J/\psi) = (0.15 \pm 0.00)\%$ obtained[78] in an earlier measurement

by the MARK II Collaboration. The electromagnetic interaction predicts a rate which is more than an order of magnitude smaller than the observed rate and therefore appears to be excluded. The decay might arise from an isospin breaking amplitude as in the decay $\eta \to 3\pi$.

c) They find evidence[79] for a new state below the J/ψ mass both in the inclusive photonspectrum of J/ψ and ψ' decay and in exclusive channels. The state has a mass of 2978 ± 9 MeV and a total width less than 20 MeV.

The photon spectrum, plotted in Fig. 18a,b, clearly shows mono-

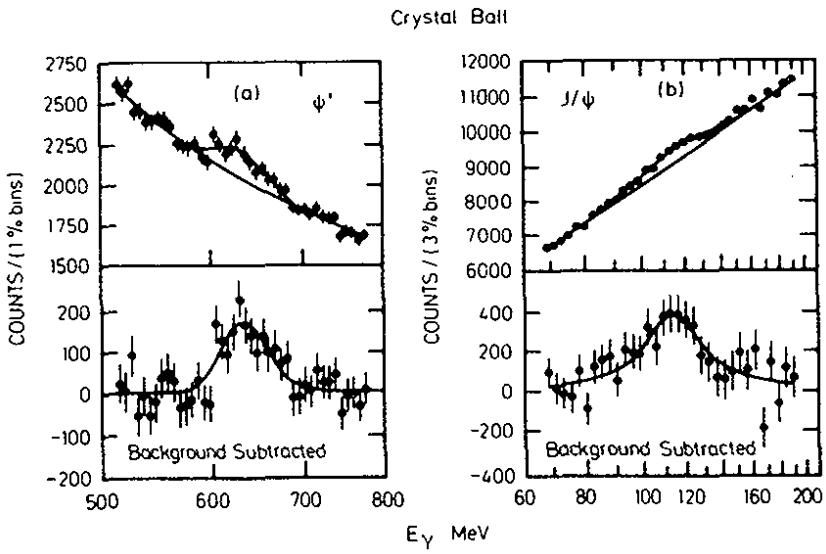

Fig. 18 a, b, Inclusive photon spectrum $\psi' \to \gamma x$ and $J/\psi \to \gamma x$ as measured by the Crystal Ball Collaboration shown with and without a smooth background subtraction.

chromatic photon lines leading to a state slightly below the J/ψ mass. It is natural to identify this state with the missing 1^1S_o $(c\bar{c})$ pseudoscalar partner to the J/ψ. Additional evidence comes from the observation of inclusive decay modes by the Crystal Ball Collaboration[79] and the MARK II group[80]. The MARK II group reports an enhancement for $\psi' \to \gamma$ X candidate events in the $\pi^\pm K^\mp K^o_s$ final state at 2980 ± 8 MeV. The photon energy spectrum (Fig. 19) for candidate events $J/\psi \to \gamma\, \eta\, \pi^+\pi^-$ measured by the Crystall Ball group has a clear peak at E_γ = 120 MeV. The combined data are listed in Table 7.

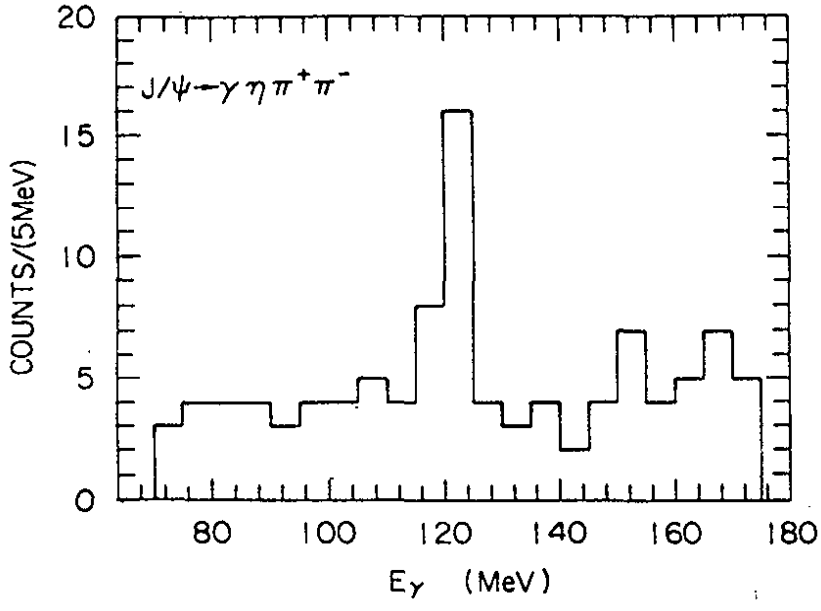

Fig. 19
The photon spectrum observed by the Crystal Ball Collaboration in $J/\psi \to \gamma\eta\pi^+\pi^-$ *candidate events.*

Table 7 – η_c *decays*

Decay mode	Branching ratio (%)
$J/\psi \to \gamma\eta_c$	$\sim$ 1
$\psi' \to \gamma\eta_c$	$0.43 \pm 0.08 \pm 0.18$
$\eta_c \to K\bar{K}\pi$	10^{+7}_{-6}
$\eta_c \to \eta\pi^+\pi^-$	3
$\eta_c \to 2\pi^+2\pi^-$	$1.3^{+1.5}_{-1.0}$
$\eta_c \to \pi^+\pi^-K^+K^-$	$0.9^{+1.5}_{-0.7}$
$\eta_c \to p\bar{p}$	$0.2^{+0.2}_{-0.1}$
$\eta_c \to \pi^+\pi^-p\bar{p}$	< 1.1 (90% C.L.)

4.2 $b\bar{b}$ states

The properties of the Υ and the Υ' have been investigated first at DORIS[21,22] and later at CESR[23]. The DORIS data demonstrated that the states are longlived - i.e. they are presumably the 1^{--} $b\bar{b}$ states of a new quark b. Quigg, Rosner and Thacker[81] have evaluated the electronic widths for Υ and Υ' in a wide varity of $Q\bar{Q}$ models and the results are

shown in Fig. 20.

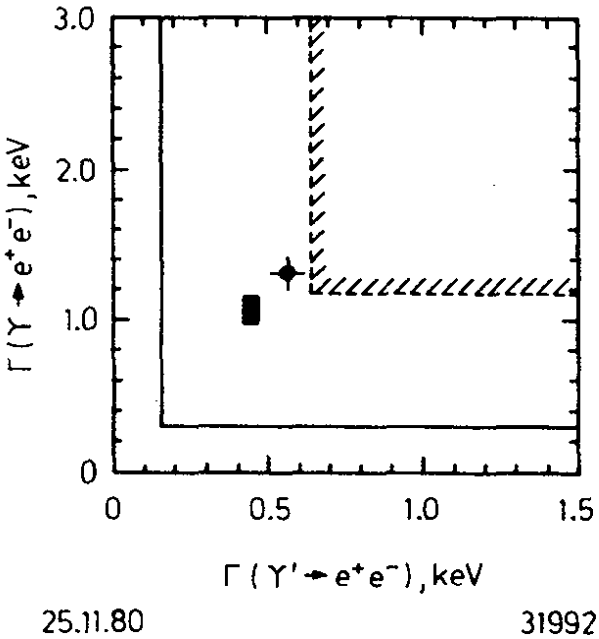

Fig. 20
The predicted leptonic width for $\Upsilon(1S)$ *and* $\Upsilon(2S)$ *in a* $Q\bar{Q}$ *model. The solid lines show the lower limit for a charge 1/3 quark, the dotted line the lower limit for a charge 2/3 quark. The average value of the DORIS data (•) and the average value of the CESR data (▮) are shown.*

The solid lines indicate the lower limit of the quark charge $e_q = 2/3$, the dotted lines the lower limits for $e_q = 1/3$. The average values obtained by the DORIS experiments and by the CESR experiments are shown. Both values favour $e_q = 1/3$. Furthermore the value of the total cross section measured by the PETRA groups above $b\bar{b}$ threshold are consistent with $e_q = 1/3$ and excludes $e_q = 2/3$ as discussed later.

The data have been extended to higher energies by the CUSB[23,82] and the CLEO[23,83] Collaborations at CESR and their total cross section results are plotted in Fig. 21 and in Fig. 22 respectively. Both experiments find clear evidence for two new resonances Υ'' and Υ'''. The Υ'' like the Υ and Υ', has a width consistent with the energy spread of the beams whereas the Υ''' is much wider. It is natural to assume that the threshold for $b\bar{b}$ production is located between the Υ'' and Υ''' resonance.

The resonance parameters for the four Υ-states observed so far are listed in Table 8.

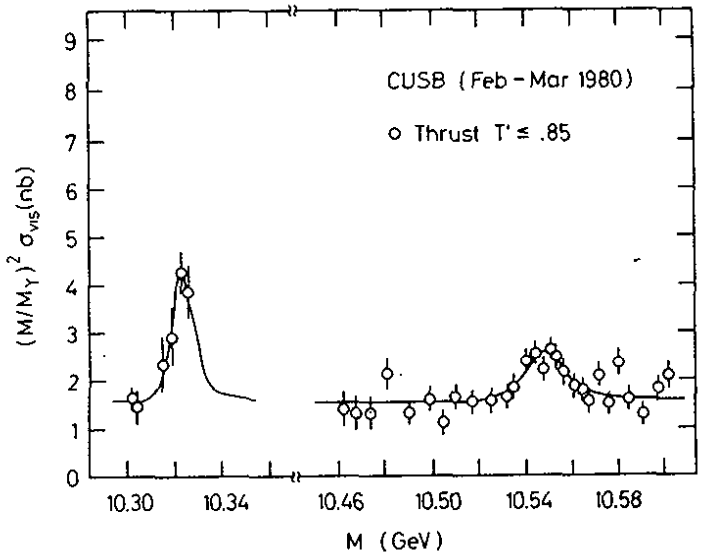

Fig. 21
The total hadronic cross section measured by the CUSB Collaboration for c.m. energies between 10.3 GeV and 10.6 GeV.

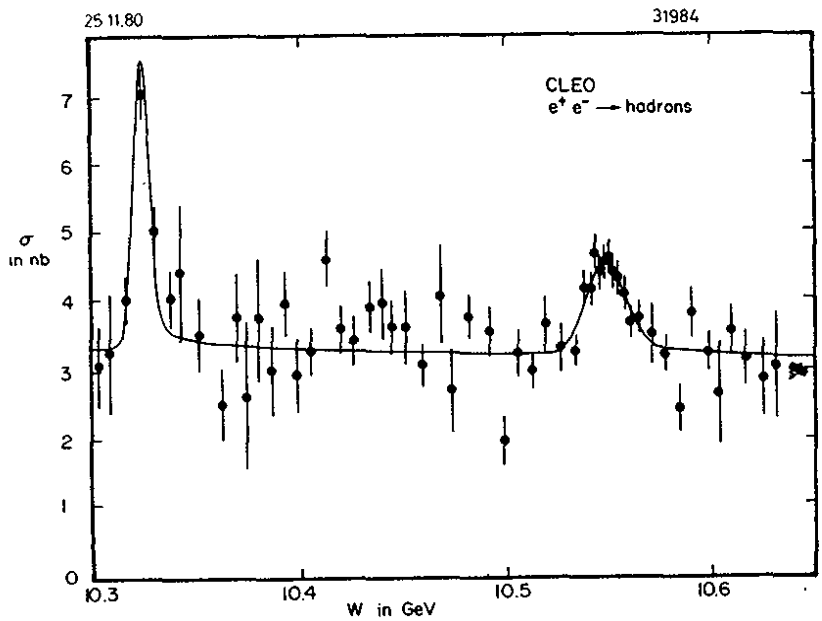

Fig. 22
The total hadronic cross section measured by the CLEO Collaboration.

Table 8 - Resonance parameters for the states

State	Mass MeV	Excitation energy MeV	Γ_{ee} (keV)	Ref.
Υ	9462±10	-	1.29 ± 0.09 ± 0.13	84
	9433±28	-	1.02 ± 0.07 ± 0.15	23
Υ'	-	553 ± 10	0.58 ± 0.08 ± 0.26	84
		560 ± 3	0.46 ± 0.03 ± 0.04	23
Υ''		889 ± 4	0.33 ± 0.03 ± 0.03	23
Υ'''		1114 ± 5	0.24 ± 0.02 ± 0.03	23

The first evidence for the cascade $\Upsilon \to \pi^+\pi^-\Upsilon$ has been presented by the LENA group[85] at DORIS and by the CUSB[82] and the CLEO[83] groups. Based on a few events they find a branching ratio on the order of 10%-30%. The branching ratio for $\Upsilon \to x\Upsilon$ can also be obtained from a comparison of the inclusive spectra measured at the Υ' and the Υ resonance. The spectra measured[83] by CLEO is shown in Fig.23 and the excess at small momenta observed in the Υ' spectrum is presumably due to $\Upsilon' \to x\Upsilon$ decay. A fit yields 21.6 ± 3.5%. The LENA group obtained[85] a branching ratio of 27 ± 9% from a similar measurement.

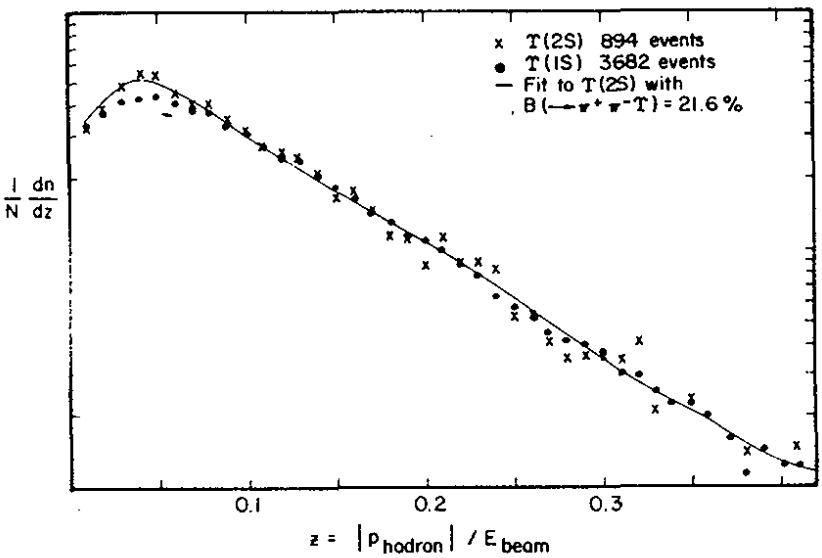

Fig. 23 Inclusive momentum spectrum of charged particles from the Υ and Υ'' with the continuum subtracted. The data were obtained by the CLEO Collaboration.

4.3 Comparison to theory

The observed $c\bar{c}$ and $b\bar{b}$ states identified by the spectroscopic notation $n^{2S+1}L_J$ are plotted in Fig. 24 as a function of excitation energy. The level ordering is in agreement with the spectrum shown in Fig. 15 for two non-relativistic fermions bound in a steeply rising potential. The excitation energy E^* measured with respect to the 1^3S_1 state and the ratio $R_{ee} = \Gamma_{ee}(1^{--}) / \Gamma_{ee}(1^3S_1)$ of the leptonic widths are listed in Table 9. By considering ratios of leptonic widths it is hoped that some of the uncertainties caused by higher order QCD radiative effects will cancel and that the data can be compared to first order calculations. Analogous to positronium decays such corrections may reduce the first order calculations by a factor[86] $(1 - 16\alpha_s/3\pi)$.

Two different approaches are in use to extract detailed information on the strong forces from the spectroscopic data.

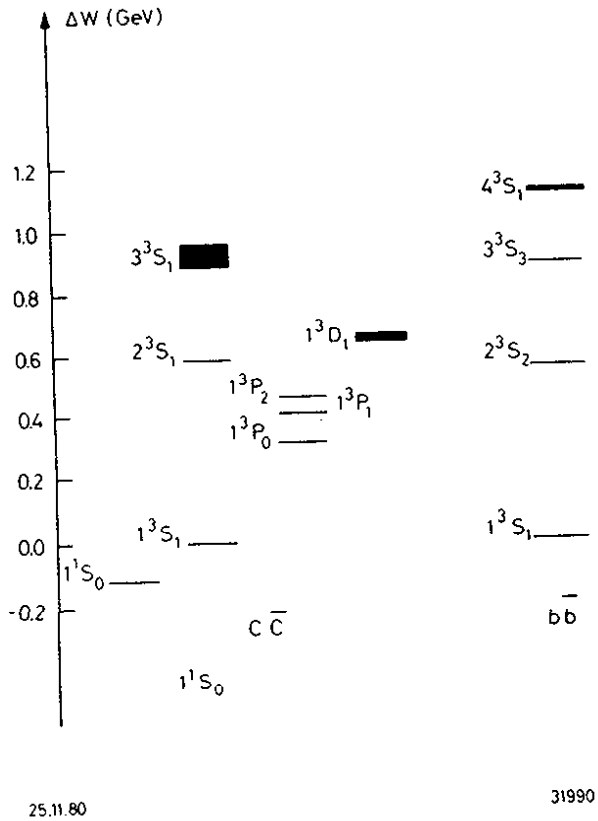

Fig. 24
Observed $c\bar{c}$ and $b\bar{b}$ states plotted versus excitation energy. The states are identified using the spectroscopic notation $n^{2S+1}L_J$.

Table 9 – Properties of the $c\bar{c}$ and the $b\bar{b}$ system

	Measured		Emp.Potential[88]		QCD Potential[90]	
State	E^*(MeV)	R_{ee}	E^*(MeV)	R_{ee}	E^*(MeV)	R_{ee}
'	589.1 ± 0.1	0.44 ± 0.06	589	0.35	589	0.45
''	671 ± 2		705		715	
$^3P_{2,1,0}$	426 ± 4		425		425	
(2S)	553 ± 10	0.45±0.06±0.02	560	0.43	500	0.45
	560 ± 3	0.45±0.03±0.04				
(3S)	889 ± 4	0.32±0.03±0.03	890	0.28	890	0.32
(4S)	114 ± 5	0.24±0.02±0.03	1120	0.20	1160	0.26

One approach is to directly derive[87] the potential from the observed levels using the inverse scattering formalism. It has also be shown[88] that a rather simple potential of the form $V(r) = A + B\ r^\nu$ with the parameters determined by the lowest levels can fit both the $c\bar{c}$ and the $b\bar{b}$ states using identical parameter values.

In a complementary approach one tries to derive a potential from first principles. Richardson[89] has obtained a QCD potential of the

form:

$$V(q^2) = -\frac{4}{3}\,\frac{12\pi}{33 - 2N_f}\,\frac{1}{q^2}\,\frac{1}{\ln(1 + q^2/\Lambda^2}} \qquad (16)$$

written in momentum space. The potential has only one parameter Λ which may be identified with the characteristic strong interaction mass. The Fourier transform results in a potential which is proportional to 1/r at small distances as expected for the confining term. The potential, with second order QCD corrections[90] included, is plotted in Fig. 25

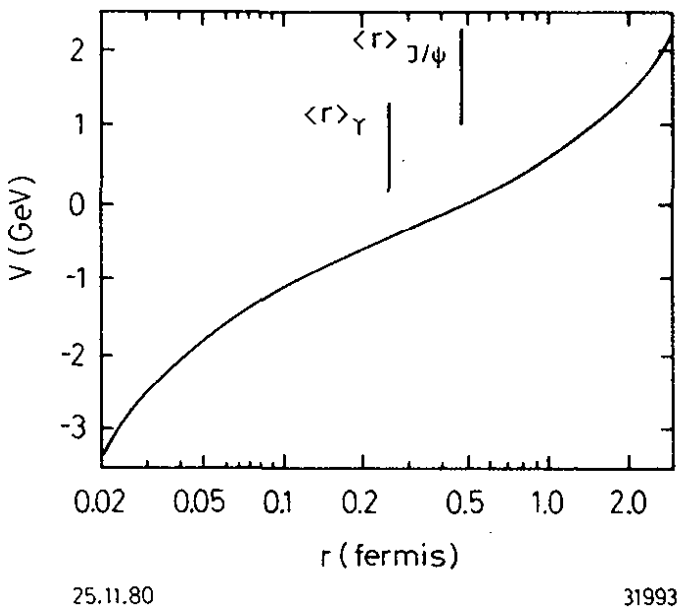

Fig. 25
The modified Richardson potential versus r.

versus r. The average r values for the J/ψ and the Υ are indicated. It is clear that both the $c\bar{c}$ and the $b\bar{b}$ family are mainly sensitive to the intermediate part of the potential between the Coulombic and the linear part. A fit to the observed spectrum gives $\Lambda_{\overline{MS}} = 0.508$ GeV which is consistent but larger than the value of α_s determined in other processes. The results are also listed in Table 9.

The observed data are reproduced rather well by the QCD model but also the simple ad hoc potential gives an adequate representation. Both the $c\bar{c}$ and the $b\bar{b}$ spectra can be fit using the same values of the parameters[88,90] and this shows that the strong force does not depend on the quark flavour.

4.4 Upsilon decays

1^{--} states in QCD decays dominantly via a 3 gluon intermediate state. The energy distribution of the gluons can be written as:

$$\frac{1}{\Gamma}\frac{d\Gamma}{dx_1 dx_2} = \frac{6}{\pi^2-9}\,\frac{x_1^2(1-x_1)^2 + x_2^2(1-x_2)^2 + x_3^2(1-x_3)^2}{x_1^2\,x_2^2\,x_3^2} \qquad (17)$$

where $x_i = E_i/E_b$ is the scaled energy.

This should lead to flat events defined by the three gluons fragmenting into three jets of hadrons. However, T decays yield in general two energetic gluon jets plus one low energy gluon jet. The symmetric case $x_1 = x_2 = x_3 = 2/3$ is rather unlikely and even in this case each jet will on the average have an energy of only 3 GeV. The data on $e^+e^- \to$ hadrons do not show a clear jet structure at 6 GeV in c.m.

PLUTO has analyzed the hadron data[25] from T decays using triplicity[91], a generalization of thrust to three axis. In this method the final state hadrons with momenta $\vec{p}_1$, $\vec{p}_2$ ....$\vec{p}_N$ are grouped into three classes C_1, C_2 and C_3 with momenta $\vec{p}(C_N) = \Sigma|\vec{p}_i|$ where the sum is over all particles assigned to class C_N. Triplicity T_3, is then defined as:

$$T_3 = \frac{1}{\Sigma_i |p_i|} \cdot \max\{|\vec{p}(C_1)| + |\vec{p}(C_2)| + |\vec{p}(C_3)|\} \qquad (18)$$

T_3 is 1 for a perfect 3-jet event and 3 $(\sqrt{3/8})$ = 0.65 for a spherical event.

The momenta of the three jets are given by $\vec{p}_1 = \vec{p}(C_1)$, $\vec{p}_2 = \vec{p}(C_2)$ and $\vec{p}_3 = \vec{p}(C_3)$ and the angles between these vectors θ_1, θ_2, and θ_3 are the angles between the three jets. The triplicity and the thrust distribution for events on the T are plotted in Fig. 26 and Fig. 27 respectively. The data include both neutral and charged tracks and they

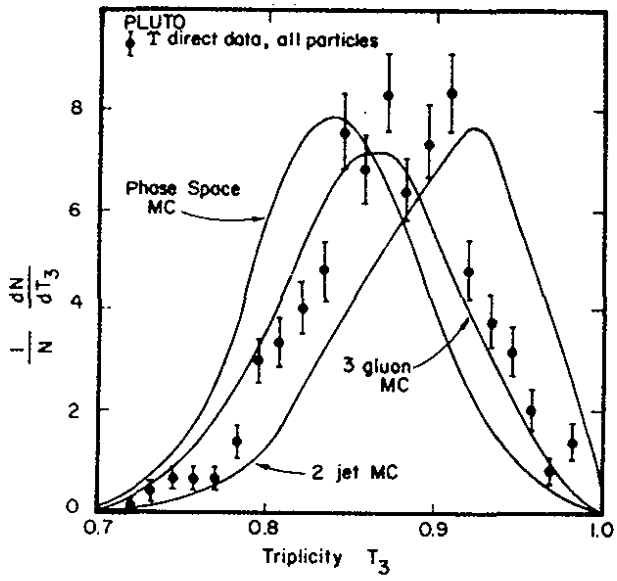

Fig. 26
The triplicity distribution on the T(9.46) resonance.

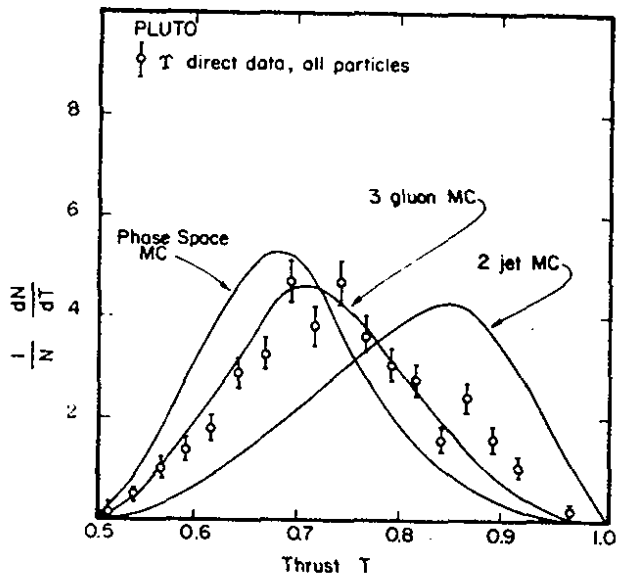

Fig. 27
The thrust distribution on the T(9.46) resonance.

have been corrected for the continuum contribution $e^+e^- \to q\bar{q}$ and for the vacuum polarisation. The triplicity and thrust distributions for the following decay modes have been evaluated:

i) $e^+e^- \to T \to$ hadrons, where the hadrons are distributed according to phase space.

ii) $e^+e^- \to T \to q\bar{q}$. Such a distribution might be expected if the T decays via a one gluon intermediate state. Also $e^+e^- \to T \to$ gg would lead to a similar topology.

iii) $e^+e^- \to T \to ggg$. This is the lowest order diagram in QCD.

The results are also plotted in Fig. 26 and Fig. 27 and it is clear that the 3 gluon distribution agrees well with the data whereas neither phase space nor twobody $q\bar{q}$ (gg) decays fit the observed distributions. The thrust distribution for events collected in the continuum adjacent to the T peak is plotted in Fig. 28. This distribution is peaked at large values of thrust and is well fit by $e^+e^- \to q\bar{q}$ but not by $e^+e^- \to ggg$. With a colourless gluon T could decay [92] via one gluon emission producing a final state with two collinear hadron jets as observed in the continuum and resulting in a similar thrust distribution on and off resonance. The marked difference in event topology observed on and off the resonance is strong indirect evidence that the gluon has colour.

The angular distribution of the thrust axis for T events is plotted in Fig. 29. The dotted and the solid lines show the predictions [93] for vector and scalar gluons respectively. The data clearly favour a vector gluon.

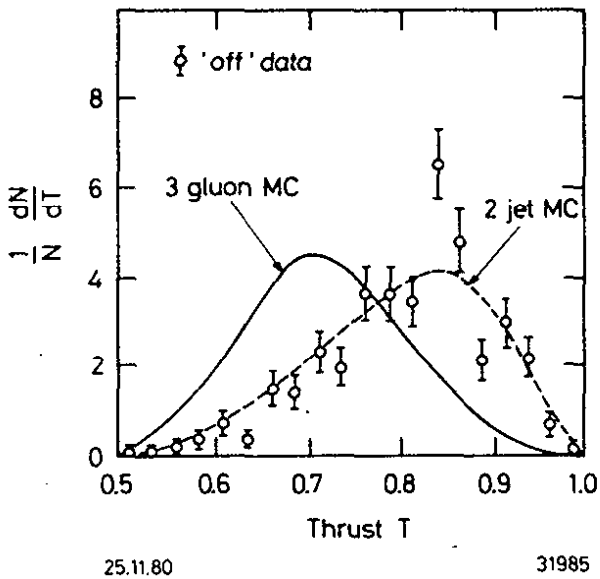

Fig. 28
The thrust distribution in the continuum at energies adjacent to the T(9.46) resonance.

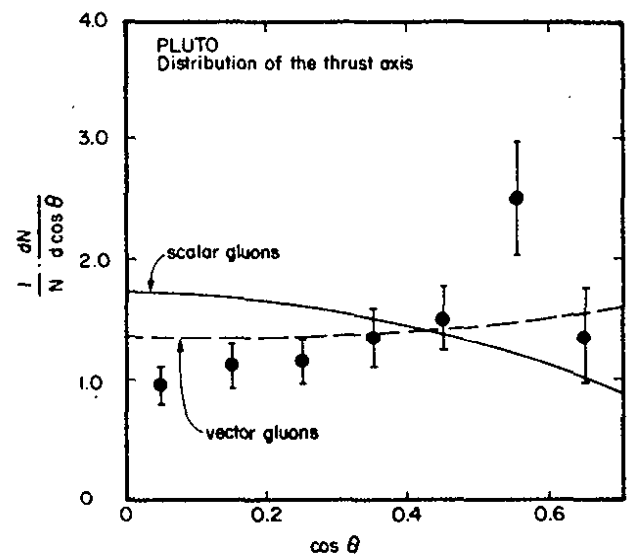

Fig. 29
Data on the distribution of the thrust axis observed in T (9 46) decay with respect to the beam axis. The theoretical distribution for scalar and vector gluons are also shown.

Since the data agree with the QCD predictions they can be used to determine the quark gluon coupling constant α_s. Combining Eq. 15 and Eq. 16 yields:

$$\Gamma_{ggg} = \frac{10(\ ^2 - 9)}{9\pi\alpha^2} \cdot \alpha_s^3 \, \Gamma_{ee} \qquad (19)$$

$$\Gamma_{ggg} = \Gamma_{tot} - \Gamma_{ee} - \Gamma_{\mu\mu} - \Gamma_{\tau\tau} - R\Gamma_{\mu\mu} = \Gamma_{tot} - (3+R)\Gamma_{ee} \qquad (20)$$

where the term $R\Gamma_{\mu\mu}$ is the contribution from the vacuum polarisation. The average over all DORIS data yield[84]:

$$\Gamma_{ee} = 1.29 \pm 0.09 \pm 0.13 \quad \text{and} \quad B_{ee} = B_{\mu\mu} = (3 \pm 0.8)\%. \qquad (25,26)$$

This yields

$$\Gamma_{tot}(1^3S_1) = \Gamma_{ee}/B_{ee} = (43\ ^{+20}_{-10})\ \text{keV}$$

which is the first direct measurement of the T width. Inserting these values into Eq. 19 leads to:

$$\alpha_s = 0.17 \pm 0.02 \text{ at the T.}$$

Using the same method to evaluate α_s at the J/ψ yields:

$$\alpha_s = 0.19 \pm 0.02.$$

These values are in good agreement with the values of α_s determined from quark gluon bremsstrahlung asdiscussed below.

4.5 Direct photon decays of the J/ψ

Replacing one of the gluons in the decay $^3S_1 \rightarrow ggg$ by a photon results in a final state which consists of one photon and two gluons. The photon spectrum is predicted to be nearly proportional to $x = k_\gamma/E$ such that the favoured topology is a high energy photon recoiling against two nearly collinear gluons. The leading order QCD calculation[94] based on the Feynman graph shown in Fig. 30, predicts for the ratio of the decay widths:

$$\Gamma_{\gamma gg} / \Gamma_{ggg} = \frac{36}{5} \left(\frac{\alpha}{\alpha_s} \right) \left(\frac{e_Q}{e} \right)^2 \qquad (21)$$

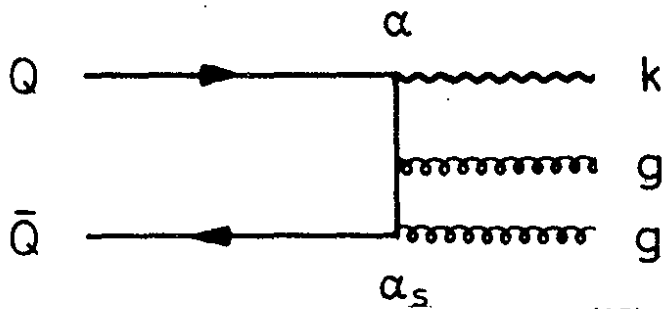

Fig. 30
Feynman graph for $1^{--} \rightarrow \gamma + gg$

The MARK II Collaboration has observed[95] the single photon spectrum in J/ψ decays. The difference between the data and the estimated background from π^o and η decay is plotted in Fig. 31 versus x. This difference is ascribed to the direct decay J/$\psi \rightarrow \gamma + X$. The leading order QCD calculation smeared by the resolution is shown as the solid curve in Fig. 31.

The theoretical spectrum is harder than the observed, but including QCD radiative effects and the mass of the final state hadrons may soften the predicted spectrum.Measured and predicted rates are in good agree-

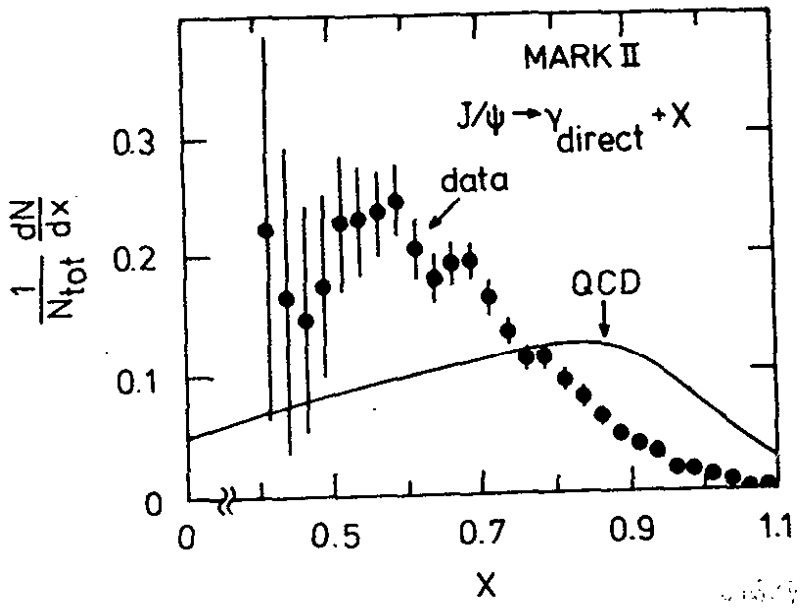

Fig. 31
The direct photon spectrum observed in J/ψ decays. The leading order QCD prediction smeared by the experimental resolution is shown as the solid curve.

ment. Integrating the spectrum for $x \geq 0.6$ results in an inclusive branching ratio of $(4.1 \pm 0.8)\%$ compared to 5% predicted by the first order QCD calculation. The MARK II Collaboration has also investigated the properties of the hadronic system recoiling against the photon. They find[96] the charged multiplicities and the K^o fractions to be similar to those observed in e^+e^- annihilation at the corresponding c.m. energy.

4.6 Search for the gluonium

Two or more gluons are expected[97] to form gluonium states, bound colourless particles with a massspectrum starting may be around 1-1.5 GeV. The direct photon decay $J/\psi \to \gamma gg \to \gamma$ hadrons is a good place to search for these states. Also radiative decays[3] $J/\psi \to \gamma\, \eta\, (\eta' f)$ seem to proceed mainly by diagrams similar to the one shown in Fig. 30.

The inclusive photon spectrum $J/\psi \to \gamma X$ measured[98] by the Crystal Ball group is plotted in Fig. 32. In addition to the well known transitions $J/\psi \to \gamma\eta$ and $J/\chi \to \gamma\eta'$ a new state is observed which they tentatively identify with the E(1420). The MARK II Collaboration sees evidence[96] for the same state in the channel $J/\psi \to \gamma\, (K_s K^{\pm}\pi^{\mp})$. The $K_s K^{\pm}\pi^{\mp}$ mass distribution for candidate events, plotted in Fig. 33a and b, shows a peak centered at 1440 MeV. From a fit to the 5C distribution in Fig.33a they find $M = 1440^{+10}_{-15}$ MeV, $\Gamma = 50^{+30}_{-20}$ MeV and $B(J/\psi \to \gamma E) \cdot B(E \to K\bar{K}\pi) = (3.6 \pm 1.4) \cdot 10^{-3}$. The large branching ratio $J/\psi \to \gamma E$ has lead the experimentators to suggest that the E might be a gluonium state.

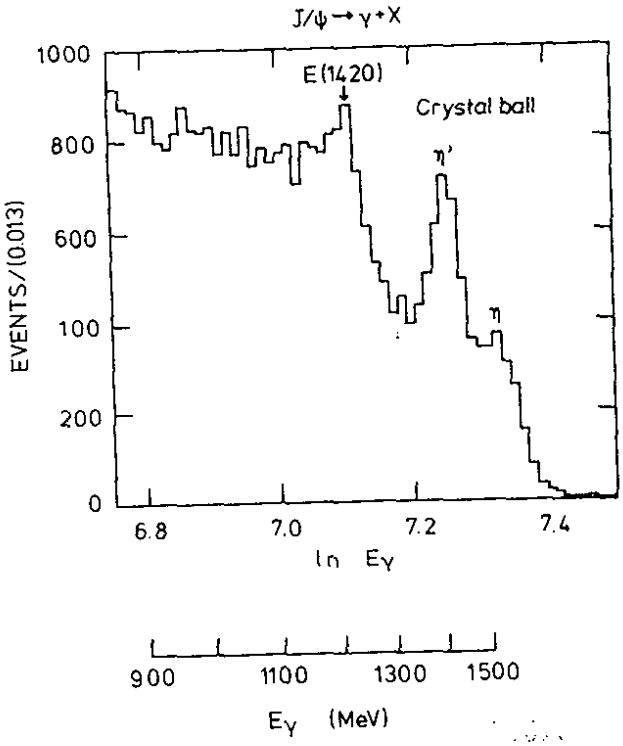

Fig. 32
The inclusive photon spectrum $J/\psi \to \gamma X$ observed by the Crystal Ball Collaboration.

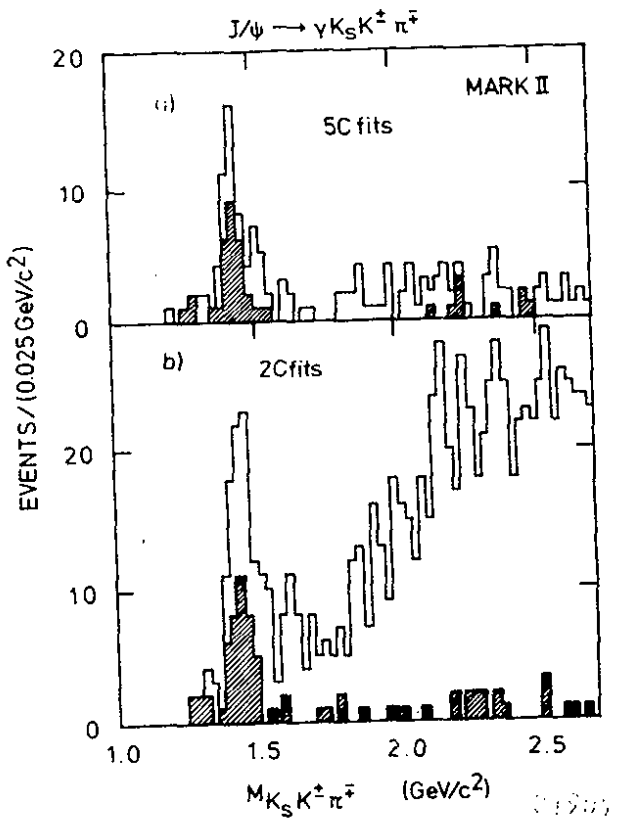

Fig. 33
The $K_S K^{\pm}\pi^{\mp}$ mass spectrum for $J/\psi \to \gamma\, K_S K^{\pm}\pi^{\mp}$ candidate events which satisfy
a) a 5C fit to this hypothesis
b) a 2C fit (observation of the photon not required).
Events in the shaded region have $m_{K\bar{K}} < 1.05$ GeV. The data were obtained by the MARK II Collaboration.

Recently Dionisi et al. determined[99] the spin parity of the E meson to be $J^P = 1^+$ from an analysis of the $E \to K^*K$ decay mode. The MARK II Collaboration, however, found no evidence for this decay mode,

but rather observed the $\delta\pi$ to be a prominent decay mode. If the axial vector assignment is confirmed for the resonance observed in the radiative decays then it becomes natural to include it with the $\tilde{D}(1285)$, A_1 and Q_A in the same nonet. In this case there is no evidence for gluonium state in radiative J/ψ decays.

5.
STATES WITH OPEN CHARM

5.1 The D^o and $D^{\pm}$ states

Possible transitions between the corresponding Q-values are summarized in Fig. 34 for the known D states.

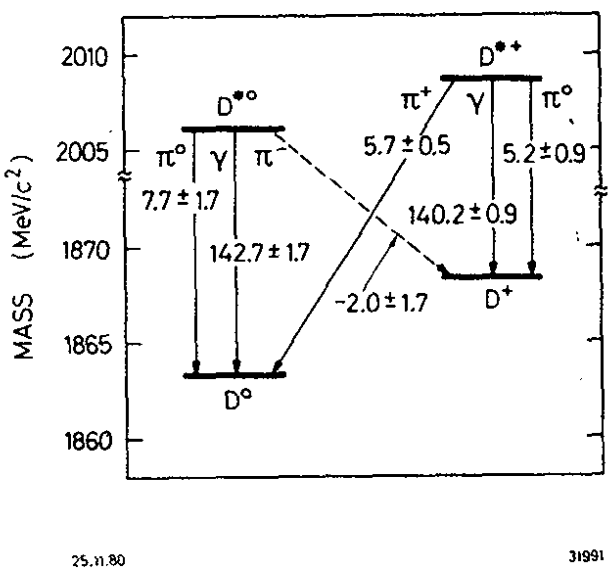

Fig. 34
Q-values for $D^* \to D$ transitions.

The ψ'' decays to a good approximation only into $D\bar{D}$ final states. The production cross sections for these mesons at the ψ'' resonance were determined[100] by the MARK II Collaboration to:

$$\sigma(D^o) = (8.0 \pm 1.0 \pm 1.2) \text{ nb}$$
$$\sigma(D^+) = (6.0 \pm 0.7 \pm 0.1) \text{ nb}$$

For comparison, the cross section predicted for $e^+e^- \to Z^o \to c\bar{c}$ is on the order of 4 nb. An additional advantage is that the D's are produced almost at rest and the favourable kinematics allow a precise determination of the mass $M_o = \sqrt{E^2 - p^2}$ where E is the beam energy and p the D momentum. These nice features have been exploited by the groups working at SPEAR and have lead to a wealth of data[101] on the D states.

e^+e^- COLLIDING BEAM EXPERIMENTS

Mass-spectra for $K^{\pm}\pi^{\mp}$, $K^{o}_{s}\pi^{\mp}\pi^{\pm}$ and $K^{\pm}\pi^{\mp}\pi^{\pm}$ measured at the ψ'' by the MARK II Collaboration[102] are shown in Fig. 35. From such data groups working at SPEAR found m_{D^o} = (1864.3 ± 0.9 MeV) and m_{D^+} = (1868.4 ± 0.9 MeV).

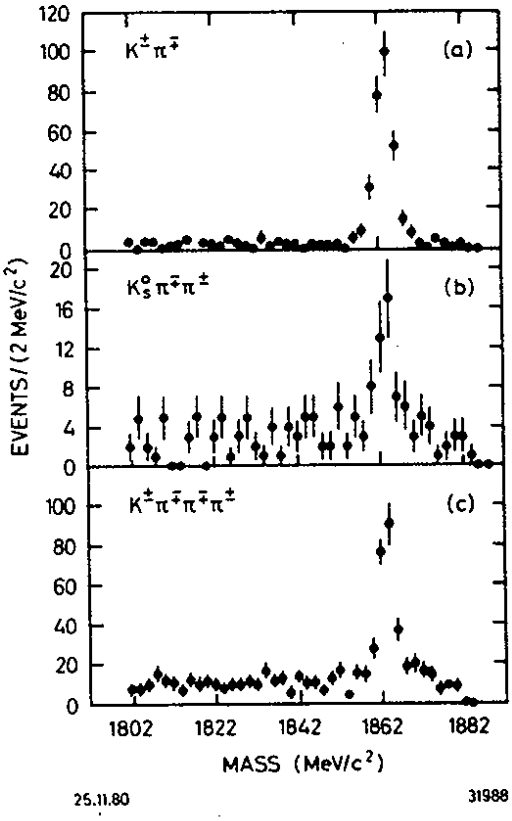

Fig. 35
Mass spectra for $\psi'' \to D^o\bar{D}^o$ *candidate events with*
a) $D \to K^{\pm}\pi^{\mp}$
b) $D \to K^{o}_{s}\pi^{\mp}\pi^{\pm}$
c) $D \to K^{\pm}\pi^{\mp}\pi^{\mp}\pi^{\pm}$
The data were obtained by the MARK II Collaboration.

A complete list of D branching ratios can be found in Ref. 101. Below we want to discuss a measurement of the lifetimes and a determination of the GIM mixing angles.

5.2 Lifetime of charmed mesons

Possible Cabibbo favoured decay modes of charmed mesons into light hadrons are shown in Fig. 36. An assumption often made was that the charmed quark would decay according to $c \to -\sin\theta \cdot d + \cos\theta \cdot s$ with the second quark merely acting as a spectator. This mechanism, shown in Fig. 36a, c and d predicts that all charmed mesons should have the same lifetime. It has been pointed out by Pais and Treiman[103] that $\Gamma(D^+ \to \ell \bar{\nu}_c X) = \Gamma(D^o \to \ell \bar{\nu}_c X)$ since $|\Delta I = 0|$ for the Cabibbo allowed decay $c \to \bar{\ell}\, \nu_e\, s$. The semileptonic branching ratios can therefore be used to determine the ratios of the lifetimes:

$$\frac{B(D^+ \to \bar{\ell}\, \nu_e\, X)}{B(D^0 \to \bar{\ell}\, \nu_e\, X)} = \frac{\sigma_{tot}(D^0 \to X)}{\sigma_{tot}(D^+ \to X)} = \frac{\tau(D^+)}{\tau(D^0)} \qquad (22)$$

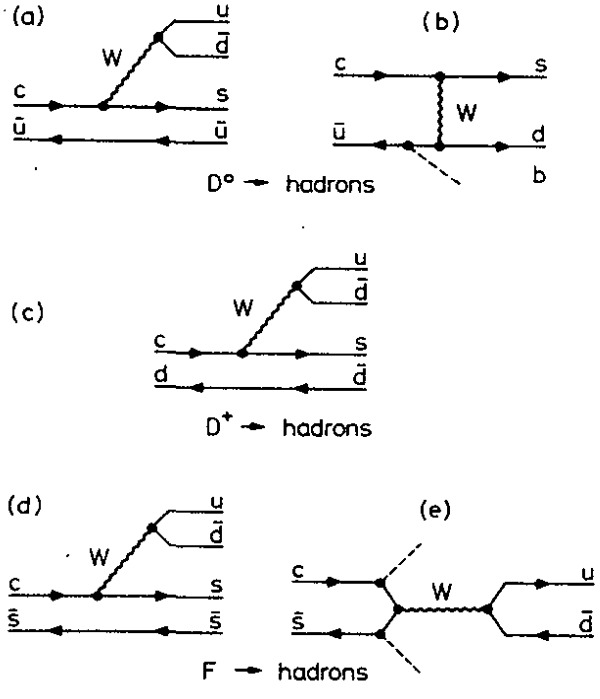

Fig. 36
Possible Cabibbo favoured decay modes of charmed mesons into light hadrons.

Both the DELCO[104] and the MARK II[102] collaborations report results on this ratio. DELCO finds[104]

$$\tau(D^+ / \Gamma(D^0) > 4.3 \qquad \text{and} \qquad B_e(D^+) = 22\ ^{+4.4}_{-2-2}\ \%.$$

The results were extracted from a sample of $D\bar{D}$ events in which one or both of the charmed mesons decayed semileptonically.

The MARK II Collaboration determined[102] the branching ratios from an inclusive measurement of charmed meson production. The events were tagged by identifying either a charged or a neutral D meson and measuring the decay products of its partner. In this way the semileptonic branching ratios are determined directly and they find:

$$\tau(D^+) / \Gamma(D^0) = 3.1\ ^{+4.6}_{-1.4} \quad \textit{and} \quad B_e(D^+) = 18.6 \pm 6.4\%.$$

The lifetime of charmed particles has been determined directly using emulsions[105, 106]. Although the data still have rather limited statistics they show that the D^0 indeed may have a shorter lifetime than

the D^+. Niu et al.[106] reports the following lifetimes in units of 10^{-13} s

$$\tau(D^o) = 1.01\ ^{+0.43}_{-0.27} \qquad \tau(D^+) = 10.3\ ^{+10.5}_{-\ 4.1} \quad \text{and} \quad \tau(F^+) = 2.2\ ^{+2.8}_{-1.0}$$

The D^+ lifetime combined with the average branching ratio for $D^+ \to e^+ \nu_e X$ results in a semileptonic width:

$$(D^+ \to e^+ \nu_e X) = (2 \pm 1) \times 10^{11}\ \text{sec}^{-1}.$$

Cabbibo, Maiani and Corbo have evaluated[107] the semileptonic width in the spectator model and they find:

$$\Gamma_{SL} = \frac{G_F^2 m_c^5}{192\pi^3}\ g(\varepsilon)\ \left(1 - \frac{2\alpha_s}{B\pi}\ f(\varepsilon)\right) \qquad (23)$$

with $\varepsilon = m_s/m_c$. Here $g(\varepsilon)$ is a phase space correction due to the finite mass of the s quark and the terms in the bracket is a QCD strong interaction correction. With $m_c = 1.75\ \text{GeV/c}^2$ they find $\Gamma_{SL} = 1 \times 10^{11}\ \text{sec}^{-1}$ consistent with the experimental results. This indicate that the D^o must have additional decay modes.

Additional decay modes resulting from W^+ annihilation are indeed Cabibbo allowed both for D^o and F^+ decays whereas they are Cabibbo forbidden for D^+ decays. These decay modes, shown in Fig. 36 d and e may account for a factor of 5 in the lifetime ratio $\tau(D^o)/\tau(D^+)$.

5.3 The G I M mechanism

The GIM mechanism[16] predicts that the charmed quarks decay predominantly into a strange quarks according to:

$$c \to \sin\theta_B \cdot d + \cos\theta_B \cdot s \qquad (24)$$

The mixing angle θ_B is identified with the familiar Cabibbo angle θ_A which is found to be 13^o from strange particle decays. Both angles θ_A and θ_B can be determined from a measurement of the two-body decay modes

$$D^o \to K^-\pi^+ \quad , \quad D^o \to K^-K^+ \quad , \quad D^o \to \pi^-\pi^+$$

as shown in Fig. 37.

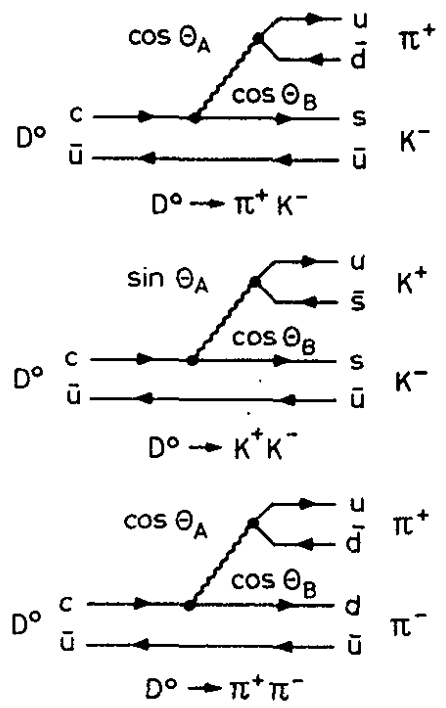

Fig. 37
Diagrams for two body D^O decays
a) $D^O \to \pi^+K^-$
b) $D^O \to K^+K^-$
c) $D^O \to \pi^+\pi^-$

These decays yield

$$tg^2\theta_A = 1.08\,\frac{\Gamma(D^O \to K^-K^+)}{\Gamma(D^O \to K^-\pi^+)} \quad \text{and} \quad tg^2\theta_B = \frac{0.93 \cdot \sqrt{(D^O \to \pi^-\pi^+)}}{\Gamma(D^O \to K^-\pi^+)}$$

Invoking SU(3) invariance and the GIM mechanism yields

$$tg^2\theta_A = tg^2\theta_B = tg^2\theta_{Cabibbo} = 0.05.$$

The MARK II Collaboration has determined[108] these decay modes making use of the fact that at the ψ'' D^O's are pairproduced with a unique momentum of 288 MeV/c. The invariant mass spectra obtained for the two-body decay modes are shown in Fig. 38. The peak occurs at the D^O mass if the two particles are identified correctly and shifted by about $\pm$ 120 MeV/c^2 if one of the particles is misidentified. Both a $\pi^+\pi^-$ and a K^-K^+ signal is observed yielding:

$$\frac{\Gamma(D^O \to \pi^-\pi^+)}{\Gamma(D^O \to K^-\pi^+)} = 0.033 \pm 0.015 \quad \text{and} \quad \frac{\Gamma(D^O \to K^-K^+)}{\Gamma(D^O \to K^-\pi^+)} = 0.113 \pm 0.030.$$

The data show that Cabibbo forbidden decays occur at roughly the level predicted. The two standard deviation effects observed in the K^-K^+ rate may imply that SU(3) is violated either in the strong or in the weak

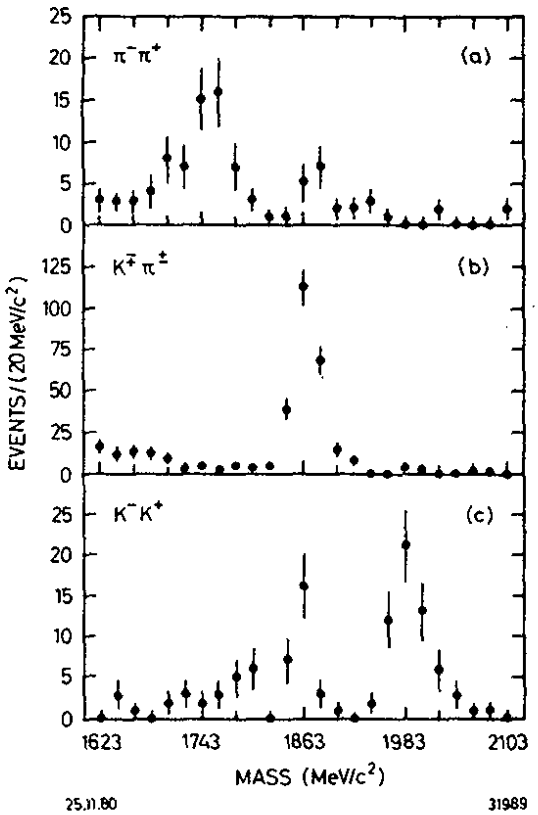

Fig. 38
Invariant mass distribution of candidate events for:
a) $D^0 \to \pi^-\pi^+$
b) $D^0 \to K^\mp\pi^\pm$
c) $D^0 \to K^-K^+$
The data were obtained by the MARK II Collaboration.

interaction. Improved data are needed to settle this question.

5.4 Evidence for the F meson

The DASP Collaboration observe[18] a signal at 4.42 GeV in c.m. which they attribute to $F^+ \to \eta\,\pi^+$. A scatter plot of the $\eta\pi^+$ mass versus the fitted recoil mass assuming $e^+e^- \to FF^*$ is shown in Fig. 39 for events at 4.42 GeV and events outside the region. At 4.42 GeV there is a cluster of 6 events, whereas at other energies the events have a smooth mass distribution. Of the 6 events observed at 4.42 GeV less than 0.2 events can be ascribed to the background. This was estimated from the measured luminosity and the number of events observed outside of 4.42 GeV in the same mass region with the conservative assumption that all these events are background events. The cluster at 4.42 GeV gives,

$$m_F = 2.03 \pm 0.06 \text{ GeV/c}^2 \quad \text{and} \quad m_{F^*} = 2.14 \pm 0.06 \text{ GeV/c}^2,$$

including systematic uncertainties.

The DASP data also indicate, with large errors, a structure in the η inclusive cross section which they ascribe to F production.

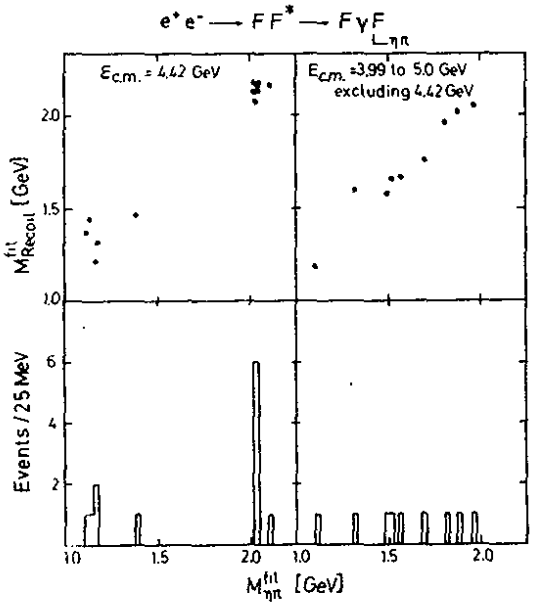

Fig. 39
Fitted mass versus fitted recoil mass, assuming $e^+e^- \to FF^*$, where $F^* \to \gamma F$ and $F \to \eta\pi$. a) at 4.42 GeV c) all other energies excluding 4.42 GeV. Histograms (b) and (d) are the projections of (a) and (c) respectively, along the $M(\eta\pi)$ axis. The data were obtained by the DASP Collaboration.

Recent data[109] by the Crystal Ball Collaboration do not confirm this structure.

Supporting evidence for the F has come from a photoproduction experiment in the Ω' spectrometer at the SPS and from emulsion exposures. The WA4 Collaboration at the SPS observe[110] a signal in the decay modes $F \to \eta\pi$, $\eta 3\pi$ and $\eta' 3\pi$. The results are shown in Fig. 40 and summarized in Table 9.

Table 10 - Evidence for F-photoproduction

Decay mode	Width (MeV) predicted	observed	Mass (MeV)	B · σ (nb)
$\eta\ \pi$	75	108 ± 31	2047 ± 25	12 ± 3
$\eta\ 3\pi$	50	38 ± 24	2021 ± 15	60 ± 15
$\eta'\ 3\pi$	40	48 ± 34	2008 ± 20	20 ± 8

The best estimate of the mass gives $m_F = (2020 \pm 0.010)$ GeV/c^2.

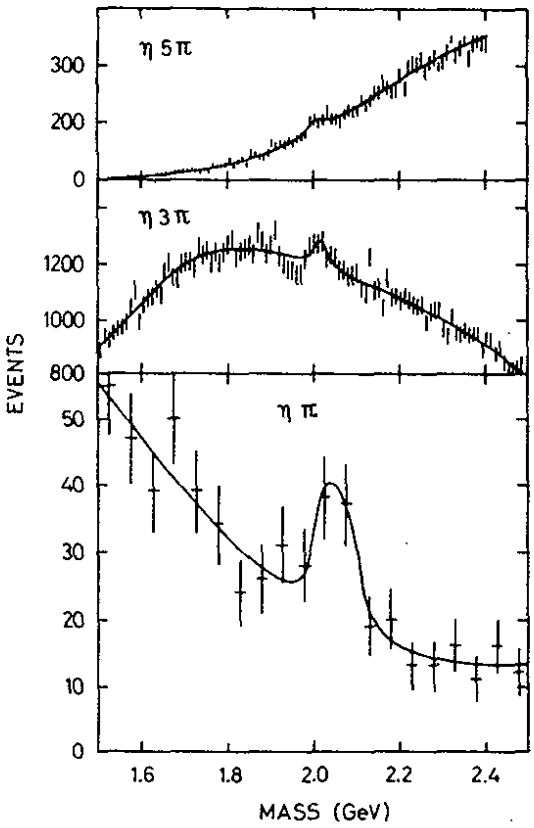

Fig. 40
Mass spectra of photoproduced η + nπ final states measured by the WA4 Collaboration at CERN.

Three F candidate events are found in the emulsion data[106]. The observed decay modes and mass values in MeV/c^2 are:

$\pi^-\pi^+\pi^-\pi^o$ (2026 ± 56)
$K^+\pi^-\pi^+K^o$ (2089 ± 121) and
$\pi^+\pi^+\pi^-\pi^o$ (2017 ± 25).

The mass values observed in the new experiments are consistent with the values reported by the DASP Collaboration.

6.

STATES WITH OPEN BEAUTY

The large width of the T(4S) compared to the width of the adjacent T(3S) state shows that lightest B meson must have a mass 5.18 GeV < m_B < 5.28 GeV using the DORIS energy scale. A search[82] by the CUSB Collaboration for monochromatic photon lines which may occur in the decay

$B^* \to \gamma B$ lead to a negative result. It is therefore likely that the T(4S) cannot decay into B^*B^* or BB^*. This fact and the observed width of the T(4S)leads to an estimated[26] mass m_B=5.27 ± 0.01 GeV.

In the standard Kobayashi-Maskawa[111] model the b quark is the partner of a charge 2/3 quark in a weak doublet. In this model the b quark is expected to decay semileptonically with a branching ratio $B(b \to e\,\bar{\nu}_e\ \text{hadrons}) = B(b \to \mu\bar{\nu}_\mu\ \text{hadrons}) \approx 17\%$. Furthermore the b quark decays via a flavour cascade $b \to c \to s$ leading to a strong increase in the kaon yield above $b\bar{b}$ threshold.

This model predicts that on the average (2.4 ± 0.5 ± 0.5) kaons (charged and neutral) are produced per B decay.

The production of a new quark with a flavour respected by the strong and the electromagnetic interaction will lead to step in the cross section for mixed lepton hadron events at bb threshold. The CUSB[82] and the CLEO[83] Collaborations have measured the yield of mixed electron hadron events in the vicinity of the T(4S) resonance. The data are plotted in Figs. 41 and 42 and as a function of c.m. energy. Both experiments only accept electrons with momenta above 1 GeV/c. This cut strongly reduces the number of events resulting from charm production whereas 2/3 of the B decays survive. Both experiments show a strong increase in the inclusive electron yield at the T(4S) state. CUSB finds that the observed rate is consistent with a branching ratio $B(B \to e\nu_e X)$ between

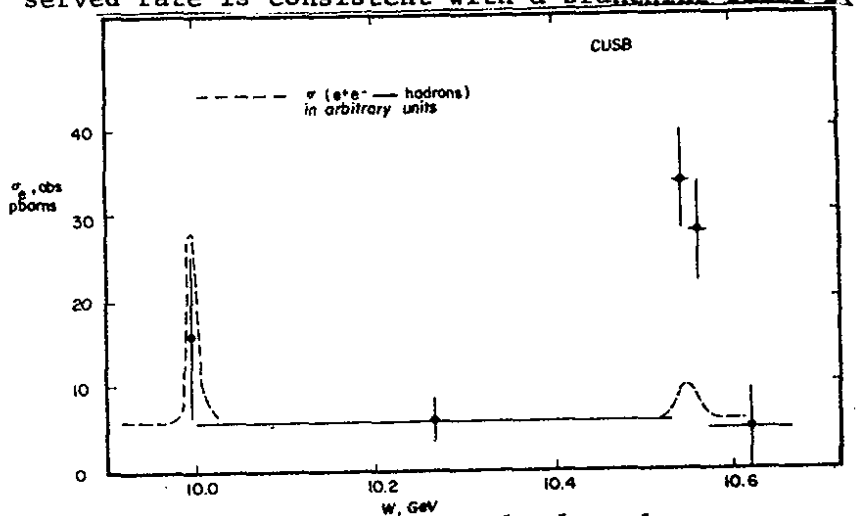

Fig. 41 The observed cross section for $e^+e^- \to e\,\nu_e$ hadrons measured by the CUSB Collaboration plotted versus c.m. energy. The total cross section in arbitrary units is shown as the dotted curve.

arbitrary units is shown as the dotted curve.

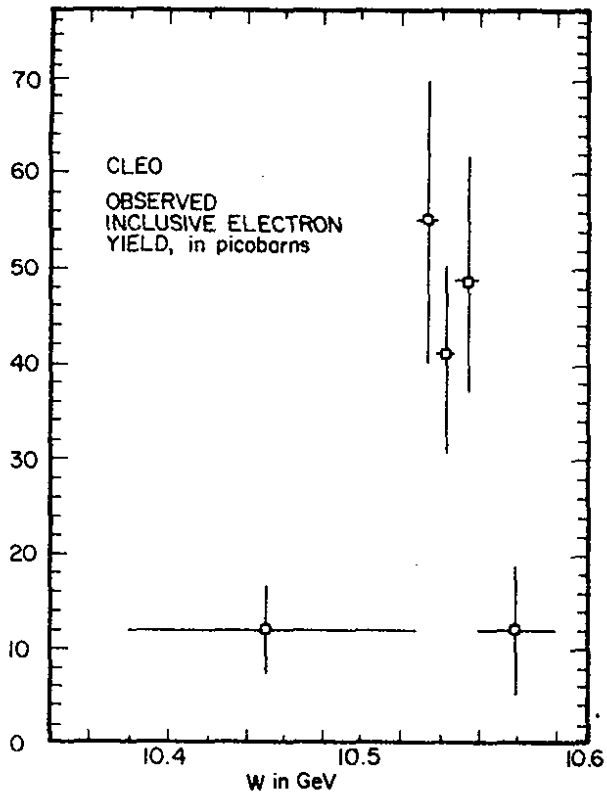

Fig. 42a
The observed cross section for $e^+e^- \to e^\pm$ + hadrons plotted versus c.m. energy. The data were obtained by the CLEO Collaboration.

10% and 20%. CLEO finds $B(B \to e\, \nu_e\, X) = (13 \pm 3 \pm 3)\%$. The CLEO Collaboration has also measured the yield of mixed muon hadron events. The results plotted in Fig.42b versus energy show a strong peak of the T(4S) corresponding to $B(B \to \mu \nu_\mu X) = 9.4 \pm 3.6$.

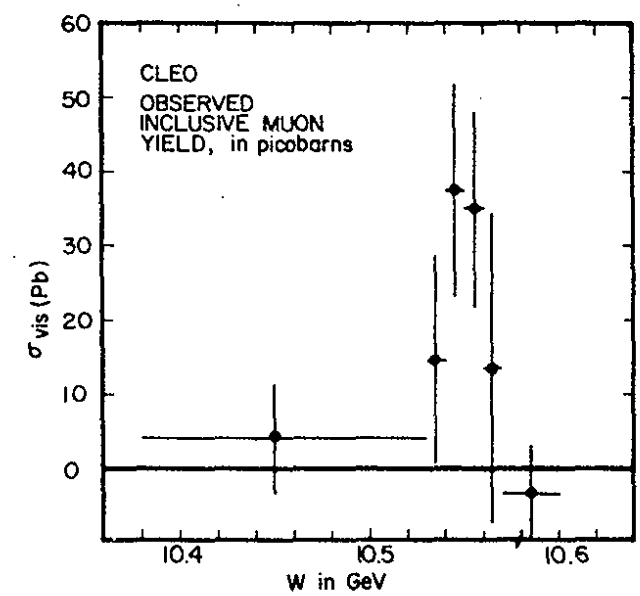

Fig. 42b
The observed cross section for $e^+e^- \to \mu^\pm$ + hadrons plotted versus c.m. energy. The data were obtained by the CLEO Collaboration.

The inclusive lepton-hadron data show conclusively that the T(4S) state is indeed decaying mainly into hadrons with a new flavour.

The K/π ratio for momenta between 0.6 GeV and 1.0 GeV/c has been measured[83] by the CLEO Collaboration for c.m. energies in the vicinity of the T(4S) state. The data, plotted in Fig. 43 show a clear 4 standard deviation peak for energies at the resonance. A total of $0.40 \pm 0.09 \pm 0.02$ charged kaons per event is observed in the peak compared to $0.06 \pm 0.01 \pm 0.01$ kaons per event observed in the continuum. The peak value should be compared to 0.22 ± 0.08 charged kaons per event predicted assuming $b \to W\bar{c}$ and 0.06 ± 0.01 charged kaons per event predicted for $b \to W\bar{u}$..

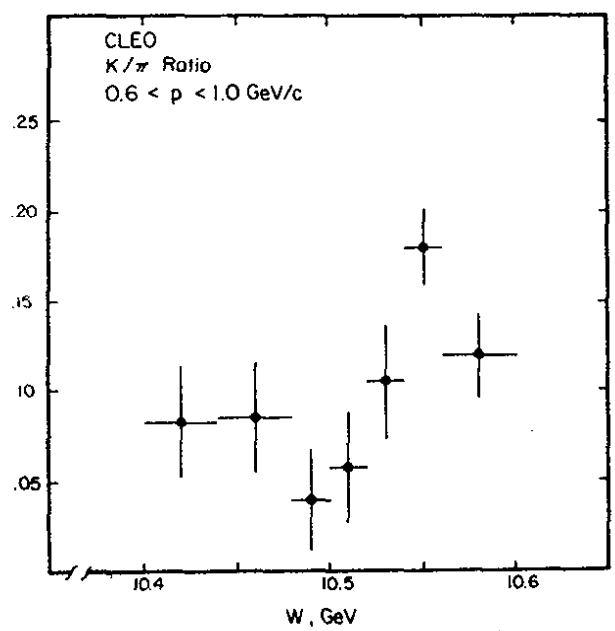

Fig. 43
The K/π ratio as measured by the CLEO Collaboration plotted versus s c.m. energy.

The data available on the decay of the B mesons favour the conventional model and rule out most of non standard model. It is indeed very likely that the t quark does exist.

7.

HADRON PRODUCTION IN e^+e^- ANNIHILATION AT HIGH ENERGIES

It has been conjectured[27-30] in the naive parton model that hadron production in e^+e^- annihilation proceeds by quark-antiquark pair production as shown in Fig. 44, where the electromagnetic current couples

Directly to the charge of a pointlike quark. The neutral weak current is expected to contribute on the order of 1% to the total cross

e^+e^- COLLIDING BEAM EXPERIMENTS

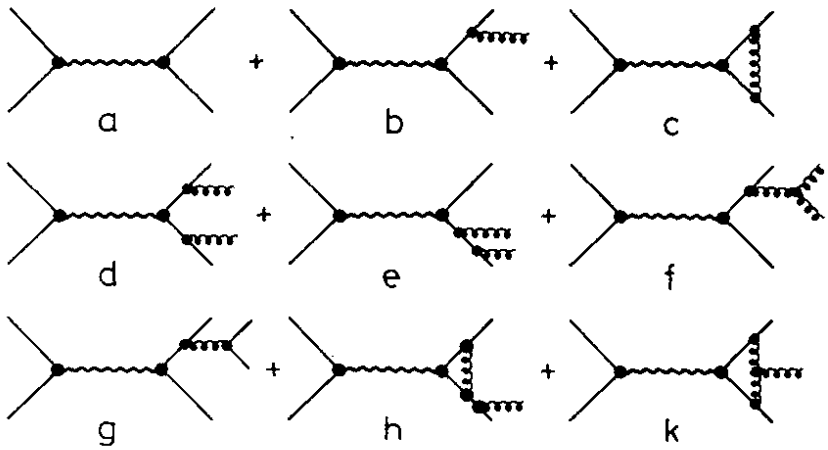

Fig. 44
Some of the diagrams for hadron production in e^+e^- annihilation up to second order in α_s.

section at s = 1000 GeV^2 energies and is neglected. The total cross section for hadron production in this approximation should therefore be proportional to the cross section for muon pair production with the constant of proportionality:

$$R = 3 \Sigma e_i^2 \quad . \tag{25}$$

where e_i is the charge of the ith flavour and the sum is over all flavours with masses less then the beam energy. The hadrons should appear in two nearly collinear jets with small and maybe constant momenta transverse and large and growing momenta parallel to the jet axes. The single particle distribution should scale i.e. s $d\sigma/dx$ with $x = E_h/E_{beam}$ should become independent of energy at large energies. The charged particle multiplicity would be expected to increase logarithmically with s = $(2E)^2$. The data[31] from SPEAR and DORIS at lower energies support the gross features of this picture.

This naive parton picture will be modified in any field theory[32] of strong interactions. In a field theory e^+e^- annihilation proceeds to lowest order by the Feynman graphs shown in Fig. 44b, c. The produced quark radiate field quanta (gluons) and the gluons are expected to materialize as hadron jets in the final state.

This has well defined experimental implications[32,112]: The mean transverse momentum of the hadrons with respect to the jet axis will increase with energy. If the quark-gluon coupling constant is small only one of the two original jets will broaden. A primordial $q\bar{q}g$ state is necessarily planar and the final hadron configuration should retain the planarity. In a small fraction of the events the gluon may be radiated

at an angle which is large compared to the angular spread of the hadron jet. Such events will be very striking with three visible jets of hadrons defining a plane. Higher order multiple gluon emission diagrams (Fig. 44 d-f) are expected to become more visible at high energies since the angular spread of the hadrons resulting from the non-perturbative fragmentation of a single quark or gluon decreases rapidly with energy, enabling one to pick out at higher energies jets from gluons radiated at smaller angles relative to the primordial q and $\bar{q}$ directions. Such multijet events are of course not planar in general and will lead to an increase of the momentum transverse to the event plane. A field theory of the strong interactions will also modify the value for R given above, the multiplicity will grow faster than ln s and the single particle distribution will no longer scale[32].

At present quantum chromodynamics (QCD)[24] is the leading candidate for a theory of strong interactions. The coupling strength in this theory depends on a characteristic strong interaction mass Λ and a typical momentum transfer q in the process. The functional form is given by:

$$\alpha_s(q^2) = g^2/4\pi = \frac{12\pi}{(33-2N_f)\ \ln(q^2/\Lambda^2)} \qquad (26)$$

where N_f is the number of flavours with mass below threshold.

Although the exact value of Λ is still a subject of some controversy it is presumably rather small, on the order of one to a few hundred MeV.

Here I will first discuss the gross properties of the final state, then summarize the evidence for gluon bremsstrahlung and finally discuss the properties of the gluon in some detail.

8.

GENERAL PROPERTIES OF THE FINAL STATE IN e^+e^- → HADRONS

The basic diagrams (Fig. 44) governing e^+e^- → qq(g) → hadrons are very simple. The properties of the hadrons in the final state can therefore be directly related to the properties of quarks and gluons and their fragmentation into hadrons.

e^+e^- COLLIDING BEAM EXPERIMENTS

8.1 Thrust and sphericity distributions

Two methods to determine the jet axis, sphericity[29] and thrust[113] are in general use:

Sphericity S is defined as:
$$S = \frac{3}{2} \min \frac{\sum_i (p_T^i)^2}{\sum_i (p^i)^2} \qquad (27)$$

Here p^i is the momentum and p_T^i the transverse momentum of a track with respect to a given axis. The jet axis is defined as the axis which minimizes transverse momentum squared. Sphericity measures the square of δ, the jet cone opening angle. $S = 3/2 \langle\delta^2\rangle$ and is 0 for a perfect jet and 1 for a spherical event.

Thrust T is defined as:
$$T = \max \frac{\sum_i |p_\parallel^i|}{\sum_i |p^i|} \qquad (28)$$

Here p^i is the momentum of a track and $p_\parallel^i$ its projection along a given axis. The jet axis is defined as the axis which maximizes the directed momentum. Expressed in terms of δ, $T \underset{\sim}{>} (1-\langle\delta\rangle^2)^{1/2}$ and it will approach 1 for a perfect jet event and 1/2 for an isotropic event.

The deviation between the true jet axis and the axis found by either the sphericity or the thrust method has been determined from a Monte Carlo calculation. This calculation shows that the jet axis is determined to 5° or better nearly independent of method for c.m. energies above 20 GeV in c.m.

The energy dependences of the average sphericity $\langle S\rangle$ and $(1 - \langle T\rangle)$, where $\langle T\rangle$ is the average thrust are plotted versus c.m. energy together with data obtained at lower energies in Figs. 45 and 46.

Both quantities decrease with increasing energies as expected if the jets become more collimated with increasing energies. The jet cone half opening angle, as indicated from the sphericity distribution, shrinks from about 31° at 4 GeV in c.m. to 17° near 36 GeV. However, this decrease is slower than that expected in a pure $e^+e^- \to q\bar{q}$ model. The observed decrease is in agreement with computations including gluon bremsstrahlung. Note that the distributions are smooth indicating the absence of thresholds in the energy range above the $b\bar{b}$ threshold.

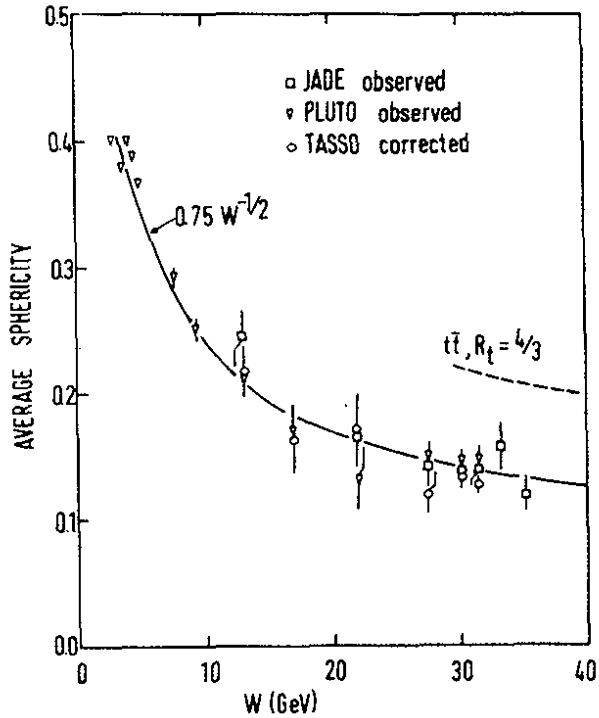

Fig. 45
The average sphericity plotted as a function of c.m. energy.

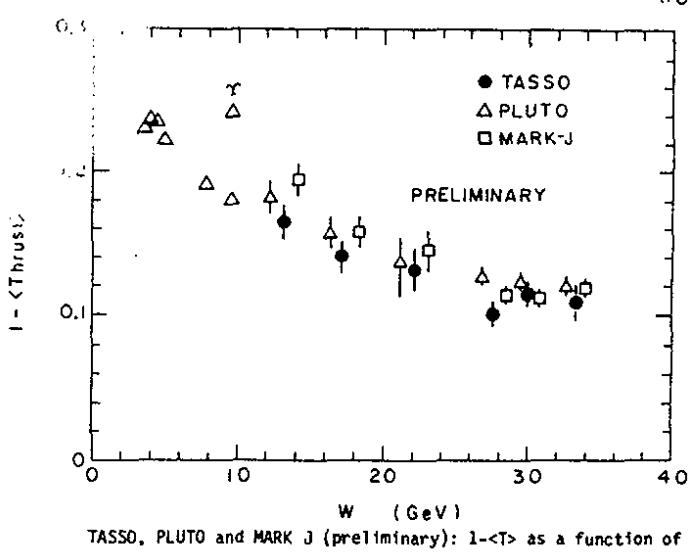

TASSO, PLUTO and MARK J (preliminary): 1-<T> as a function of energy

Fig. 46
The average of 1 - T plotted as a function of c.m. energy.

8.2 The total cross section

R, the total hadronic e^+e^- annihilation cross section in units of the point cross section can be written[114] in the first order QCD as:

$$R = 3 \Sigma e_i^2 \left(1 + \alpha_s/\pi \right) \qquad (29)$$

where α_s is the running coupling constant defined in Eq. 26.

The PETRA groups report[41] data on R for center of mass energies between 12 GeV and 36.5 GeV. The data, corrected for radiative effects including the vacuum polarization, and with the contribution from τ pair

production removed, are plotted versus c.m. energy in Fig. 47 together with data obtained at lower energies[115].

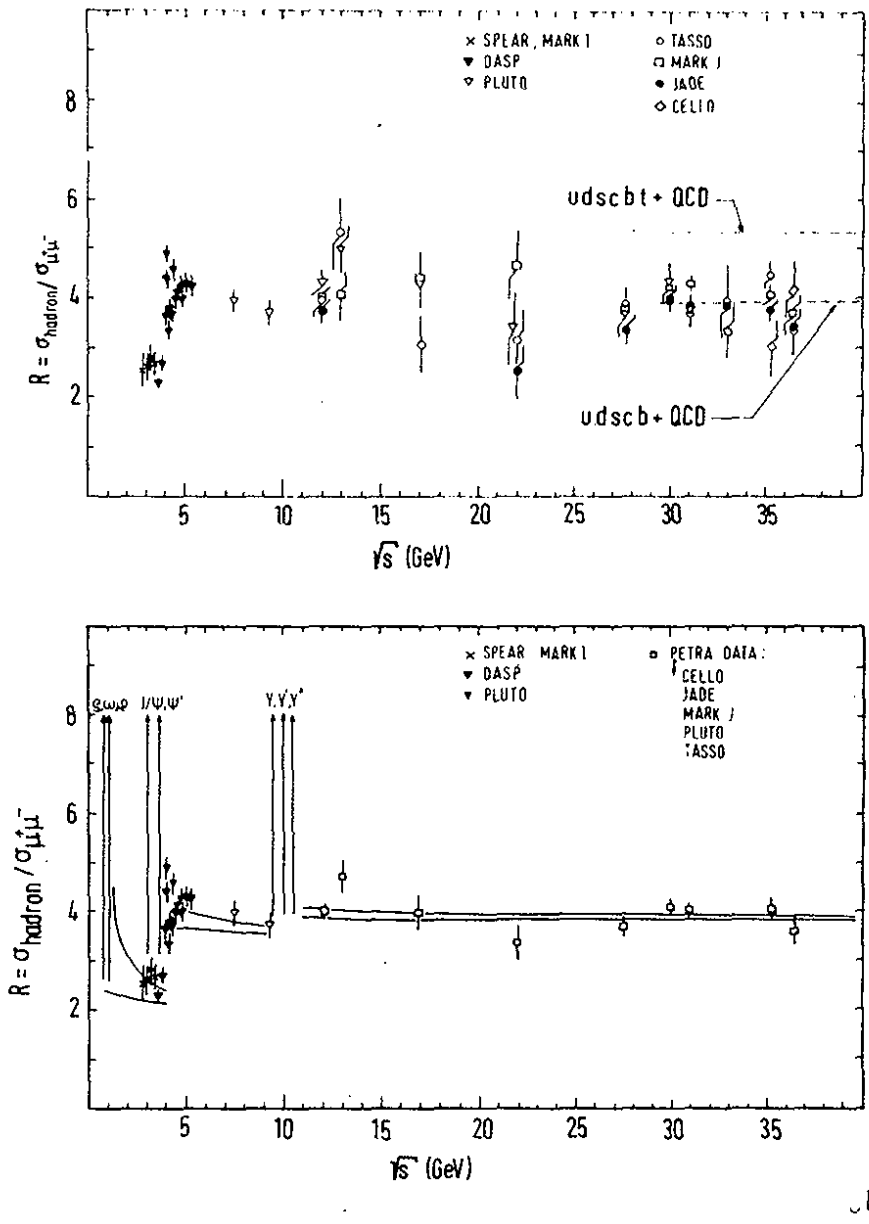

Fig. 47

a) The ratio R of the total hadronic cross section normalized to the muon pair cross section is plotted as a function of c.m. energy.

b) The value of R obtained by averaging the data of all the PETRA groups. The solid line represents two QCD predictions with Λ = 1.0 GeV (upper curve) and Λ = 0.1 GeV (lower curve).

The MARK I Collaboration has measured[116] R for c.m. energies between 5.5 GeV and 7.5 GeV with good statistics and an estimaed systematic uncertainty of 10%. A careful comparison[117] of these data with QCD shows that the experimental values are on the average 16% above the theoretical QCD prediction.

In some respects a measurement of the total cross section is easier at high than at low energies. A comparison between data and theory might therefore be more significant at high energies although the effects are smaller.

At $s = 1000\ GeV^2$, α_s/π is of the order of 5% yielding $R \simeq 3.9$. Higher order terms[114] depend on the renormalization scheme used but they are smaller than the first order term. The QCD prediction, plotted in Fig. 47b, is in agreement with the data.

Are the QCD corrections needed to fit the data ? Clearly not, since the systematic errors are believed to be of the order of 10%. However, note from Fig. 47 that the data which were collected using different trigger conditions and analysed using different cuts are in agreement within the statistical errors. This indicates that the systematic errors may be smaller than 10% and indeed there are good reasons to expect that R can eventually be measured rather well in the PETRA energy range.

It is therefore tempting to add the data from the various groups and the resulting cross section is plotted in Fig. 47. The solid lines are QCD predictions corresponding to $\Lambda = 1.0$ GeV and 0.1 GeV respectively. Averaging all the data above 20 GeV in c.m. yields $R = 3.97 \pm 0.06$. An error of 0.16 was computed from the fluctuations of the individual measurements. First order QCD at $s = 1000\ GeV^2$ predicts $R = 3.87$ for $\Lambda = 100$ MeV or $R = 3.94$ for $\Lambda = 500$ MeV.

8.3 The neutral energy fraction

The JADE Collaboration has determined[118] the fraction of the total energy converted into photons by a direct measurement of the photon energy deposited in lead glass counters surrounding the detector. They have also determined the total neutral energy fraction by measuring the energy carried away by charged particles and subtracting this from the known c.m. energy. The results, listed in Table 11, show that the neutral energy fraction, which includes K_s^o and Λ's, increases with energy.

Also the energy fraction carried off by photons seems to increase. However, in this case the errors are rather larger.

Table 11 - Energy fraction carried off by photons and by neutral particles

$\sqrt{s}$ (GeV)	Energy fraction carried off by Photons %	Neutral particles %
12	21.3 ± 7.0	31.2 ± 4.1
30.4	26.1 ± 5.9	37.5 ± 3.7
34.9	30.7 ± 6.0	43.8 ± 4.1

8.4 Charged multiplicities

The average charged multiplicity $\langle n_{ch} \rangle$ observed at high energies[119-121] is plotted in Fig. 48 together with data obtained at lower energies[122].

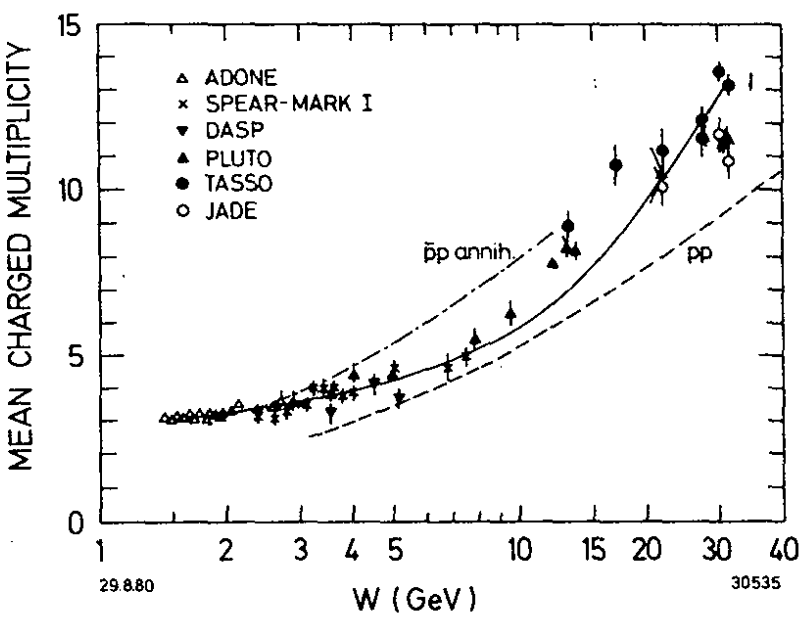

Fig. 48 Average charged particles multiplicity versus the c.m. energy. The solid line is a combined fit to the low energy data and the TASSO data at high energies.

The high energy data points from the various groups are in reasonable agreement and are well above the multiplicities obtained by extrapolating the lower energy data according to a + b ln s as predicted by the naive quark-parton model. For comparison, the multiplicities observed in pp[123] and $p\bar{p}$[124] are also shown.

The average multiplicity in QCD may[125,126] increase as $n = n_o + a \exp(b\sqrt{\ln s/\Lambda^2})$, and the data can indeed be fitted over the whole

energy range using this form. The values of the parameters obtained by fitting the TASSO and the PLUTO data are listed in Table 12. The fit considers only the statistical errors and the results were obtained assuming Λ = 0.5 GeV/c.

Table 12 - Fits to the charged particle multiplicity

Group	n_o	a	b
TASSO	2.92 ± 0.04	2.85 ± 0.07	0.0029 ± 0.0005
PLUTO	2.38 ± 0.09	1.92 ± 0.07	0.04 ± 0.01

The asymptotic value[126] of a = 2.4 in QCD. However, note that the fragmentation of the gluon in three jet events is expected to increase the average multiplicity by less than one unit at the highest energy.

8.5 Inclusive particle spectra

The scaled cross sections s dσ/dx for inclusive charged particle production as determined by DASP[122], SLAC-LBL[127] and TASSO[118,128] for c.m. energies between 5 GeV and 36.6 GeV are plotted in Fig. 49 versus x.

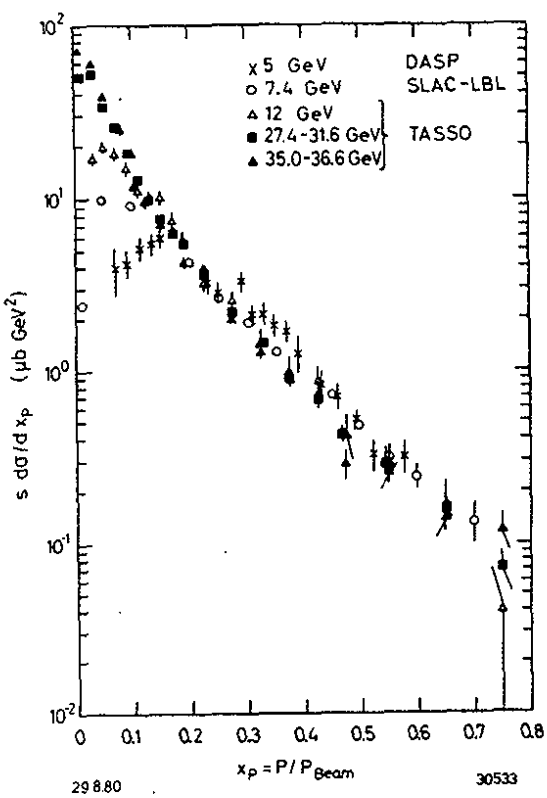

Fig. 49
The scaled cross section s dσ/dx ($x = p/p_{beam}$) for inclusive charged particle production.

e^+e^- COLLIDING BEAM EXPERIMENTS

The cross section for x > 0.2 scales to within 30% between 5 GeV and 36.6 GeV. For x < 0.2 the cross section increases dramatically with energy and shows that the observed increase in multiplicity is due to slow particles. Gluon emission will lead[32] to a depletion of particles at large x and a corresponding increase in the yield at small x, since the energy is now shared between the quark and the gluon. In QCD these are rather small effects except at very large or very small x. In general the effects are only of the order of 10 - 20% at PETRA energies since q^2 is very large compared to Λ^2.

During the past year the PETRA experiments have succeeded in identifying hadrons over a considerable range in momentum. The available data[118] are summarized in Table 13.

Table 13 - Experiments measuring particle separated cross section

Type of particle	Experiment	Technique	Momentum range (GeV/c)	Remark
$\pi^\pm$	JADE	dE/dx [118]	< 0.7, 2-7	preliminary
	TASSO	TOF[129]	< 1.1	
		Cerenkov[118]	< 5.0	preliminary
$K^\pm$	JADE	dE/dx [118]	< 0.7	preliminary
	TASSO	TOF[129]	< 1.1	
		Cerenkov[118]	< 5.0	preliminary
$K^o, \bar{K}^o$	PLUTO	$K^o_s \to \pi^+\pi^-$ [118]	all p	preliminary
	TASSO	$K^o_s \to \pi^+\pi^-$ [118]	all p	
p, $\bar{p}$	JADE	dE/dx [118]	< 0.9	preliminary
	TASSO	TOF[129]	< 2.2	
		Cerenkov[118]	< 4.0	

The scaled cross section $s/\beta\, d\sigma/dx$ for charged pions is plotted in Fig. 50 versus x. The TASSO and the JADE data[118, 129] are in agreement and seem to fall below the DASP 5.2 GeV data[116, 129].

The data [118,129,130] for neutral and charged kaons measured by TASSO and PLUTO at high energies and by the MARK I Collaboration[131] at lower energies are plotted versus x in Fig. 51. The data are in

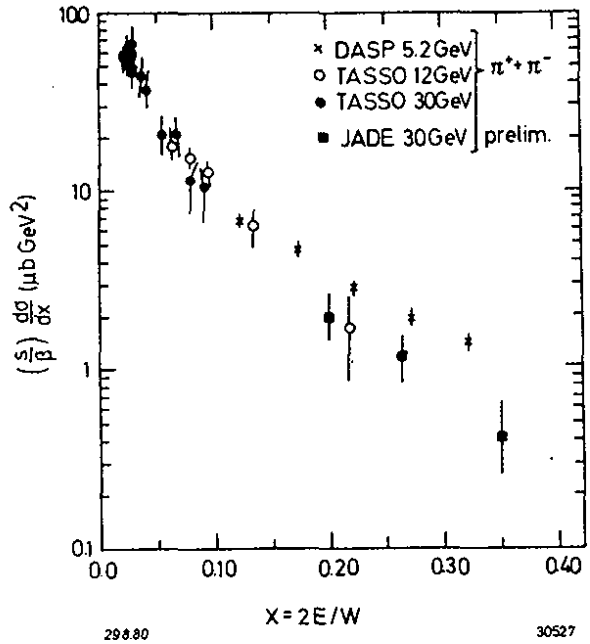

Fig. 50
The scaled cross section s/β dσ/dx for charged pions.

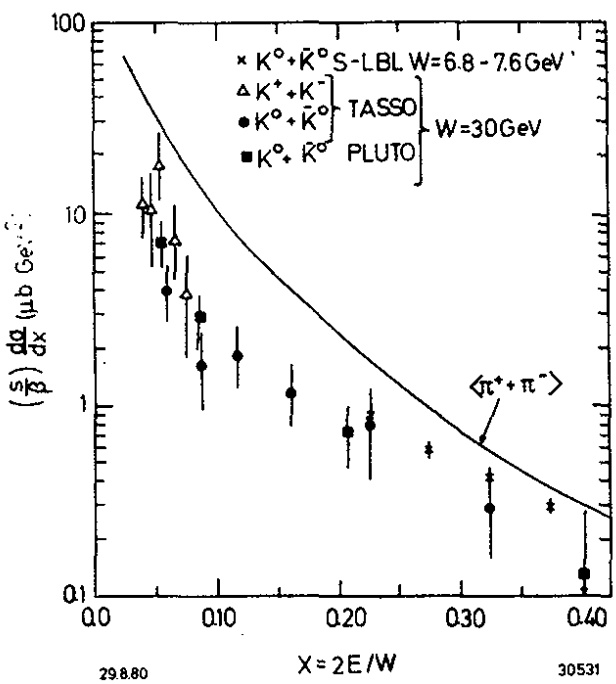

Fig. 51
The scaled cross section sβ dσ/dx for neutral and charged kaons. The average pion cross section is shown as the solid curve.

general agreement, and in particular the cross sections for charged and neutral kaon production are similar. The average value for charged pion production is shown as the solid line. The kaon cross section is a factor of 2 to 4 below the pion cross section at low x but seem to approach the pion data at large x.

The proton data[118,129] are plotted in Fig. 52 and compared to the charged pion data represented by the solid lines. Within the rather large error bars the cross section for kaon and proton production are si-

milar. The large p, $\bar{p}$ cross section seems surprising.

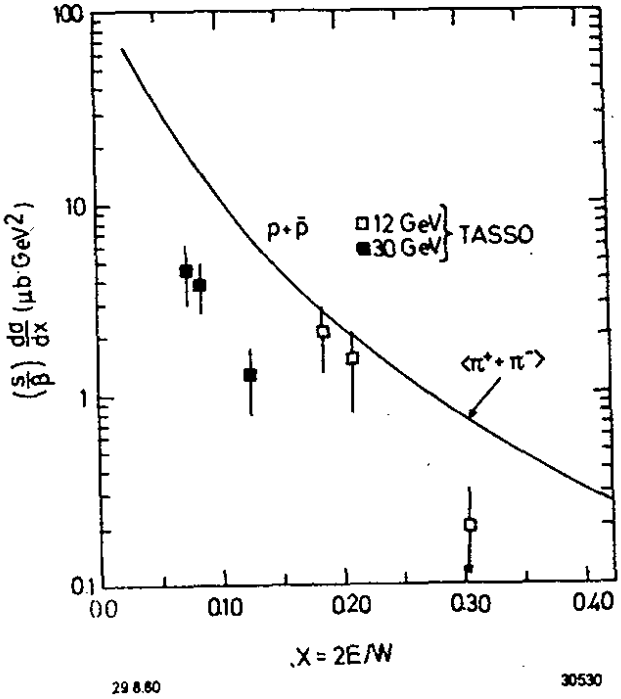

Fig. 52
The scaled cross section $s/\beta d\sigma/dx$ for protons. The average charged pion cross section is shown as the solid curve.

The relative fractions of charged pions, kaons and protons observed at 30 GeV in c.m. are plotted in Fig. 53 as a function of particle momentum. At low momenta nearly all the particles are pions, however, the kaon and the proton yield rises rapidly with momentum such that at a momentum of 3.0 GeV/c the ratio of

$$\pi^{\pm} \text{ to } K^{\pm} \text{ to } p^{\pm} \quad \text{is roughly} \quad 55 \text{ to } 35 \text{ to } 10.$$

An average event at a center of mass energy of 30 GeV consists of roughly $10\pi^{\pm}$, 1.4 $K^0\bar{K}^0$ and 0.4 $p\bar{p}$ i.e. about one out of 5 events has a p, $\bar{p}$ pair in the final state.

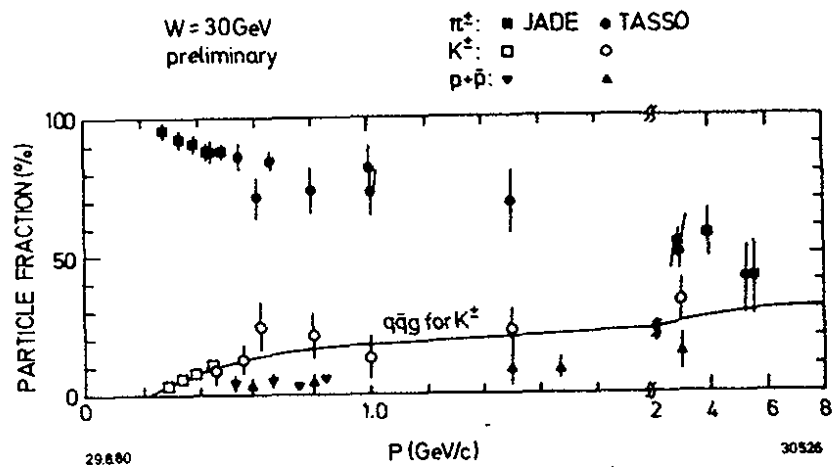

Fig. 53
The relative fraction of charged pions, kaons and protons observed at 30 GeV in c.m.

8.6 Charge correlations

The back to back produced quarks have opposite charge. According to the standard picture they will fragment into hadrons by a neutral quark-gluon cascade conserving the initial charge. Therefore, apart from fluctuations, the charge found in one jet should be correlated[132] with the charge of the other jet. Furthermore one expects this long range correlation to be found among the fast particles and that the slow particles should exhibit short range correlation only. The TASSO group reports[133] the first evidence for long range correlation.

To investigate the charge correlations they evaluate the function

$$\bar{\Phi}(y, y') = - \frac{1}{\Delta y \Delta y'} \langle 1/n \sum_{k=1}^{n} \sum_{i \neq k} e_i(y)\, e_k(y') \rangle \qquad (30)$$

In this expression $e_i(y)$ is the charge of a particle i at rapidity y in the interval Δy and $e_k(y')$ is the charge of a particle k at a rapidity y' in the interval $\Delta y'$. The rapidity is defined as

$$y = \frac{1}{2} \ln \left(\frac{(E + p_{\parallel})}{(E - p_{\parallel})} \right) \qquad (31)$$

where $p_{\parallel}$ is the particle momentum along the jet axis. The function $\bar{\phi}(y,y')$ is related to the probability that the particles i and k have opposite sign charges minus the probability that the charges have the same sign. Since the event as a whole is neutral the function $\bar{\phi}(y,y')$ simply shows how the charge of particle i at a rapidity y is being compensated. The normalization is choosen such that $\int \bar{\phi}(y,y')dy' = 1$. In Fig.54a, the ratio $\phi(y,y') = \bar{\phi}(y,y')/ \bar{\phi}(y,y')dy$ is plotted versus y with the test particle in the rapidity interval $-0.75 \leq y' < 0$, i.e. a slow particle. This distribution peaks at small negative values of y and shows that the charge of a slow particle is indeed compensated locally as expected if only short range correlations are present. The observed peak has an rms width of 1.3.

In Fig.54b the same quantity is plotted as a function of y for the test particle at $-5 \leq y' \leq -2.5$. Although the bulk of the charge is compensated locally there is now a significant signal at the opposite end of the rapidity plot. Integrating the distribution for $y > 2.5$ yields 0.101 ± 0.033 compared to the 0.011 ± 0.014 found for the test

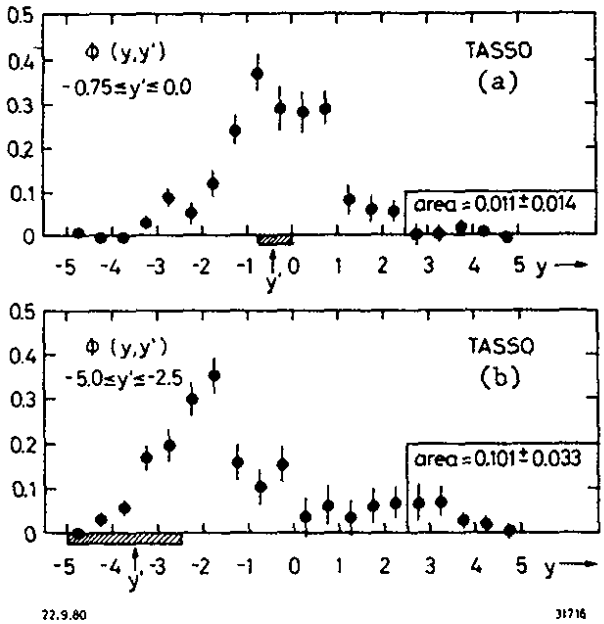

Fig. 54
The charge compensation function Φ(y, y') with the test particle a) at $-0.75 \leq y' \leq 0$ and b) at $-5.0 \leq y' \leq -2.5$.

particle at $-0.75 \leq y' \leq 0$. There is therefore a clear signature for a long range correlation extending over some seven units in rapidity.

It is interesting to compare the charge correlation to the particle density distribution defined by:

$$\bar{\rho}(y,y') = \frac{1}{\Delta y \Delta y'} \quad \frac{1}{n(n-1)} \sum_{k=1}^{n} \sum_{i \neq k} \langle |e_i(y)| |e_k(y')| \rangle \qquad (32)$$

The quantity $\rho(y,y') = \bar{\rho}(y,y') / \int \bar{\rho}(y,y')\, dy$ with $\iint \bar{\rho}(y,y')\, dydy' = 1$ is the probability to find a charged particle with rapidity y if there is another charged particle with rapidity y'. This particle density function is plotted in Fig. 55a and b for the test particle at $-0.75 \leq y' \leq 0$ and at $-5 \leq y' \leq -2.5$. Comparing Figs. 54 and 55 shows that the particle density function is wider than the charge correlation function – i.e. unlike sign particles are on the average closer in ra-

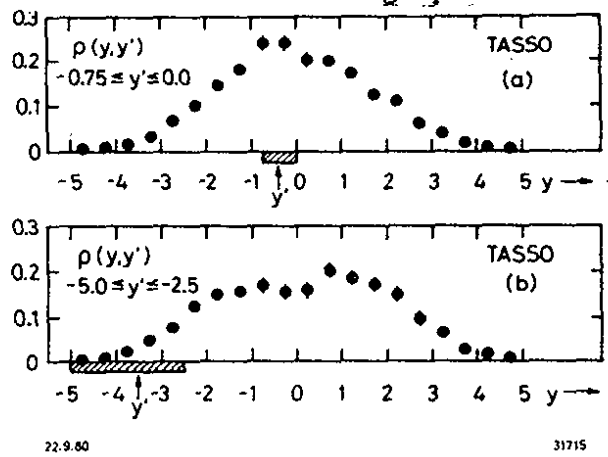

Fig. 55
The particle density function ρ with the test particle a) at $-0.75 \leq y' \leq 0$ and b) at $-5.0 \leq y' \leq -2.5$.

pidity than like sign particles.

The particle density function with the test particles at $-5 \leq y' \leq -2.5$ is rather smooth with no sign of long range correlations.

The correlation functions contain information on the primordial quarks and are more sensitive tests of the fragmentation process than the single particle distributions.

9.
EVENT TOPOLOGY AND THE FINAL STATE ANALYSIS

The topology of the hadrons in e^+e^- annihilation can be used to identify the production mechanism

a) Pair production of light quarks with only collinear gluon bremsstrahlung will manifest itself as two collinear jets of hadrons.

b) Single wide angle gluon bremsstrahlung $e^+e^- \rightarrow q\bar{q}g$ leads to planar events with large and growing momenta in the plane and small and limited momenta transverse to the plane. Multiple gluon bremsstrahlung will lead to more isotropic events.

c) Pair production of heavy quarks will yield nearly spherical events close to threshold.

In the next paragraphs we briefly describe the Monte Carlo simulations and the methods used to determine the topology of the hadrons in the final state.

9.1 Inputs to the Monte Carlo simulation

All groups have made extensive Monte Carlo computations to confront the various production mechanisms with the data. The inputs to these calculation are summarized below:

a) Quark pairs are pair-produced proportional to e_i^2. Light quark pairs are created from the vacuum in the ratio $u\bar{u} : d\bar{d} : s\bar{s} = 2 : 2 : 1$.

b) The basic gluon bremsstrahlung process (Fig. 44) is treated to first order in the strong coupling constant α_s by Hoyer et al.[134] whereas the computation by Ali et al.[135] includes all second order diagrams except those with internal gluon lines (Fig. 44h, k).

The formalism of Field and Feynman[136] or the one set up by the Lund group[137] is then used to compute the fragmentation of the constituents.

c) The fragmentation of the quarks is described by 3 parameters in the Field-Feynman model:

i) a_F: The quark fragments $q \to q' + k$ according to a distribution function $f^h(z) = 1 - a_F + 3a_F(1-z)^2$ with $z = (p + E)_h/(p + E)_q \cdot a_F$ is the same for u, d and s quarks and is determined experimentally. For the heavy quarks c and b; $f^h(z)$ = constant.

ii) σ_q: The primordial transverse momentum distribution of the quarks with respect to the jet axis is given by $\exp(-p_T^2/\sigma_q^2)$.

iii) P/(P+V): Only pseudoscalar (π, K ...) and vector mesons (ρ, K ...) are produced; P/V is the ratio of pseudoscalar to vector mesons produced in the primordial cascade.

Field and Feynman found[136] that deep inelastic lepton-hadron reactions and also hadron-hadron interactions can be simultaneously described by the following values of parameters:

$$a_F = 0.77, \quad \sigma_q = 0.30 \text{ GeV/c} \quad \text{and} \quad P/(P+V) = 0.5.$$

d) The fragmentation of gluons is treated as a two-step process in which the gluon first fragments into a $q\bar{q}$ pair which subsequently fragments into hadrons as outlined above. In the Hoyer et al. program[134] the gluon imparts all its energy to one of the quarks - i.e. in this model quark and gluon fragmentation are identical. Ali et al.[135] describe $g \to q\bar{q}$ by the splitting function[137] $f(z) = z^2 + (1-z)^2$ where $z = E_g/E_q$.

9.2 Event topology

The production mechanism can be delineated from the event shape. There are by now several methods used to determine the shape and the topology of an event. Some of these methods are briefly discussed below.

The shape of an event is conveniently evaluated by constructing the second rank tensor[29,31]

$$M_{\alpha\beta} = \sum_{j=1} p_{j\alpha} \cdot p_{j\beta} \quad (\alpha, \beta = x, y, z) \tag{33}$$

where $p_{j\alpha}$ and $p_{j\beta}$ are momentum components along the α and β axes for the jth particle in the event. The sum is over all charged particles in the event. Let $\vec{n}_1$, $\vec{n}_2$, $\vec{n}_3$ be the unit eigenvectors of this tensor associated with the normalized eigenvalues Q_i, where $Q_i = \Sigma(\vec{p}_j \cdot \vec{n}_i)^2/\Sigma\vec{p}_j^2$.

These eigenvalues are ordered such that $Q_1 \leq Q_2 \leq Q_3$ and are normalized with $Q_1 + Q_2 + Q_3 = 1$. The principal jet axis is then the $\vec{n}_3$ direction. The event plane is spanned by $\vec{n}_2$ and $\vec{n}_3$; and $\vec{n}_1$ defines the direction in which the sum of the square of the momentum component is minimized. Every event can be represented in a two dimensional plot of aplanarity $A = (3/2)\, Q_1$ (i.e. normalized momentum squared out of the event plane) versus sphericity $S = (3/2)(Q_1 + Q_2)$. In such a plot two jet events will cluster at small values of A and S, planar events have small values of A whereas both A and S will be large for spherical events. This is borne out by the Monte Carlo results shown in Fig. 56 b and c. This method has been used by TASSO[33] and JADE[36].

MARK J[34,139] uses a linear method based on energy flow where the coordinate system is defined as follows: the $\vec{e}_1$ axis coincides with the thrust axis which is defined as the direction of maximum energy flow. They next investigate the energy flow in a plane perpendicular to the thrust axis. The direction of maximum energy flow in that plane defines a direction $\vec{e}_2$ with a normalized energy flow

$$\text{major} = \sum_i |\vec{p}^i \cdot \vec{e}_2| \;/\; E_{vis}, \tag{34}$$

where $E_{vis} = \Sigma|\vec{p}^i|$. The third $\vec{e}_3$ is orthogonal to both the thrust and the major axis $\vec{e}_2$, and it is very close to the minimum of the momentum projection along any axis i.e.

$$\text{minor} = \sum_i |\vec{p}^i \cdot \vec{e}_3| \;/\; E_{vis}. \tag{35}$$

The PLUTO group[140] has developed a two step cluster method to determine the event topology. The first stage associates all particles into preclusters irrespective of their momenta. Particles belong to the same precluster if the angles between any two tracks are less than a limiting angle α. The momentum of a precluster is the sum of the momenta of all the particles assigned to that precluster. The preclusters are then combined to clusters if the angle between the momentum vectors is less than a given value β. The number of clusters n is defined as the minimum number of clusters which fulfil the inequalities:

$$\sum_{i=1}^{n} E_{ci} > E_{vis}\,(1 - \varepsilon) \tag{36}$$

where E_{ci} is the cluster energy and ε a small number. If the energy of a cluster, defined as the sum of the energies of all particles assigned to the cluster, exceeds a threshold energy E_{th} then the cluster is called a jet. Typical values for the various parameters are $\alpha = 30^\circ$, $\beta = 45^\circ$, $\varepsilon = 0.1$ and $E_{th} = 2.0$ GeV.

9.3 Evidence against new quarks

The distribution of events in the A, S plane observed[141] by the TASSO Collaboration at c.m. energies between 27.4 and 36.6 GeV is shown in Fig. 56a. The data cluster at small values of S and A with a long tail of planar events as expected for light quark production including gluon bremsstrahlung as shown in Fig. 56b.

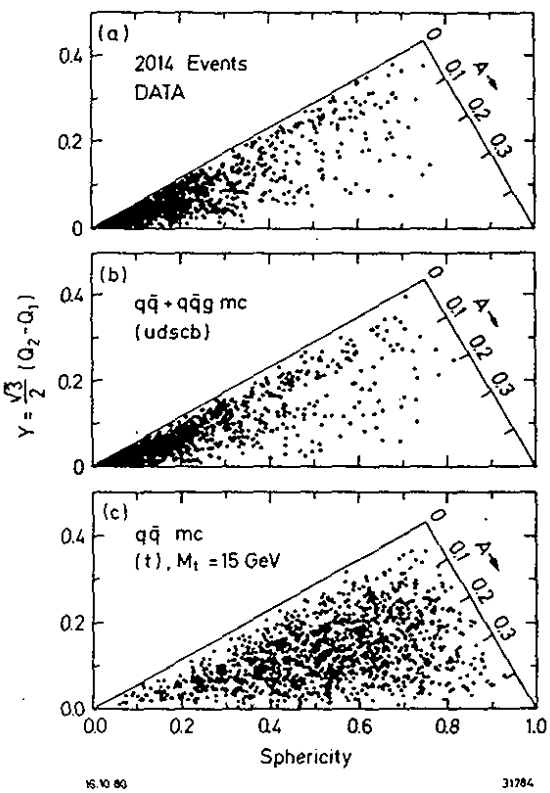

Fig. 56

a) The event distribution in aplanarity and sphericity observed by the TASSO Collaboration between 27.4 GeV and 36.6 GeV in c.m.

Monte Carlo created events in apalanarity and sphericity at 30 GeV in c.m. for

b) $e^+e^- \to q\bar{q}g$ with $q = u, d, s, c, b$.

c) $e^+e^- \to t\bar{t}$ with $m_t = 15$ GeV and a c.m. energy of 35 GeV.

In the data at $35.0 \leq W \leq 36.6$ GeV there are 2 events with A> 0.15, whereas for heavy quark pairproduction we expect a total of 57 events if the quark has a charge of 2/3 and 14 events if the charge is 1/3. Combining these data with similar data[141] from JADE and MARK J excludes a charge 2/3e heavy quark with a mass between the b quark and 18 GeV by some 12 standard deviations. The existence of a charge 1/3 quark is also rather unlikely in the mass range explored at PETRA.

A scan of the cross section in 20 MeV steps did not produce any evidence for narrow peaks. The limit is $\Gamma_{ee} \cdot B_h < 0.4$ keV for c.m. energies between 35.0 and 35.6 GeV. For a charge 2/3e quark or a 1/3e quark we expect to find respectively $\Gamma_{ee} = 5$ keV or 1.3 keV.

10.

GLUONS

At present QCD is the only theory of strong interactions available, and it is obviously crucial to carry out clean experiments which either support or refute this theory. The first step is to demonstrate that field quanta, gluons, indeed do exist. However, this is not sufficient since presumably any field theory of strong interactions contains gluons. To "prove" QCD one must demonstrate that the gluon is a flavour neutral, coloured vector particle with gauge couplings.

10.1 The evidence for gluons

Gluon bremsstrahlung $e^+e^- \to q\bar{q}g$ (see Fig. 44) has well defined experimental signatures.

A) The average transverse momentum of the hadrons with respect to the jet axis will grow with energy. Normalized transverse momentum distributions, measured by TASSO and evaluated with respect to the sphericity axis are plotted in Fig. 57 versus p_T^2 for different c.m. energies. The observed p_T^2 distribution clearly broadens with energy. In QCD the growth is explained as hard non-collinear gluon emission. Fits based on this mechanism are shown in Fig. 57. However, it is also possible to fit the data up to moderate values of p_T^2 by increasing σ_q as a function of c.m. energy.

B) If hard non-collinear gluon emission is a rare process as expected in QCD, then there should usually be only one wide-angle gluon per event: In fact the probability of emitting two gluons in one event compared to single gluon emission is proportional to α_s. Hence only one of the jets should broaden.

To test this prediction the jets in an event are divided into a narrow and a wide jet. The data obtained by PLUTO[35] are shown in Fig. 58. Plotted are $\langle p_T^2 \rangle$ versus $z = p/p_{beam}$ at low and high energies

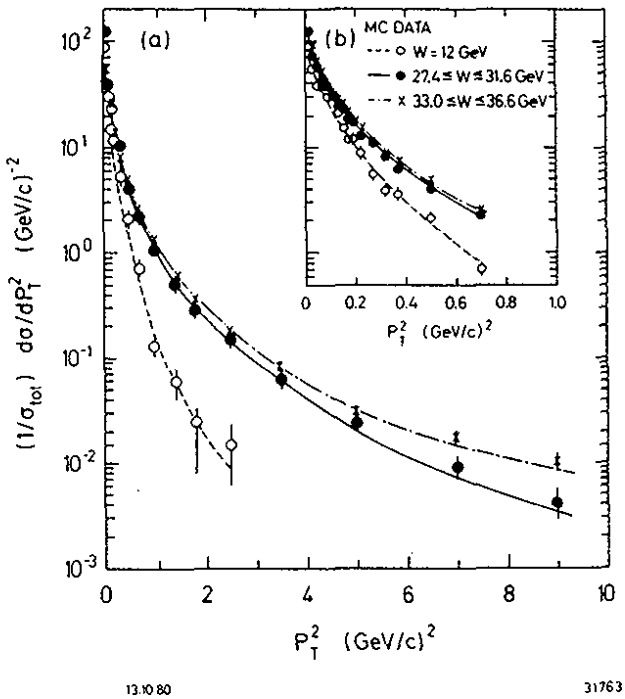

Fig. 57
$1/\sigma\ d\sigma/dp_T^2$ at 12 GeV, 27.4 - 31.6 GeV and 33.0 - 36.6 GeV as a function of p_T^2. The curves are QCD fits to the data with σ_q = 320 MeV/c.

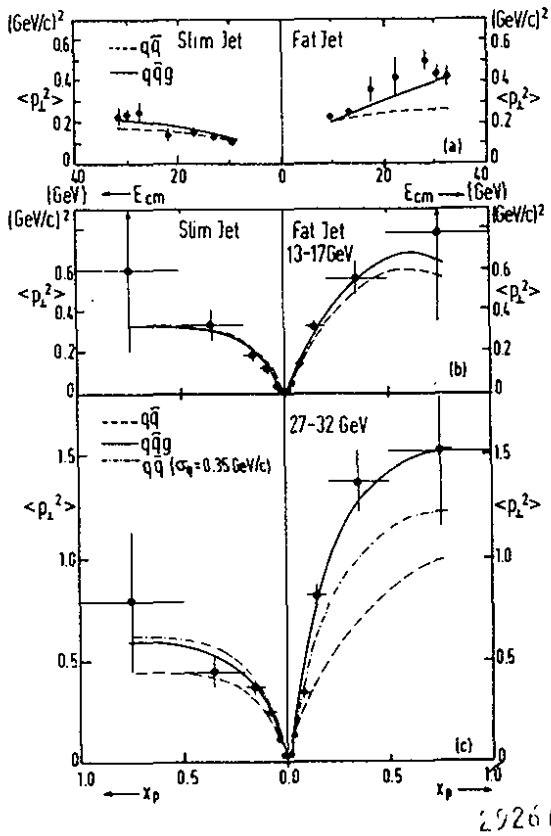

Fig. 58
Data obtained by PLUTO on $<p_T^2>$ as a function of $z = p/p_{beam}$ for wide and narrow jets. The solid and the dashed curves are the $q\bar{q}g$ and $q\bar{q}$ predictions, respectively.

for the wide and the narrow jet separately. A large asymmetry between the two jets is observed at high energies. Unlike the asymmetry observed at low energy the PLUTO group find that this cannot be explained

by fluctuations in the two jet events.

C) Planarity. Regardless of the value of σ_q (or the mean p_T), hdrons resulting from the fragmentation of a quark must on the average be uniformly distributed in azimuthal angle around the quark axis. Therefore, apart from statistical fluctuations, the two jet process $e^+e^- \to q\bar{q}$ will not lead to planar events whereas the radiation of a hard gluon, $e^+e^- \to q\bar{q}g$ will result in an approximately planar configuration of hadrons with large transverse momentum in the plane and small transverse momentum with respect to the plane. Thus the observation of such planar events, at a rate significantly above the rate expected from statistical fluctuations of the $q\bar{q}$ jets, shows in a model independent way that there must be a third confined particle in the final state. The third particle is not a quark since it has baryon number zero and cannot have 1/2 integer spin.

We first compare the distribution of $\langle p_T^2 \rangle_{out}$, the momentum component normal to the event plane squared, with that of $\langle p_T^2 \rangle_{in}$, the momentum component in the event plane perpendicular to the jet axis.

The data obtained by the TASSO group are plotted in Fig. 59 and Fig. 60 for c.m. energies between 12 GeV and 36.6 GeV. The distribution of $\langle p_T^2 \rangle_{out}$ changes little with energy in contrast to the distribution of $\langle p_T^2 \rangle_{in}$ wich grows rapidly with energy,in particular there is a long tail of events not observed at lower energies. Fits to the data assuming $e^+e^- \to q\bar{q}$ and σ_q = 300 MeV/c (solid curves) or σ_q = 450 MeV/c (dotted curves) are also shown. The $\langle p_T^2 \rangle_{out}$ distribution at high energies is not fit by σ_q = 300 MeV/c, however a good fit can be obtained by increasing σ_q to 450 MeV/c. The $q\bar{q}$ model however, completely fails to reproduce the long tail observed in $\langle p_T^2 \rangle_{in}$ at high energies. This discrepancy cannot be removed by increasing the mean transverse momentum of the jet. Fig. 60 shows a fit assuming σ_q = 450 MeV/c (which gives a good fit to $1/\sigma\ d\sigma/dp_t^2$ and to $\langle p_T^2 \rangle_{out}$). The agreement is poor. We therefore conclude that the data include a number of planar events not reproduced by the $q\bar{q}$ model independent of the average p_T assumed.

Gluon bremsstrahlung offers a natural mechanism to explain the observed planarity of the events. Fig. 60 shows a second order QCD fit to the data using the Monte Carlo method outlined above. The fit assumed a constant value of σ_q = 320 MeV and α_s = 0.17 (see below). The long

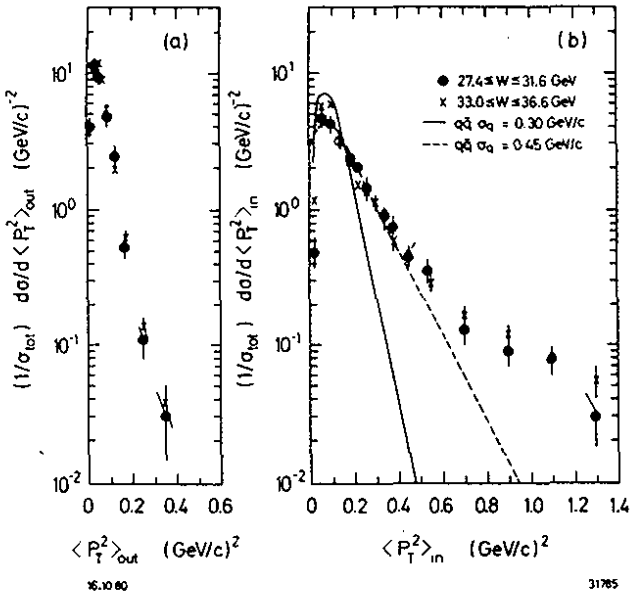

Fig. 59
Distributions of mean transverse momentum squared per event for charged particles, normal to ($\langle p_T^2\rangle_{out}$) and in ($\langle p_T^2\rangle_{in}$) the event plane measured by the TASSO Collaboration at low and high energies. The curves are the predictions for a $q\bar{q}$ final state with σ_q = 300 MeV/c (solid lines) and σ_q = 450 MeV/c (dashed lines).

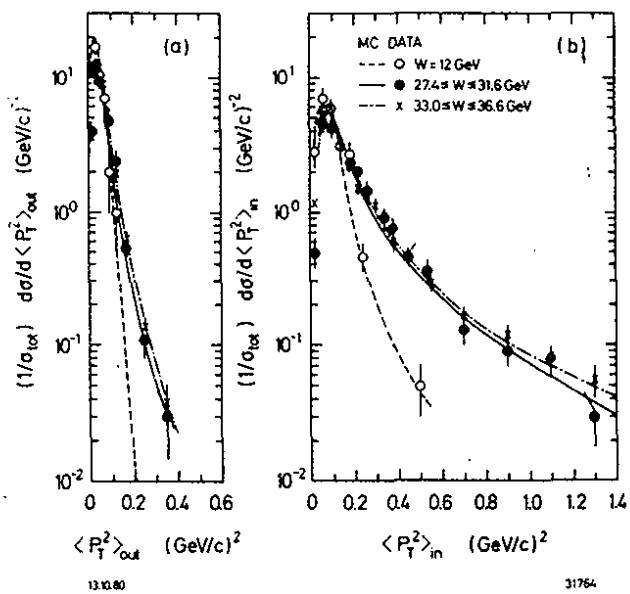

Fig. 60
Same plot as above. The curves are the second order QCD predictions with α_s = 0.17 and σ_q = 320 MeV/c.

tail in $\langle p_T^2\rangle_{in}$ is reproduced in this model. Note that the growth in $\langle p_T^2\rangle_{out}$ is explained by the occurence at small fraction of 4 (or more) jet events which, in general, are not planar.

The data from PLUTO[35] and JADE[36] analyzed in a similar manner are in full agreement with the findings of the TASSO group.

The planarity of the events is also observed[34, 139] by the MARK J group using a different technique. They divided each event into two hemispheres using the plane defined by the major and the minor axis (see above) and analyzed the energy distribution in each hemisphere as if it

were a single jet. The jet with the smallest transverse momentum with respect to the thrust axis is defined as the narrow jet. The other as the broad jet. The oblateness defined as O = Major - Minor is a measure of the planarity of the event and is zero for phase space and two jet events and finite for three jet final states. The normalized event distribution measured for c.m. energies between 27 and 37 GeV is plotted versus oblateness in Fig. 61 for the narrow and the wide jet separately and compared to the predictions for $e^+e^- \to q\bar{q}$ (dashed curve) and $e^+e^- \to q\bar{q}g$ (solid line). A good fit is obtained with the $q\bar{q}g$ final state whereas the $q\bar{q}$ final state do not fit the oblateness distribution for the broad jet.

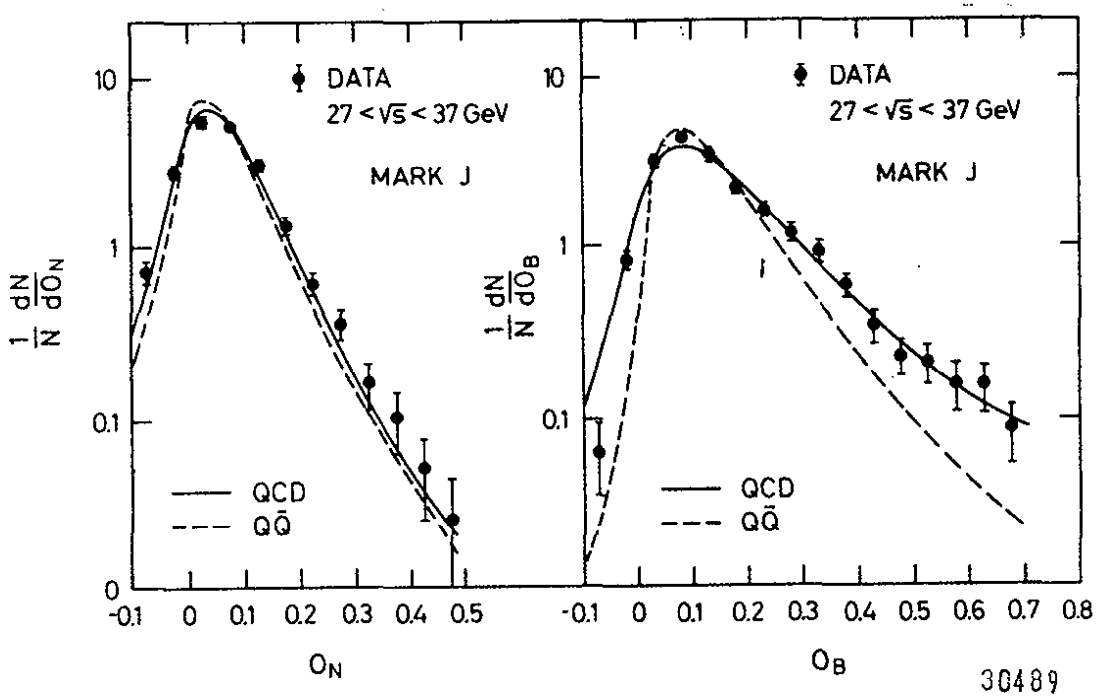

Fig. 61

The distribution 1/N dN/dO determined by the MARK J Collaboration as a function of oblateness O for the narrow and the wide jet separately. The solid curves are predictions based on $e^+e^- \to q\bar{q}g$, the dashed curve shows the prediction for $e^+e^- \to q\bar{q}$.

The data discussed above prove conclusively that the observed planar events cannot result from the fluctuations in quark pair production with a Guassian distribution in transverse momentum around the jet axis of the hadrons. Each PETRA group has now observed on the order of 200 planar events with an estimated background from fluctuations of two jet

events of about 20%. Wide angle gluon bremsstrahlung $e^+e^- \to q\bar{q}g$ naturally result in planar events. The observed rate for such events is consistent with the QCD predictions. Besides this source there are two ad hoc possibilities; a flat phase space of unknown origin, or that the transverse momentum distribution of the quark fragmentation has a long non-Gaussian tail. The first possibility can be excluded by observing events with 3 axes, the second by excluding the possibility that the 3 axes are defined by 2 multiparticle jets and a single high momentum particle at a large angle with respect to the jet axes.

D) Properties of planar events. The TASSO Collaboration use a generalization[142] of sphericity to define three-jet events. In this method the tracks are projected on to the event plane defined by $\vec{n}_2$ and $\vec{n}_3$ (see above). The projections are divided into three groups and the sphericity for each group S_1, S_2 and S_3 determined. The three axes and the particle assignment to the three groups are defined by minimizing the sum of S_1, S_2 and S_3. This defines the direction of the three jets and assigns the particles to these jet directions.

In Fig. 62 the TASSO events are plotted versus tri-jettiness J_3 defined as

$$J_3 = \langle p_T^2 \rangle_{in} \; / \; \left(\frac{1}{2} \; (300 \text{ MeV/c}^2)^2 \right).$$

Here $\langle p_T^2 \rangle_{in}$ is evaluated for all charged tracks in an event with respect to their assigned axies. Thus for three jet events with a mean

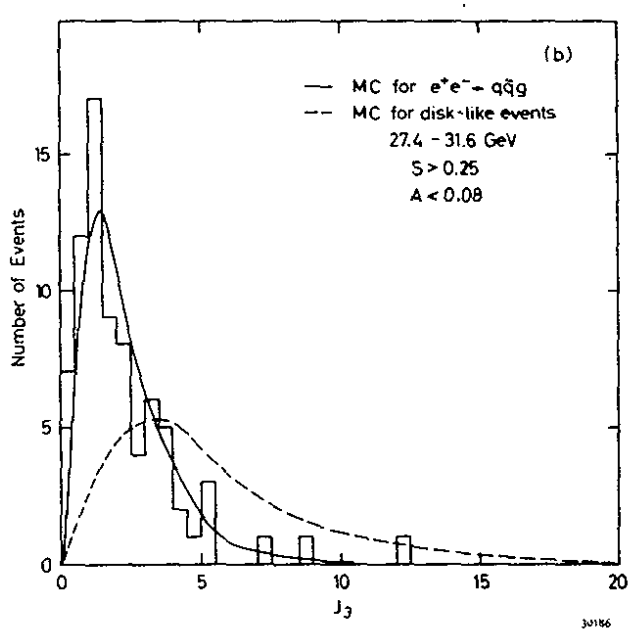

Fig. 62
Planar events ($S \geq 0.25$, $A \leq 0.08$) measured by the TASSO Collaboration and plotted versus the tri-jettiness J_3. The Monte Carlo predictions for $e\,e^- \to q\bar{q}g$ (solid) and for $e\,e^- \to$ hadrons (phasespace dashed).

transverse momentum of 300 MeV with respect to the jet axis we expect to find the events clustered around $J_3 = 1$, compared with a wide distribution in J_3 in case of a flat phase space distribution. The data agree with the expectations for $e^+e^- \to q\bar{q}g$, shown as the solid line and disagree with the phase space distribution plotted as the dashed curve.

The TASSO group has also evaluated the transverse momentum of charged particles from three jet events with respect to the jet axes to which they were assigned, This distribution $1/N\ dN/dp_T^2$ is plotted as the solid points in Fig. 63 versus p_T^2. It is compared to the p_T^2 distribution found with respect to the jet axis in two jet events shown as the open points. The agreement is very good and demonstrates that the mean p_T is constant independent of energy, when the events are analyzed as three jet events.

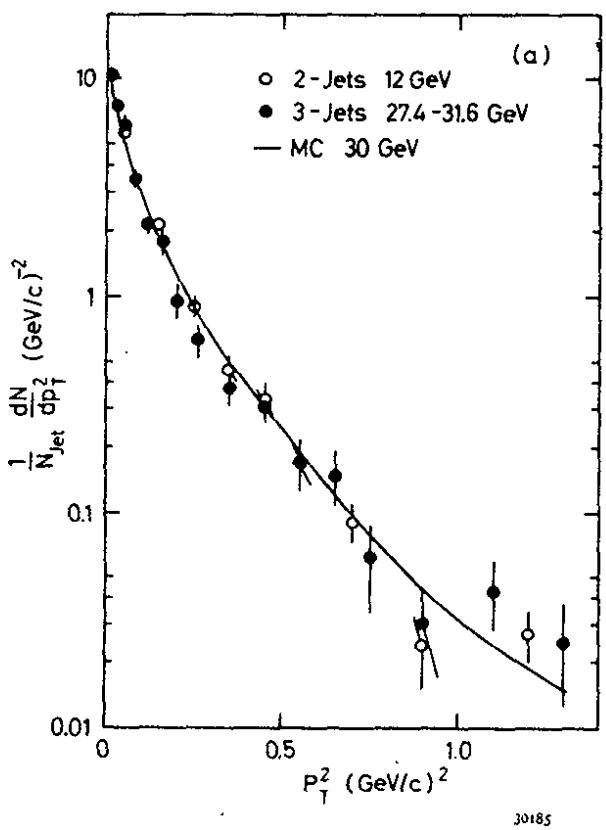

Fig. 63
The transverse momentum distribution $1/N\ dN/dp_T^2$ of the hadrons in the planar events with respect to the three axes found by the generalized sphericity method is shown as the full points. The open points represent the transverse momentum distribution with respect to the jet axis in 2 jet events at lower energies. The solid curve represents the Monte Carlo calculation of $e\ e^- \to q\bar{q}g$ at 30 GeV. The data were obtained by the TASSO group.

The MARK J group observes a three jet structure in their energy flow analysis. To enhance effects resulting from gluon emission they select events with low thrust $T < 0.8$ and large oblateness $O > 0.1$. Fig. 64 shows the energy distribution of these events in the plane defined by $\vec{e}_1$ and $\vec{e}_2$. Plotted is the energy deposited in 5° bins as a

function of angle. A clear three peak structure is seen. Plotted are the predictions from QCD, phase space + $q\bar{q}$ with σ_q = 300 MeV/c and $q\bar{q}$ only with σ_q = 500 MeV. Normalized to the total event sample, only the gluon bremsstrahlung hypothesis fits the data.

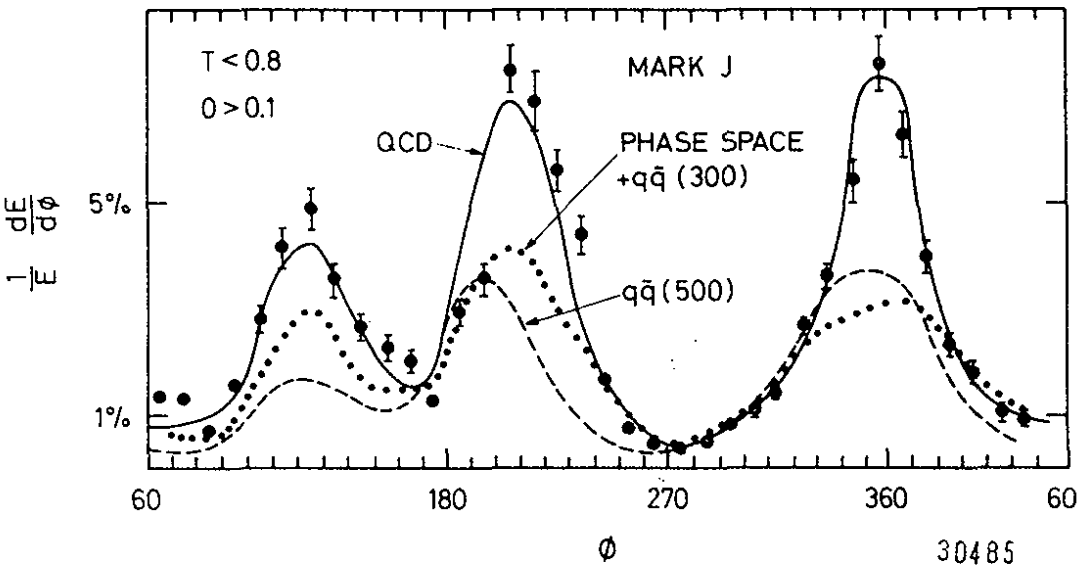

Fig. 64

A plot of the energy distribution in the plane defined by the thrust and the major axes for all events with thrust < 0.8 and oblateness > 0.1. The measurements were done by the MARK J group. The QCD fit is shown by the solid line, a mixed phase space and $q\bar{q}$ model is shown as the dotted line, a pure $q\bar{q}$ model with σ_q = 500 MeV is given by the dashed line.

The JADE group[143] uses an independent method suggested by Ellis and Karliner[144] to demonstrate the existence of three jet events. From the data taken at c.m. energies around 30 GeV they select planar events which satisfy the condition $Q_2 - Q_1 > 0.1$ and determine the thrust axis for each event. The event is then divided into two jets by a plane normal to the thrust axis and the p_T for each jet computed separately; the jet with the smallest p_T is called the slim jet, the other broad jet. The particles in the broad jet are then transformed into its own rest system. If the broad jet consists of two jets they will now appear as two back to back jets along the new thrust axis T^*. The distribution of T^* in this system is plotted in Fig. 65 together with the thrust distribution of two jet events measured at 12 GeV. The two distributions are in excellent agreement. Also other quantities like the invariant mass, mean p_T and

charged multiplicity evaluated for the broad jet in its own rest system are in agreement with the same quantities evaluated for a two jet event at 12 GeV. The data therefore exhibit a three jet structure as expected for gluon bremsstrahlung.

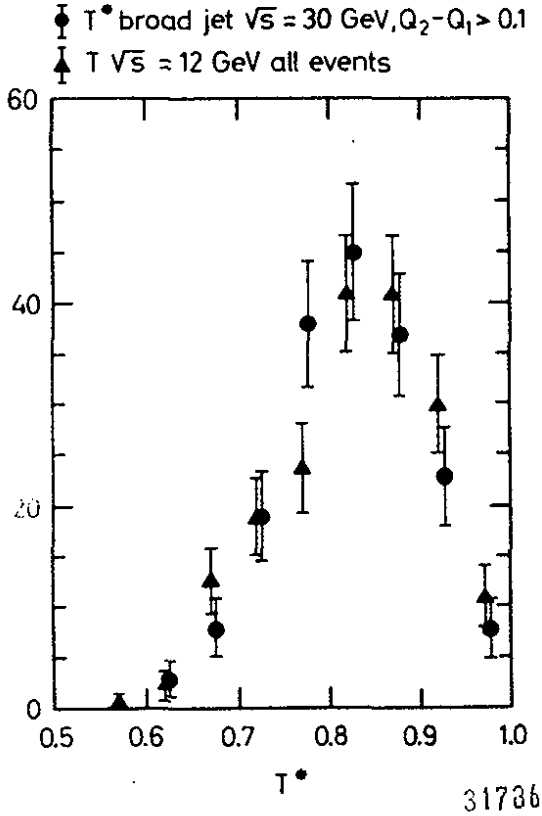

Fig. 65
Distribution of thrust for the broad jet of planar events at 30 GeV compared with the thrust distribution at 12 GeV. The data were obtained by the JADE COllaboration.

The PLUTO group has analyzed[140,145] their data using the cluster method discribed above. The distribution of the observed number of jets per event are listed in Table 14 and compared to the predictions based on $q\bar{q}$, $q\bar{q}$ + $q\bar{q}g$ (α_s = 0.15) and phase space. The models are all normalized to the number of observed events. The data clearly favour a clustering of the particles around 3 axes.

Table 14 - Number of clusters

n_j	1	2	3	4	5	6	7
Data	2	551	249	53	3	1	
phase space	1	30	154	306	268	86	14
$q\bar{q}$	3	680	152	23	1		
$q\bar{q}$ + $q\bar{q}g$	3	567	247	46	2		

e^+e^- COLLIDING BEAM EXPERIMENTS

The remaining question is then to decide whether the third jet is defined by a single particle or a group of particles. This can be done by examining the events. Figs. 66 a and b show typical candidates for three jet events observed by JADE and TASSO. Note that several tracks cluster around each axis.

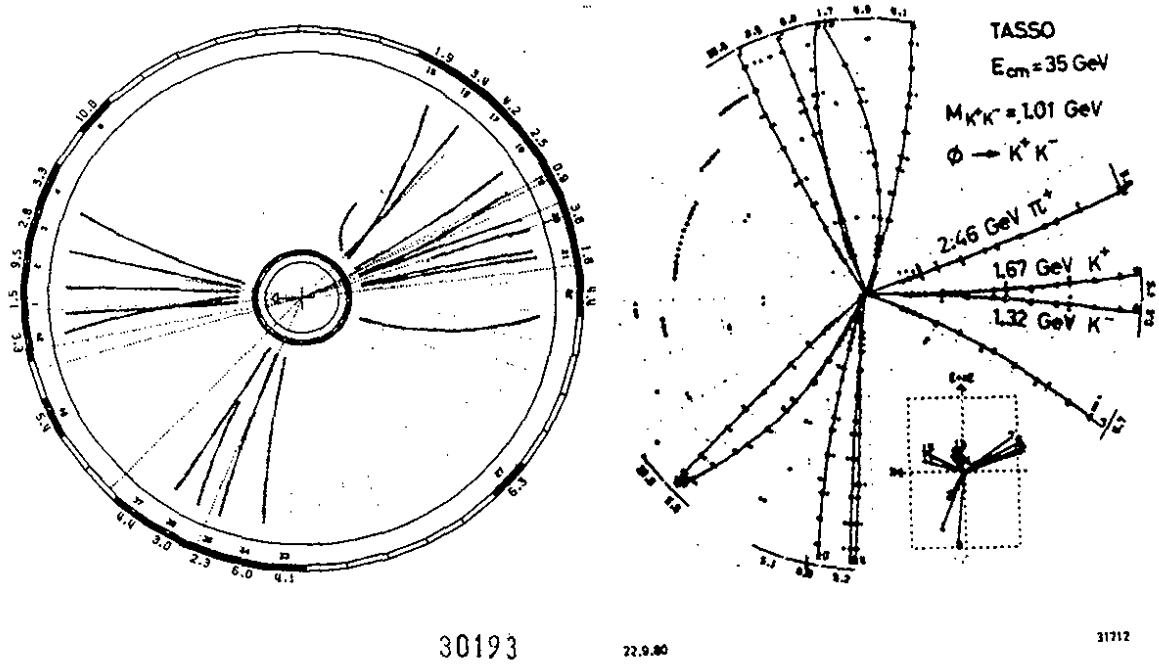

Fig. 66 – Example of three jet events observed by a) JADE and b) TASSO

In Fig. 67 the multiplicity distribution of the three jets determined by the TASSO group is shown. The jets are ordered according to $E_1 > E_2 > E_3$. The energies of the jets were computed from the observed opening angles between the jets neglecting parton masses. Furthermore only events for which the acceptance of the drift chamber is nearly complete were considered. It is clear that each jet in general consists of several charged particles and that the multiplicity distribution is reproduced by the QCD calculation.

In conclusion: all the properties observed in $e^+e^- \rightarrow$ hadrons can be explained naturally by gluon bremsstrahlung and there is no other alternative mechanism known which explains all the data. However, to prove that the gluon observed is the QCD gluon one must show that the gluon is a coloured, flavour neutral vector particle with gauge couplings.

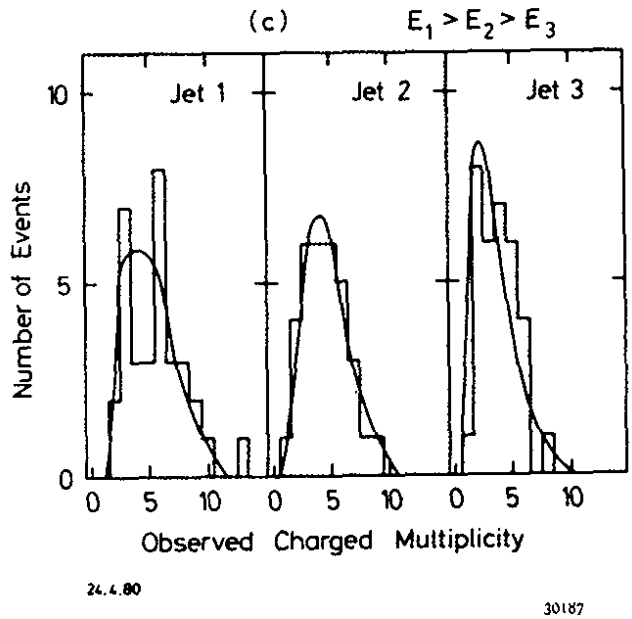

Fig. 67
The charged particle multiplicity distribution observed by TASSO in each of the three jets in a planar event with the jets ordered according to energy.

10.2 The spin of the gluon

It is obviously crucial to determine the spin of the gluon from a sample of clean three jet events resulting from gluon bremsstrahlung. $e^+e^- \to q\bar{q}g$. This process can conveniently be described in Dalitz plot using the variables $x_i = E_i/E_b$ where the energy carried off by the quark or the gluon E_i is measured in units of the beam energy E_b. The variables are ordered such that $x_3 < x_2 < x_1$. The thrust of the $q\bar{q}g$ event is then given by x_1, and $x_1 + x_2 + x_3 = 2$. The distribution of the events as function of x_i, averaged over production angles relative to the incident e^+e^- directions, can be written as:

$$\frac{1}{\sigma_o}\left(\frac{d\sigma}{dx_1 dx_2}\right)_V = \frac{2\alpha_s}{3\pi}\left(\frac{x_1^2 + x_2^2}{(1-x_1)(1-x_2)} + \text{cyclic permutations of } 1,2,3\right) \quad (37)$$

for the vector case and as:

$$\frac{1}{\sigma_o}\left(\frac{d\sigma}{dx_1 dx_2}\right)_S = \frac{\tilde{\alpha}_s}{3\pi}\left(\frac{x_3^2}{(1-x_1)(1-x_2)} + \text{cyclic permutations of } 1,2,3\right) \quad (38)$$

for the scalar case.

The TASSO group[146] has determined the spin using the variable $\cos\tilde{\theta} = (x_2 - x_3) / x_1$ suggested by Ellis and Karliner[144]. $\tilde{\theta}$ is the angle between the parton 1 and the axis of the parton 2 and 3 system boosted to its own rest frame. To ensure that the spin analysis is not affected by higher order terms one should avoid x_i close to 1. Further-

more, for x_1 close to 1 the distributions are varying rapidly so that smearing effects caused by the non-perturbative fragmentation of gluons and quarks are important. For these reasons only events with $1 - x_1 > 0.1$ are used in the analysis.

A total of 248 events remained after this cut with an estimated two jet event background of 17% and 18% for scalar and vector gluons respectively.

The distribution of the events as a function of $\cos\tilde{\theta}$ is plotted in Fig. 68 and compared with the distributions predicted for vector (solid) and scalar (dotted) gluons. The prediction was made using the model of Hoyer et al.[134]. Note that the distributions are normalized to the number of events in the plot i.e. the scalar and vector cases are discriminated using the shape only.

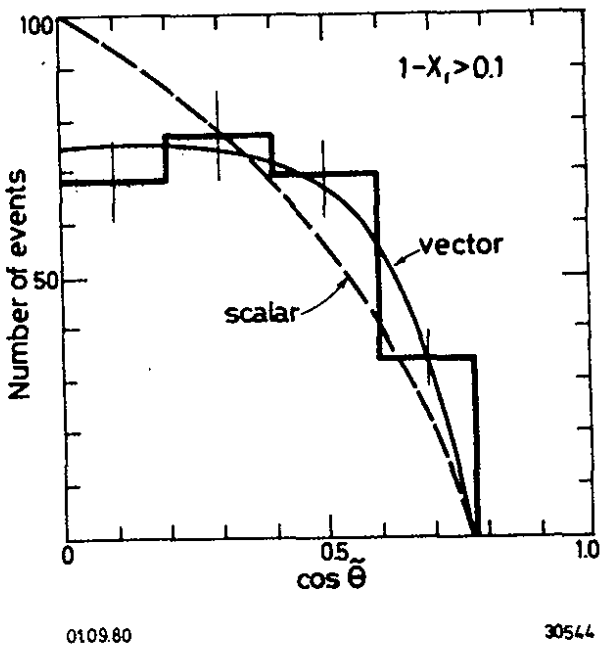

Fig. 68
Observed distribution of the data observed by TASSO in the region $1 - x_1 > 0.10$, as a function of the cosine of the Ellis-Karliner angle $\tilde{\theta}$.
The solid line shows the QCD prediction and the dotted line the prediction for scalar gluons, both normalized to the number of observed events.

The data clearly favour the vector case. A fit to the data gives for three degrees of freedom $\chi^2 = 1$ for the vector gluon and $\chi^2 = 14.9$ for the scalar gluon - i.e. scalar gluons are disfavoured by 3.1 standard deviations.

One way to avoid binning effects is to evaluate the mean value of the $\tilde{\theta}$. The experimental value of $\langle\cos\tilde{\theta}\rangle_{exp} = 0.349 \pm 0.013$ can be compared to the values $\langle\cos\tilde{\theta}\rangle_V = 0.341 \pm 0.004$ and $\langle\cos\tilde{\theta}\rangle_S = 0.298 \pm 0.003$ for vector and scalar gluons respectively. The experimental value differs from the vector gluon prediction by 0.6 standard deviations and

by 3.8 standard deviations for the scalar case.

This conclusion is remarkably insensitive both to the exact value of α_s and the details of the fragmentation. Varying the coupling constants by $\pm$ 20% changes the computed value of $\langle\cos\tilde{\theta}\rangle$ by about $\pm$1%. Evaluating $\langle\cos\tilde{\theta}\rangle$ in the elementary model without fragmentation leave the scalar prediction unchanged and increases the predicted value for a vector gluon by about 2%.

Another analysis[140,145] of the gluon spin has been made by the PLUTO Collaboration. They investigate the x_1 distribution - i.e. the distribution of the most energetic jet in three jet events. This distribution is plotted in Fig. 69 with the $q\bar{q}$ contribution subtracted.

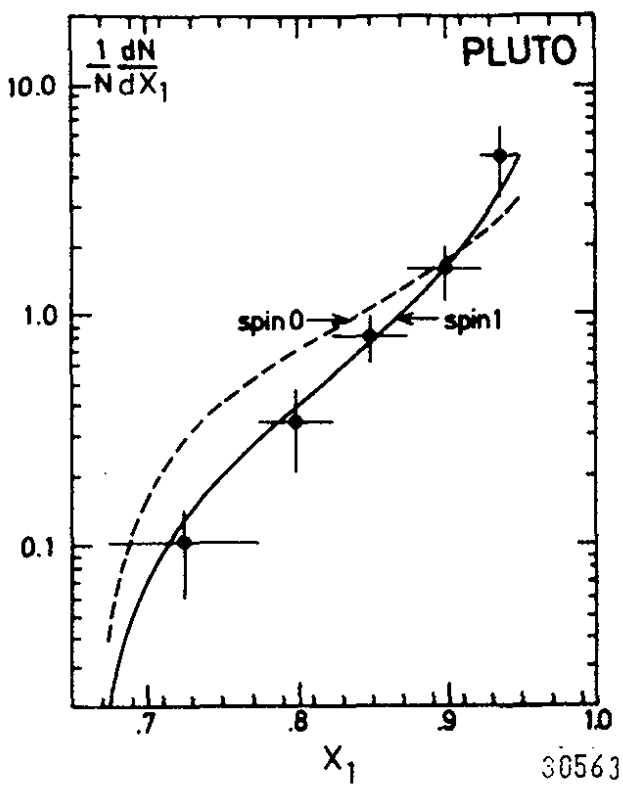

Fig. 69
The thrust distribution observed by PLUTO in three jet events. The solid line represents the spin 1 case and the spin 0 case is shown by the dotted line. The $q\bar{q}$ contribution has been subtracted.

The prediction for the vector and the scalar case normalized to the number of events is shown as the solid and the dotted curve respectively. The vector curve fits the data nicely whereas the scalar curve is clearly disfavoured. However, note that PLUTO consider events with $(1 - x_1) > 0.05$. Removing the last bin would reduce the significance of this fit.

Both the TASSO and the PLUTO conclusions are based on a first order calculation in α_s.

10.3 Determination of the strong coupling constant α_s

The strong coupling constant α_s is directly related to the number of three jet events. After choosing a minimum angle between any pair of partons (q, $\bar{q}$ or g) the QCD cross section (Eq.37) can be integrated and normalized to the total e^+e^- annihilation cross section. This ratio depends only on α_s and can be compared directly to the experimental ratio of three jet events to the total number of hadronic events. In practice the analysis must consider several effects:

1) The overlap between jets due to the hadronization process and to fluctuations which might cause a two-jet event to be classified as a three jet event. These effects are not crucial as long as the minimum angle between any two partons is large compared to the opening angle of the jet.
2) The omission of neutrals in some experiments.
3) Apparent multijet contributions resulting from b-decays.
4) Corrections from higher order processes in α_s.
5) QED corrections[147], in particular hard photon emission in the initial state.

These and other effects have been taken into account using the elaborate Monte Carlo routines discussed above.

A first attempt to determine α_s at PETRA energies was made by the MARK J group[148] using data taken around 30 GeV. They found, using the Ali et al. program, $\alpha_s = 0.23 \pm 0.02 \pm 0.04$ where ± 0.02 is the statistical error and ± 0.04 the systematic uncertainty. A recent analysis[139] based on further data and which also includes the hard photon correction omitted in the first analysis yields as a preliminary value $\alpha_s = 0.19 \pm 0.02 \pm 0.04$.

The TASSO group determined[149] α_s from the event distribution in the A, S plane. They found that α_s can be determined almost independently of the fragmentation parameters using events with $S > 0.25$. In this kinematical region three jet events dominate and non-perturbative effects are not important. The events with $S \geq 0.25$ were fitted for all allowed values of a_F and $P/(P+V)$ with α_s and σ_q as free parameters. This fit gave α_s values between 0.14 and 0.17 with a mean value of 0.16. Therefore $\alpha_s = 0.16 \pm 0.04$ is independent of the fragmentation parameters.

The fragmentation parameters were then determined in a further analysis using events with low sphericity S < 0.25. This region is dominated by two jet events and is insensitive to α_s.

Simultaneous fits were made to: i) The x distribution ($x = p_h/E_b$). ii) The $\langle p_T^2 \rangle_{out}$ distribution. iii) The charged multiplicity distribution.

The fits yielded $a_F = 0.57 \pm 0.20$, $\sigma_q = 0.32 \pm 0.04$ GeV/c and $P/(P+V) = 0.56 \pm 0.15$ in agreement with the values found[136] earlier in lepton-hadron and hadron-hadron interactions. The quality of the fits is shown in Fig. 70. Using these parameter values as an input to fit the events with S > 0.25 resulted in $\alpha_s = 0.17 \pm 0.02 \pm 0.03$.

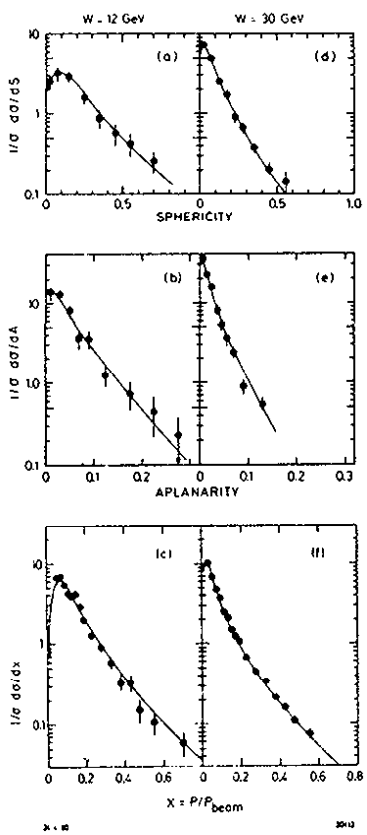

Fig. 70
Comparison of the data with the QCD model (curves) at 12 GeV and 30 GeV in c.m.

Repeating the fit using the model of Hoyer et al.[134], gave

$$\alpha_s = 0.19 \pm 0.02.$$

This is expected since this model only considers two and three jet events whereas the second order model[135] also considers four jet events. The effective value of α_s in the first order model must thus be about 10% larger. However, remember that diagrams with internal gluon lines have been neglected[150].

The JADE group basically used the procedure outlined above to determine α_s. They find[151] $\alpha_s = 0.18 \pm 0.03 \pm 0.03$ consistent with an earlier[36] determination based on the planarity distribution.

The PLUTO group used the cluster method method[140,145] described above to classify the events as two, three or four jet events. The value of α_s was then determined from the observed jet distribution. They find $\alpha_s = 0.15 \pm 0.03 \pm 0.02$.

It is clear that the values for α_s determined from the three jet events by

various methods are in good agreement with a mean value $\alpha_s = 0.17$.

The value of α_s is related to Λ, the strong interaction mass scale. It is still an open question what to use for q^2 in Eq. 26. Maybe, the best choice is $q^2 = p^2$ where p^2 is the quark-gluon effective mass squared. The p^2 distributions for the TASSO events with $S > 0.25$ are plotted in Fig. 71. Inserting the mean value $\langle p^2 \rangle = 140\ \mathrm{GeV}^2$ into the expression for $\alpha_s(q^2)$ yields

$$\Lambda = (95 \, {}^{+65}_{-35}) \text{ MeV for } \alpha_s = 0.17 \pm 0.02.$$

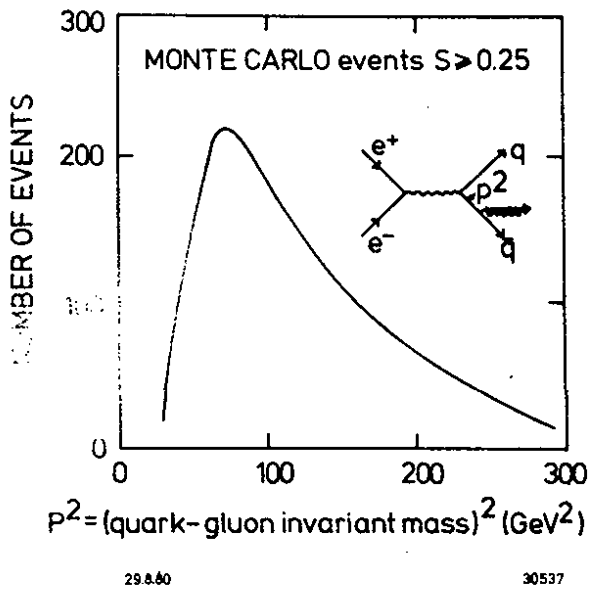

Fig. 71
Distribution of the square of the quark-gluon mass as computed for events with large sphericity.

Including the systematic error yields $\Lambda < 290$ MeV.

From deep inelastic lepton hadron interactions values for Λ between 100 and 500 MeV are found.

10.4 Soft gluon emission

So far we have primarily considered effects due to the emission of a single hard gluon at large angles. However, in the quark-gluon cascade leading to the final hadron jet most gluons are soft and emitted at small angles. The coupling constant α_s will thus be of order unity and many diagrams must be summed. It has been proposed[152] to relate the parton angular distribution within the cascade to the two particle differential cross section:

$$1/\sigma \frac{d\sigma}{d\Omega} = \sum_{a,b} \int dz_a \int dz_b \cdot z_a \cdot z_b \, \frac{1}{\sigma} \frac{d^3\sigma}{dz_a \cdot dz_b \cdot d\Omega} \qquad (39)$$

where a and b are any two particles emitted in the event with normalized momenta z_a, z_b ($z = p/p_{beam}$) and an opening angle of $\pi-\theta$.

The PLUTO Collaboration has determined[153] the two particle differential cross section for c.m. energies between 9.4 GeV and 31.6 GeV. The data at 9.4 GeV and 31.6 GeV are plotted in Fig. 72 versus θ for small angles - i.e. the particles belong to opposite jets. The dashed

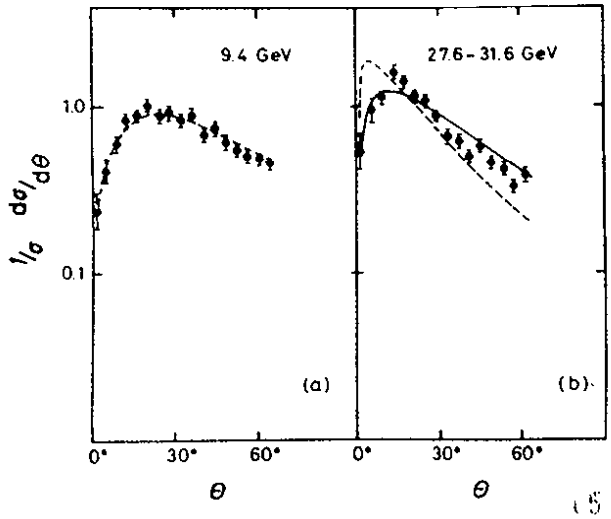

Fig. 72
$1/\sigma\ d\sigma/d\Omega$ measured by PLUTO plotted versus θ. The dashed and solid curves represent theoretical fits to the data.

curve represents a theoretical fit[154] to the data without hadronization. The fit is based on the QCD leading logarithmic approximation which is used to evaluate the fragmentation function for a parton a to produce a parton b. The parameters were determined from the 9.4 GeV data and used to predict the cross section at 30 GeV. The trend of the data is reproduced by this fit, however, the fit was much improved by including the hadronization of the partons shown as the solid line.

10.5 Do quarks and gluons fragment differently ?

A gluon may fluctuate into pairs of quarks and gluons. Furthermore the ggg coupling is 9/4 times stronger than the $q\bar{q}g$ coupling such that gluon emission is expected to be more frequent for gluons than for quarks. This leads us to expect that a gluon and a quark will fragment into hadrons differently - the hadron spectrum from a gluon fragmentation will be softer with a correspondingly higher multiplicity.

Anderson, Gustafson and collaborators have suggested[155] studying the yields of low-energy particles emitted at large angles with respect to the jet axis. The JADE group[151] has carried out this analysis using charged and neutral particles. Planar events with $Q_2 - Q_1 >$

0.10 were divided into a slim jet and a broad jet by the plane normal to the thrust axis. The broad jet is then boosted into its own rest system and the particles assigned to the two subjets. The softest jet is called the gluon jet. Monte Carlo calculations imply that this is true about 70% of the time and it simply reflects the softness of a bremsstrahlung spectrum. All the particles are then projected on to the plane defined by T, thrust axis of the event and T^* the thrust axis of the boosted two jet system. They then plot the particle densities between the gluon jet and the slim jet and the quark jet and the slim jet in terms of normalized angles θ_i/θ_{max}, where θ_{max} is the opening angle between the gluon jet and the slim jet or the quark jet and the slim jet respectively. The data plotted in Fig. 73 show that the density of tracks

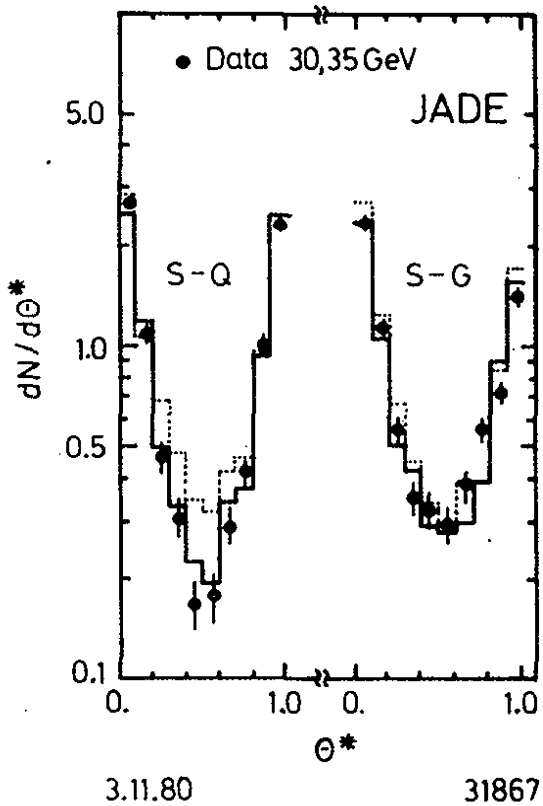

Fig. 73
Angular distribution of charged particles between the slim jet and the gluon jet and between the slim jet and the quark jet as a function of the normalized angles θ/θ_{max}.

is larger by a factor of 2 between the slim jet and the quark jet. The result of a Monte Carlo computation based on similar fragmentation functions for quarks and gluons fails to reproduce the dip observed in the particle density distribution between the quark and the slim jet, as shown by the dotted histogram in Fig. 73. The data, however, can be reproduced by assuming that the quark has a harder fragmentation function than the gluon jet, as shown by the solid histogram. This may be

a first experimental indication that quarks and gluons fragment differently.

11.
TWO PHOTON INTERACTIONS

Electron-positron collisions are also a source of photon-photon collisions[156] as shown in Fig. 74, where the mass and the energy of the spacelike photon is determined from a measurement of the scattered lepton. These processes offer a unique opportunity to vary the mass of the target and the projectile over a wide range from collisions of two nearly real photons via deep inelastic electron scattering on a photon target to collisions of two heavy photons.

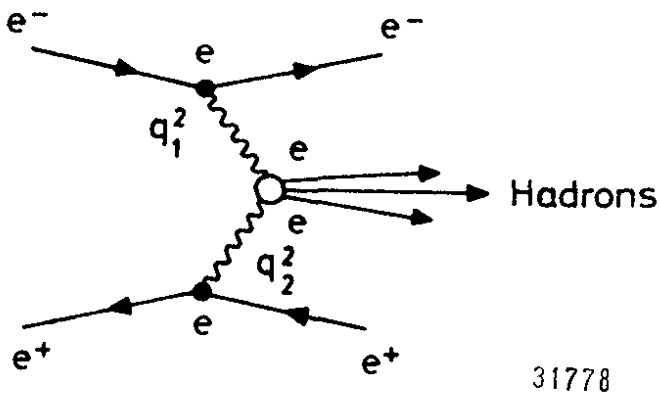

Fig. 74
Hadron production in $e^+e^- \to e^+e^- X$

Experimentally, two photon events are separated from annihilation events by a cut on the observed energy. The c.m. energy of the $\gamma\gamma$ system is in general much lower than the available energy, reflecting the products of two bremsstrahlungsspectra. The background from beamgas events is rather low as determined from the number of events which satisfy the selection criteria but originates outside of the interaction volume.

11.1 Resonance production

All hadrons with even charge conjugation and spin different from one can be produced[157] in real $\gamma\gamma$ collisions.

The MARK II Collaboration at SPEAR has published[158] data on $e^+e^- \to e^+e^-\eta'$. They found a clean η' signal in the channel $\eta' \to \rho\gamma$ which gave $\Gamma^{\eta'}_{\gamma\gamma} = (5.8 \pm 1.1)$ keV with a systematic uncertainty of 20%. With the measured branching ratio of $BR(\eta' \to \gamma\gamma) = (2.0 \pm 0.3)\%$ this yields

a total width $\Gamma_{\eta'}^{tot}$ = (293 ± 76 ± 59) keV in good agreement with the value of (280 ± 100) keV determined[159] by D.M.Binnie et al. from the reaction $\pi^- p \to \eta' n$ near threshold.

Events of the type $e^+e^- \to e^+e^-\pi^+\pi^-$ have been selected by PLUTO and TASSO at PETRA and by MARK II and the San Diego group at SPEAR to search for $\gamma\gamma$ production of resonances decaying into pairs of charged hadrons. The effective mass distribution of untagged two prong events determined by the PLUTO group[160] is plotted in Fig. 75 assuming the particles to be pions. The data show a broad maximum near 1.2 GeV decreasing steeply towards higher masses. The bulk of the two prong events results from QED reactions $e^+e^- \to e^+e^-$ ($e^+e^- \to \mu^+\mu^-$) with an amplitude proportional to e^4. (In addition there is a small contribution from $\pi^+\pi^-$ Born events). This contribution has been evaluated[161] and is shown as the solid line in Fig. 75. It describes all the data except for an ex-

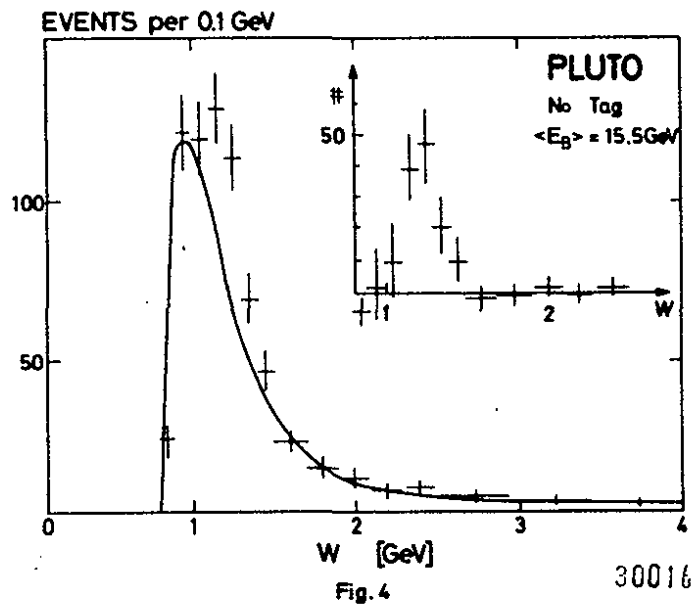

Fig. 75
Untagged two prong events from PLUTO plotted versus the pair mass. The solid line shows the QED contribution. The difference between the measured two prong yield and the QED contribution is shown in the insert.

cess near 1.25 GeV. The difference between the observed distribution and the QED prediction is a peak near 1.25 GeV as shown in the insert. It is natural to associate this peak with f^o production since the f^o has a mass of 1.27 GeV and decays into a $\pi^+\pi^-$ pair 83% of the time. A fit to the data assuming the f^o to be produced with a helicity amplitude $\Lambda = 2$ gave $\Gamma_{\gamma\gamma}^{f^o}$ = (2.3 ± 0.5 ± 0.35) keV, where the first error is statistical and the second systematic.

TASSO has obtained similar data[162] which yield a preliminary value

$\Gamma^{f^0}_{\gamma\gamma} = (4.1 \pm 0.4 \pm 0.6)$ keV.

Also the MARK II Collaboration has observed a clear enhancement at a pairmass of 1.2 GeV. However, these data can not be fit by a single Breit-Wigner resonance.

11.2 Observation of $e^+e^- \to e^+e^- \rho^0\rho^0$

The TASSO group reports[164] results on $\gamma\gamma \to \rho^0\rho^0$. The $\rho^0\rho^0$ cross section was extracted from the data by selecting neutral, four prong events with the sum of the transverse momentum with respect to the beam axis less than 0.15 GeV. The invariant $\gamma\gamma$ mass was required to be between 1.5 and 2.3 GeV. This results in 89 events, with a negligible background from beam gas events. They estimate one event from one photon annihilation and 15 events from events containing additional unobserved particles.

The cross section for $\gamma\gamma \to \rho^0\rho^0$ is plotted in Fig. 76 versus the c.m. energy of the $\gamma\gamma$-system. The cross section peaks strongly near threshold and drops rapidly with energy in disagreement with a simple V.D.M. asymptotic prediction. However, close to threshold nonasymptotic effects are expected to be important.

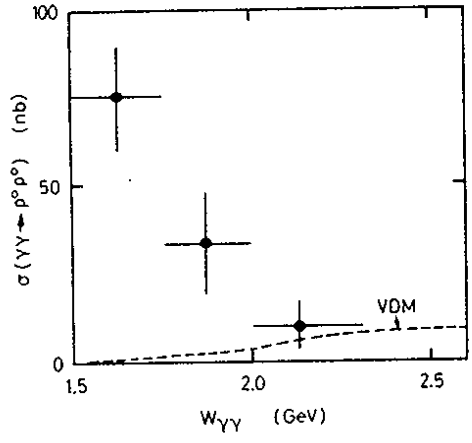

Fig. 76
The cross section for $e^+e^- \to e^+e^- \to \rho^0\rho^0$ *as measured by TASSO. An asymptotic VDM prediction is shown as the dotted line.*

11.3 Hadron production with real photons

The amplitude for $\gamma\gamma \to$ hadrons will presumably contain both the hadronlike[165] piece and the pointlike[166] piece shown in Fig. 77. In the hadronic piece the photons convert into vector mesons which subsequent-

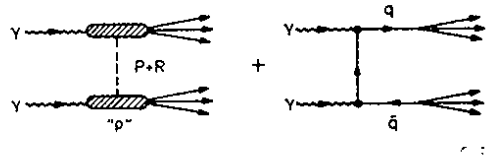

Fig. 77
The hadronlike and the pointlike contribution to $\gamma\gamma \to$ *hadrons.*

ly interact producing a final state similar to that produced in hadron hadron collisions, where the secondary hadrons tend to be produced with low transverse momenta with respect to the beam axis. In addition, however, the photon has a pointlike piece where the photon couples directly to a quark pair initiating a hard scattering process. In this case the secondary hadrons will appear in two jets of hadrons distributed roughly as $1/p_T^4$ with respect to the beam axis.

The total cross section for $\gamma\gamma \to$ hadrons can be estimated from the imaginary part of the elastic scattering amplitude to

$$\sigma(\gamma\gamma \to \text{hadrons}) = 240 \text{ nb} + \frac{270(\text{nb GeV})}{W} + \frac{C(\text{nb GeV}^2)}{W^2} \qquad (40)$$

The first term results from Pommeron exchange and was estimated from factorization $\sigma_{\gamma\gamma} \cdot \sigma_{pp} = (\sigma_{\gamma p})^2$. The second term involves f and A_2 exchange and leads to a cross section which decreases as $1/W$ where W is the energy of the hadronic system. The pointlike contribution is expected to decrease roughly as $1/W^2$.

The total hadronic cross section has been measured[162] both by the PLUTO and the TASSO Collaboration. Both groups collected data by detecting only one of the electrons leaving the other untagged. The total energy W of the produced hadron system was estimated from energy W_{vis} observed in the detector. Only charged particles were observed in TASSO whereas PLUTO also measured photons. The observed cross sections were extrapolated to $Q^2 = 0$ using the ρ- propagator:

$$\sigma_{\gamma\gamma}(W) = \sigma_{\gamma\gamma}(W, Q^2) \cdot \left[\frac{m_\rho^2}{m_\rho^2 + Q^2}\right]^{-2} \qquad (41)$$

Note that this simple Ansatz violates scaling and is not valid in electroproduction at large values of Q^2. The Q^2 dependence of the total cross section is shown in Fig. 78 together with the ρ-propagator fit.

The cross section extrapolated to $Q^2 = 0$ are plotted versus W in Fig. 79. The VDM contribution is also shown as the dotted line. Note that the TASSO data are preliminary.

In addition to the statistical errors indicated by the bands, there are systematic errors of 15% and 25% for the PLUTO and the TASSO data respectively.

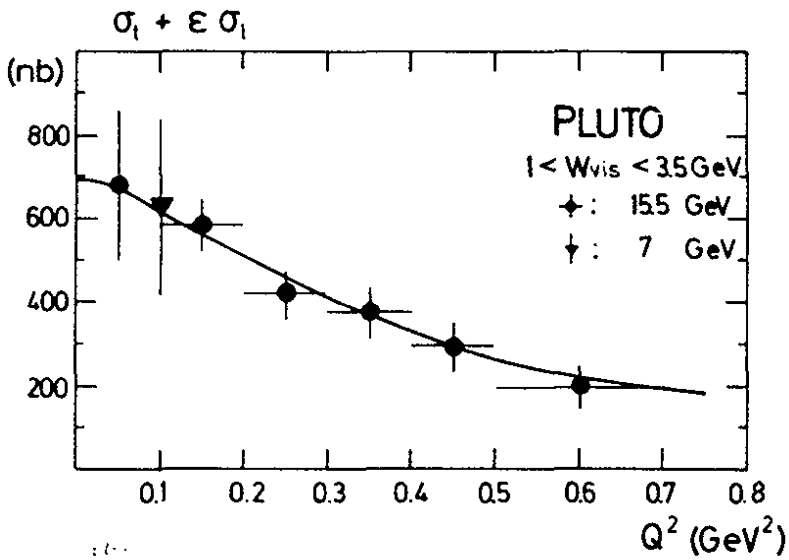

Fig. 78
Total cross section for $\gamma^{*}\gamma \rightarrow$ hadrons observed by PLUTO.

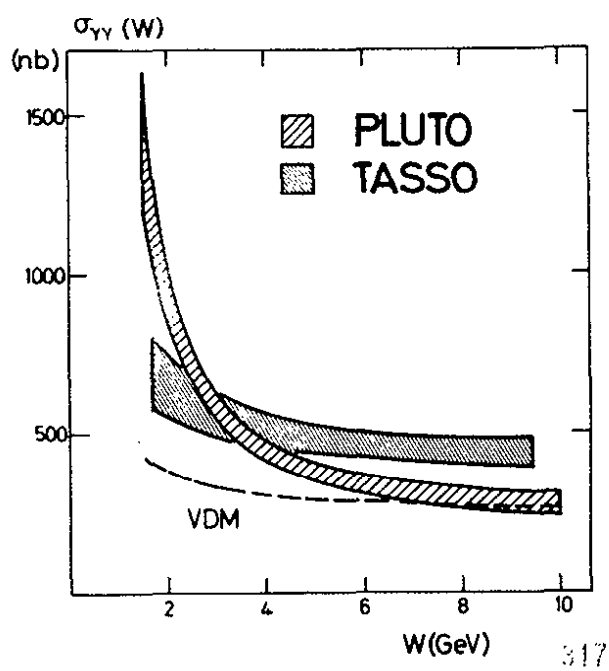

Fig. 79
The total cross section for $\gamma\gamma \rightarrow$ hadrons plotted versus the mass of the produced hadron system. Note that the TASSO data are preliminary and that only statistical errors are shown.

The data from the two groups are marginally consistent within the errors. However, the PLUTO cross section clearly decreases steeper with energy than the TASSO cross section does:
A best fit to the PLUTO data gives:

$$\sigma_{\gamma\gamma} = A\ (240\ \text{nb} + \frac{270(\text{nb GeV})}{W} + \frac{B(\text{nb GeV}^2)}{W^2}$$

with $A = 0.97 \pm 0.16$ and $B = 2250 \pm 500$, whereas the TASSO data are fit by:

$$\sigma_{\gamma\gamma} = 380\ \text{nb} + \frac{520(\text{nb GeV})}{W} \quad .$$

e^+e^- COLLIDING BEAM EXPERIMENTS

Although, the PLUTO data might suggest the presence of a pointlike term they clearly do not yet prove it. The pointlike contribution might show up more clearly in the transverse momentum distribution of the hadrons at large values of p_T where the hadron-like contribution has disappeared.

The transverse momentum distribution measured by PLUTO is plotted in Fig. 80 versus p_T^2. The spectrum drops rapidly at small values of p_T^2 and flattens at large values of p_T^2 where indeed the slope is consistent with $1/p_T^4$ as expected for the hard component. The solid line represents the contribution from the pointlike diagram.

A candidate for a hard scattering event obtained by PLUTO is shown in Fig. 81. When viewed along the beam direction the event appears as two collinear jet of hadrons. When viewed transverse to the beam direction the event is seen to have a unbalanced longitudinal momenta as expected for a $\gamma\gamma$ event.

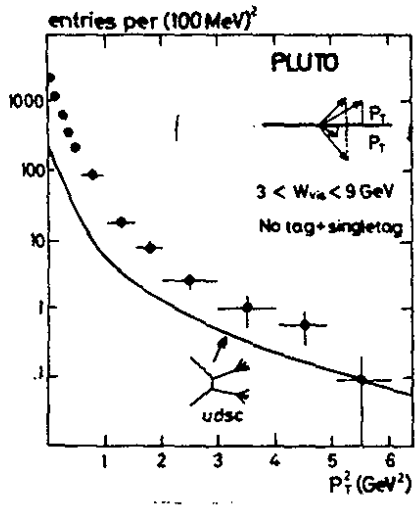

Fig. 80
Number of tracks plotted versus the square of the transverse momentum with respect to the beam axis. The solid curve is a prediction based on $\gamma\gamma \to q\bar{q} \to$ hadrons with $q = u, d, s, c$ quarks.

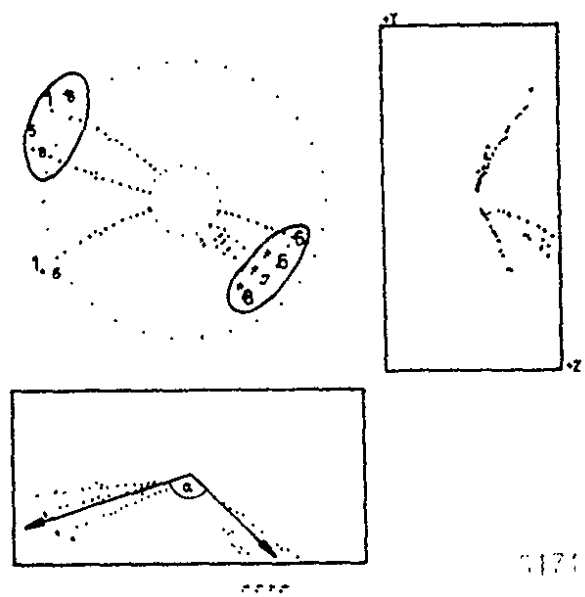

Fig. 81
Candidate for $\gamma\gamma \to q\bar{q} \to$ hadrons observed by PLUTO.

The PLUTO group has determined the two jet axes in such an event by maximizing the thrust of the event using two independent axes. It is interesting to note[167] that the mean p_T of the hadrons computed with respect to these axes is 300 MeV.

The properties of these events are strongly suggestive of a point-like production mechanism. However, it should be remembered that ordinary one photon annihilation events with radiation in the initial state could lead to events with the same topology. This mechanism, however, can be excluded if the electron is tagged on the same side as the direction of the longitudinal momentum vector of the jets. The PLUTO group finds the expected number of 2-jet events with the tagged electron on the same side as the momentum vector, appearantly excluding this background source.

11.4 Electron scattering on a photon target

The PLUTO Collaboration reports[162] the first data on deep inelastic electron-photon scattering. These data were collected by tagging one electron at scattering angles between 70 mrad and 250 mrad corresponding to values of Q^2 between 1 $(GeV/c)^2$ and 15 $(GeV/c)^2$ with a mean value of 5 $(GeV/c)^2$. The second electron was not detected yielding a nearly real target photon. A total of 120 multihadron events with this electron topology were observed.

Deep inelastic electron-photon scattering[168], as shown in Fig. 82, can be parametrized in terms of three structure functions. $F_L(x,Q^2)$ and $F_2(x,Q^2)$ corresponds to the longitudinal and to the transverse polaristion vector of the virtual photon respectively and $F_3(x,Q^2$ to the transverse polarisation vector of the target photon in the scattering plane. $x = Q^2/(Q^2+W^2)$ and W is the mass of the hadronic system. $F_3(x,Q^2)$ will average to zero since the scattering plane was not determined. Furthermore $F_L(x,Q^2)$ is expected to be smaller than $F_2(x,Q^2)$ and the PLUTO group therefore analyze their data in terms of $F_2(x,Q^2)$ only.

Both the hadronlike part and the pointlike part of the photon contributes to $F_2(x,Q^2)$ as indicated in Fig. 82b,c. In the hadronlike part the photon transforms into a vector meson and the virtual photon interacts with the quarks in the vector meson. This contribution cannot be calculated from first principles but it will have an x dependence similar to

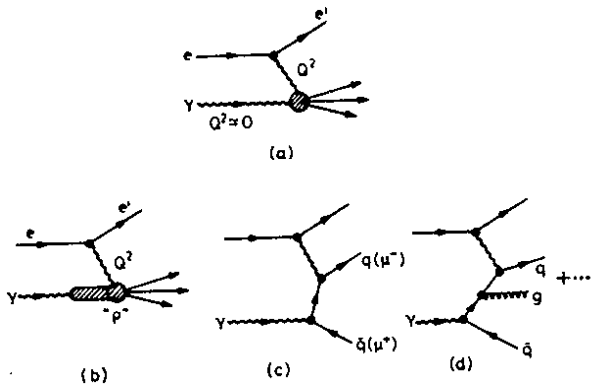

Fig. 82
Diagrams contributing to $e\,\gamma \to e'$ *hadrons.*

that observed in the structure function of the pion i.e. $F_2(x,Q^2)_{VDM} \sim (1-x)^{c_1} + c_2 \ln (\ln Q^2)$ and, just like lepton-hadron interactions, only its evolution with Q^2 is predicted in QCD. The pointlike piece (82 c) can be calculated to all orders in a perturbation theory. The lowest order calculation gives:

$$F_2(x,Q^2)_{point} = \frac{\alpha}{\pi} \sum_i e_i^4 \, x(x^2 + (1-x)^2) \cdot \ln Q^2/\Lambda^2 \qquad (42)$$

The pointlike contribution leads to a structure function which peaks at large values of x, whereas the VDM piece leads to a structure function which is large at small x and disappears at large x. The lowest order pointlike contribution is indeed proportional to the QED process $e^+e^- \to e^+e^-\mu^+\mu^-$.

Higher order QCD corresctions (Fig. 82d), including the emission of soft gluons, will soften the Born spectrum by depleting the density of fast quarks and enchancing the density of slow quarks.

The values for $(1/\alpha)F_2(x)$, extracted from the hadron data, are plotted in Fig. 83a versus x and compared to the formfactor observed in the

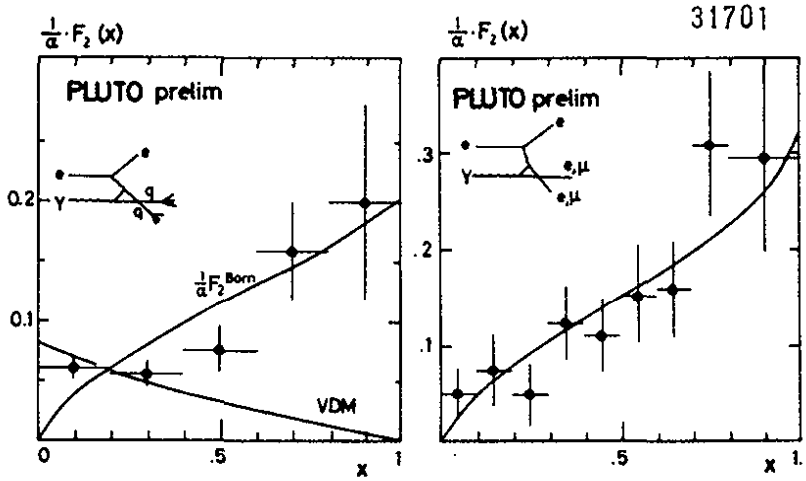

Fig. 83
The structure functions of the photon (a) and the lepton (b).

QED process $e^+e^- \to e^+e^-$ (e^+e^- + $\mu^+\mu^-$) (Fig. 83b). Both structure functions peak at large x demonstrating the existence of the pointlike piece. The Born prediction, shown as the solid curve, follows the general trend of the data quite well.

The evolution of the formfactor with increasing Q^2 will make it possible to determine Λ with good precision in a high statistics experiment. The simplicity of the target, with no finite mass effects and no higher twist effects caused by a premordial p_T distribution, makes it possible to determine Λ without the systematic uncertainties which have beset the determination in deep inelastic lepton-hadron processes. In particular it may be possible to use data in a Q^2 range such that the variation in $\ln Q^2/\Lambda^2$ are still quite large.

REFERENCES

1. G.K.O'Neill, Bull. Am.Phys.Soc. 3, 158 (1958)
2. C.Bernardini, G.F.Corazza, G.Ghigo and B.Touschek, Nuovo Cimento 18, 1293 (1960)
3. For a review of the experimental data up to the end of 1978 see: B.H.Wiik and G.Wolf, Electron-Positron Interactions, Springer Tracts in Modern Physics, Vol. 86, 1979
4. W.Barber, B.Gittelman, G.K.O'Neill, B.Richter; Phys.Rev.Lett. 16, 1127 (1966)
5. For a review of this work see: Perez-y-Jorba, Proceedings of the 4th Int.Symposium on Electron and Photon Interactions at High Energies, Liverpool, September 1969
6. For a review of this work see: C.Bernardini, Proceedings of the 1971 Symposium on Electron and Photon Interactions at High Energies, Cornell, New York, Aug. 1971
7. A.Litke et al., Phys.Rev.Lett. 30, 1189 (1973)
8. B.Richter, Proceedings of the XVII Conference on High Energy Physics, London, July 1979
9. J.J.Aubert et al., Phys.Rev.Lett. 33, 1404 (1974)
10. J.E.Augustin et al., Phys.Rev.Lett. 33, 1406 (1979)
11. G.S.Abrams et al., Phys.Rev.Lett. 33, 1453 (1974)
12. DASP Collaboration, W.Braunschweig et al., Phys.Lett.57B, 407 (1975)
13. G.J.Feldman et al., Phys.Rev.Lett. 35, 821 (1975)

e^+e^- COLLIDING BEAM EXPERIMENTS

14. T.Appelquist, H.D.Politzer, Phys.Rev.Lett.34, 43 (1975)
15. Y.Hara, Phys.Rev. 134, B 701 (1964)
    J.D.Bjorken and S.L.Glashow, Phys.Lett. 11, 265 (1969)
16. S.L.Glashow, J.Illiopoulos and L.Maiani, Phys.Rev.D2, 1285 (1970)
17. G.Goldhaber et al., Phys.Rev.Lett.37, 255 (1976)
18. DASP Collaboration, R.Brandelik et al., Phys.Lett.70B, 132 (1977) and Phys.Lett.80B, 412 (1979)
19. M.Perl et al., Phys.Rev.Lett.35, 1489 (1975)
20. S.W.Herb et al., Phys.Rev.Lett.39, 252 (1977)
    W.R.Innes et al., Phys.Rev.Lett. 39, 1240 (1977)
21. PLUTO Collaboration, Ch.Berger et al., Phys.Lett.76B, 243 (1978)
    DASP2 Collaboration, C.W.Darden et al., Phys.Lett.76B, 246 (1970)
22. J.K.Bienlein et al., Phys.Lett. 78B, 360 (1979)
    C.W.Darden et al., Phys.Lett. 78B, 364 (1979)
23. D.Andrews et al., Phys.Rev.Lett. 44, 1108 (1980) and 45, 219 (1980)
    G.Finocchiaro et al., Phys.Rev.Lett. 45, 222 (1980)
    T.Böhringer et al., Phys.Rev.Lett. 44, 1111 (1980)
24. H.Fritzsch, M.Gell-Mann and H.Leutwyler, Phys.Lett.47B, 365 (1973)
    D.Gross and F.Wilczek, Phys.Rev.Lett.30, 1343 (1973)
    H.D.Politzer, Phys.Rev.Lett.30, 1346 (1973)
    S.Weinberg, Phys.Rev.Lett.31, 31 (1973)
25. PLUTO Collaboration, Ch.Berger et al., Phys.Lett.78B, 176 (1978) and 82B, 449 (1979)
26. For a review of the recent status see:
    K.Berkelman, Proceedings of the XXth International Conference on High Energy Physics, Madison, Wisconsin, July 1980
27. S.D.Drell, D.J.Levy, and T.M.Yan, Phys.Rev.187, 2159 (1969) and Phys.Rev. D1, 1617 (1970)
28. N.Cabibbo, G.Parisi, and M.Testa, Lett.Nuovo Cimento 4, 35 (1970)
29. J.D.Bjorken and S.J.Brodsky, Phys.Rev. D1, 1416 (1970)
30. R.P.Feynman, Photon-Hadron Interactions (Benjamin, Reading Mass., p. 166 (1972)
31. R.F.Schwitters et al., Phys.Rev.Lett. 35, 1320 (1975)
    G.G.Hanson et al., Phys.Rev.Lett. 35, 1609 (1975)

32. J.Kogut and L.Susskind, Phys.Rev. D9, 697, 3391 (1974)
A.M.Polyakov, Proceedings of the 1975 International Symposium on Lepton and Photon Interactions at High Energies, Standord, August 1975
The first quantitative discussion on the experimental implications of gluon bremsstrahlung in e^+e^- annihilation was given by:
J.Ellis, M.K.Gaillard and G.G.Ross, Nucl.Phys.B111, 253 (1976) - erratum B 130, 516 (1977)

33. B.H.Wiik, Proceedings of the International Neutrino Conference, Bergen, Norway, June 1979
P.Söding, Proceedings EPS International Conference on High Energy Physics, Geneva, Switzerland, July 1979
TASSO-Collaboration, R.Brandelik et al., Phys.Lett.83B, 261 (1979)

34. MARK J Collaboration, D.P.Barber et al., Phys.Lett. 86B, 418 (1979)

35. PLUTO Collaboration, Ch.Berger et al., Phys.Lett.86B,418 (1979)

36. JADE Collaboration, W.Bartel et al., Phys.Lett. 91B, 142 (1980)

37. F.A.Berends, K.J.F.Gaemers and R.Gastmans, Nucl.Phys.B57,381 (1973); Nucl.Phys.B63, 381 (1973) and Nucl.Phys.B68, 541 (1979)
F.A.Berends and G.J.Komen, Phys.Lett.63B, 432 (1976) and private communication F.A.Berends and R.Kleiss

38. H.Salecker, Zeitschr. für Naturforschung 8a, 16 (1953) and 10a, 349 (1955)
S.D.Drell, Ann.Phys. 4, 75 (1958)
T.D.Lee and G.G.Wick, Phys.Rev. D2, 1033 (1970)

39. N.M.Kroll, Nuovo Cim. 45A, 65 (1966)

40. A.Litke, Harvard University, Thesis 1970

41. A.Böhm, Proceedings of the XX International Conference on High Energy Physics, Madison, Wisconsin, July 1980

42. JADE Collaboration, W.Bartel et al., Phys.Lett.92B, 206 (1980)
MARK J Collaboration, D.P.Barber et al., Phys.Rev.Lett.42,1110 (1979) and 43, 1915 (1979) and Phys.Lett.95B, 149 (1980)
PLUTO Collaboration, Ch.Berger et al., Z.für Physik C4, 269 (1980) and Phys.Lett. 94B, 87 (1980)
TASSO Collaboration, R.Brandelik et al., Phys.Lett. 92B, 199 (1980) and 94B, 259 (1980)

43. S.L.Glashow, Nucl.Phys.22, 579 (1961)
S.Weinberg, Phys.Rev.Lett. 19, 1264 (1967)
A.Salam, Proceedings 8th Nobel Symposium, N.Svartholm editor, Wiley NY 1968
44. J.Ellis and M.K.Gaillard, CERN 76-18
45. N.Wright and J.J.Sakurai, Phys.Rev. D22, 220 (1980)
46. MARK J Collaboration, D.P.Barber et al., RWTH Aachen, PITHA Preprint 80/08 1980
47. H.Georgi and S.Weinberg, Phys.Rev. D17, 275 (1978)
48. J.D.Bjorken, Phys.Rev. D 19, 335 (1979)
49. JADE Collaboration, R.Marshall, private communication.
50. E.H.de Groot, G.J.Gounaris and D.Schildknecht, Phys.Lett.85B, 399 (1979); Phys.Lett. 90B, 427 (1980) and Z.für Physik C5,127(1980)
51. V.Barger, W.Y.Kenny and E.Ma, Wisconsin-Hawai-Reports UW-COO-881-126 (1980); US-CO0881-133 (1980) and UW-COO-881-138 (1980)
52. DASP Collaboration, R.Brandelik et al., Phys.Lett.73B,109 (1978)
53. W.Bacino et al., Phys.Rev.Lett. 41, 13 (1978)
54. T.Kinoshita and A.Sirlin, Phys.Rev. 108, 844 (1957)
55. W.Bacino et al., Phys.Rev.Lett. 42, 749 (1979)
56. H.B.Thacker, J.J.Sakurai, Phys.Lett. 36B, 103 (1971)
Y.S.Tsai, Phys.Rev. D4, 2821 (1971)
J.D.Bjorken, C.H.Llewellyn-Smith, Phys.Rev.D7, 887 (1973)
For a recent review see: Y.S.Tsai, SLAC-PUB-2105 (1978)
57. DASP Collaboration, W.Braunschweig et al., Phys.Lett.63B, 471 (1976)
R.Brandelik et al., Phys.Lett.70B, 125 (1977);
and 70B 387 (1977)
58. DASP Collaboration, S.Yamada, Proceedings of the 1977 International Symposium on Lepton and Photon Interactions at High Energies, Hamburg, August 1977
59. G.S.Abrams et al., Phys.Rev.Lett. 43, 1555 (1979)
60. J.M.Dorfan et al., SLAC-PUB 2566, LBL 11394
61. For a review on the experimental data see:
G.J.Feldman, Proceedings of the IXX International Conference on High Energy Physics, Tokyo, 1978
62. TASSO Collaboration, R.Brandelik et al., Phys.Lett.92B,199 (1980)

63. A.M.Cnops et al., Phys.Rev.Lett. 40, 144 (1978)

64. MARK J Collaboration, MIT, Technical Report No. 113, 1980
TASSO Collaboration, R.Brandelik et al., in preparation.

65. M.S.Chanowitz, J.Ellis and M.K.Gaillard,
Nucl.Phys. B 128, 506 (1977)
A.J.Buras, J.Ellis, M.K.Gaillard and D.V.Nanopoulos,
Nucl.Phys. B 135, 66 (1978)

66. P.Fayet and S.Ferrara, Phys.Reports 32C, 249 (1977)
F.Fayet, Phys.Lett. 69B, 489 (1977)
G.R.Farrar - Proc.Int. School of Subnuclear Physics, Erice,
Italy, August 1979
G.Barbellini et al., ECFA/LEP Study Group, DESY Preprint 79/67

67. Yu. A.Gol'fand and E.P.Likhtman, JETP Letters 13, 323 (1971)
D.V.Volkov and V.P.Akulov, Phys.Lett. 46B, 109 (1973)
J.Wess and B.Zumino Nucl. Phys. B70, 39 (1974)

68. T.Appelquist and H.D.Politzer, Phys.Rev.D12, 1404 (1978)
R.Barbieri, R.Gatto, and R.Kögerler, Phys.Lett.60B, 183 (1976)
R.Barbieri, R.Gatto and E.Remiddi, Phys.Rev.Lett. 61B, 465 (1976)

69. R.Van Royen and V.F.Weisskopf, Nuovo Cimento 50A, 617 (1967)

70. L.B.Okun and M.Voloshin, Zh.Eksper.Theor.Fiz. 23, 369 (1976)
C.Rosenzweig, Phys.Rev.Lett. 36, 697 (1976)
M.Bander et al., Phys.Rev.Lett. 36, 695 (1976)
A.De Rujula et al., Phys.Rev.Lett. 38, 317 (1977)

71. R.C.Giles and S.H.H.Tye, Phys.Rev.Lett. 37, 1170 (1976)
W.Buchmüller and S.H.H.Tye, Phys.Rev.Lett. 44, 880 (1980)
P.Hasenfratz et al., CERN Preprint TH 2837

72. P.A.Rapidis et al., Phys.Rev.Lett. 39, 526 (1977)
DASP Collaboration, R.Brandelik et al., Phys.Lett.76B, 361 (1978)
J.Siegrist et al., Phys.Rev.Lett. 36, 700 (1976)
PLUTO Collaboration, J.Burmester et al., Phys.Lett.66B, 395 (1977)

73. A.A.Zholentz et al., Phys.Lett. 96B, 214 (1980)

74. DASP Collaboration, W.Braunschweig et al., Phys.Lett.67B,243 (1977)

75. J.S.Whitaker et al., Phys.Rev.Lett. 37, 1596 (1976)

76. W.Bartel et al., Phys.Rev.Lett. 79B, 492 (1978)

77. C.Biddick et al., Phys.Rev. Lett. 38, 1324 (1977)
R.Partridge et al., Phys.Rev.Lett. 44, 712 (1980)

e^+e^- COLLDING BEAM EXPERIMENTS

77. continued:
T.H.Burnett, Proceedings of the XX International Conference on High Energy Physics, Madison, Wisconsin, July 1980
78. T.M.Himel et al., Phys.Rev.Lett. 34, 1357 (1979)
79. R.Partridge et al., SLAC-PUB-2578 (1980)
K.Königsman, Proceedings of the XX International Conference on High Energy Physics, Madison, Wisconsin, July 1980
80. T.M.Himel et al., SLAC-PUB-2562 (1980)
81. J.L.Rosner, C.Quigg and H.B.Thacker, Phys.Lett. 74B, 350 (1978)
82. J.K.Yoh, Proceedings of the XX International Conference on High Energy Physics, Madison, Wisconsin, July 1980
83. E.H.Thorndike, Proceedings of the XX International Conference on High Energy Physics, Madison, Wisconsin, July 1980
K.Chadwick et al., Phys.Rev.Lett. to be published
C.Bebek et al., Phys.Rev.Lett. to be published
84. W.Schmidt-Parzefall, Proceedings of the XX International Conference on High Energy Physics, Madison, Wisconsin, July 1980
85. F.Messing, Proceedings of the XX International Conference on High Energy Physics, Madison, Wisconsin, July 1980
86. R.Barbieri et al., Phys.Lett. 57B, 455 (1978)
W.Celmaster, Phys.Rev. D 19, 1517 (1979)
87. H.B.Thacker, C.Quigg, and J.L.Rosner, Phys.Rev. D18, 274 and 287 (1978)
88. A Martin, Proceedings of the XX International Conference on High Energy Physics, Madison, Wisconsin, July 1980
and CERN-TH 2843 (1980)
89. J.L.Richardson, Phys.Lett. 82B, 272 (1979)
90. W.Buchmüller, G.Granberg, and S.H.H.Tye, Phys.Rev.Lett.45,103(1980)
91. S.Brandt and H.D.Dahmen, Z. für Physik C1, 61 (1979)
92. T.F.Walsh and P.M.Zerwas, DESY 80/20
93. K.Koller and H.Krasemann, Phys.Lett. 88B, 119 (1979)
94. T.Appelquist et al., Phys.Rev.Lett. 34, 365 (1978)
M.Chanowitz, Phys.Rev.D 12, 918 (1975)
L.Okun and M.Voloshin, Report No. ITEP-95-1976
S.J.Brodsky et al., Phys.Lett. 73B, 203 (1978)
K.Koller and T.Walsh, Nucl.Phys.B140, 449 (1978)

95. G.S.Abrams et al., Phys.Rev.Lett. 44, 114 (1980)
96. D.L.Scharre, Proceedings of the XX International Conference on High Energy Physics, Madison, Wisconsin, July 1980
97. H.Fritzsch and M.Gell-Mann, Proceedings of the XVI International Conference on High Energy Physics, Chicago 1972
H.Fritsch and P.Minkowski, Nuovo Cimento 30A, 393 (1975)
D.Robson, Nucl.Phys. B 130, 328 (1977)
98. D.G.Aschman, Proceedings of the Fifteenth Rencontre de Moriond, Les Arcs, France, March 1980
99. C.Dionisi et al., CERN Report CERN/EP 80-1, 1980
100. R.H.Schindler et al., Phys.Rev. D 21, 2716 (1980)
101. G.Goldhaber and J.E.Wiss, LBL-10652, submitted to Annual Reviews of Nuclear and Particle Science
102. R.A.J.Lankford, Proceedings of the XX International Conference on High Energy Physics, Madison, Wisconsin, July 1980
103. A.Pais and S.B.Treiman, Phys.Rev. D 15, 2529 (1977)
104. W.Bacino et al., Phys.Rev.Lett. 45, 329 (1980)
105. D.Allasia et al., CERN-EP 180-76 submitted to Nuclear Physics
G.Diambrini-Palazzi, Proceedings of the XX International Conference on High Energy Physics, Madison, Wisconsin, July 1980
106. K.Niu, Proceedings of the XX International Conference on High Energy Physics, Madison, Wisconsin, July 1980
R.Amman et al.,ibid
107. N.Cabibbo and L.Maiani, Phys.Lett. 79B, 109 (1978)
N.Cabibbo, G.Corbo, and L.Maiani, Nucl.Phys. B 155, 93 (1979)
108. G.S.Abrams et al., Phys.Rev.Lett. 43, 481 (1979)
109. F.C.Porter, Proceedings of the XX International Conference on High Energy Physics, Madison, Wisconsin, July 1980
110. B.d'Almagne, Proceedings of the XX International Conference on High Energy Physics, Madison, Wisconsin, July 1980
111. M.Kobayashi and T.Maskawa, Prog.Theor.Phys. 49, 652 (1973)
112. T.A.DeGrand, Yee Jack Ng, and S.H.H.Tye, Phys.Rev.D16,3251 (1977)
A.de Rujula, J.Ellis, E.G.Floratos and M.K.Gaillard, Nucl.Phys. B 138, 387 (1978)
G.Kramer and G.Schierholz, Phys.Lett. 82B, 102 (1979)
G.Kramer, G.Schierholz and J.Willrodt, Phys.Lett.79B, 249 (1978)

e^+e^- COLLIDING BEAM EXPERIMENTS

112. continued
P.Hoyer, P.Osland, H.G.Sander, T.F.Walsh and P.M.Zerwas, Nucl.Phys. B 161, 349 (1979)
G.Kramer, G.Schierholz and J.Willrodt, Z. für Physik C4, 149 (1980)
113. E.Farhi, Phys.Rev.Lett. 39, 1587 (1977)
S.Brandt and H.D.Dahmen, Z.Physik C1, 61 (1979)
114. T.Appelquist and H.Georgi, Phys.Rev. D8, 4000 (1973)
A.Zee, Phys.Rev. D8, 4038 (1973)
G.'t Hooft, Nucl.Phys. B 62, 444 (1973)
M.Dine and J.Sapirstein, Phys.Rev.Lett. 43, 668 (1979)
W.Celmaster and R.J.Gonsalves, UCSD Preprint UCSD-10P10-206,207(1979)
K.G.Chetyrkin, A.L.Kataev and F.V.Tkachov,Phys.Lett.85B, 277 (1979)
USSR Academy of Sciences, Institute of Nuclear Research Preprint D-0178 (1980)
115. A.Quenzer, thesis, Orsay Report LAL 1299 (1977)
A.Cordier et al., Phys.Lett. 81B, 389 (1979)
V.A.Sidorov, Proceedings of the XVIII International Conference on High Energy Physics, Tbilisi, USSR, B 13 (1976)
R.F.Schwitters, Proceedings of the XVIII International Conference on High Energy Physics, Tbilisi, USSR, July 1976
J.Perez-Y-Jorba, Proceedings of the XIX International Conference on High Energy Physics, Tokyo, 1978
PLUTO Collaboration, J.Burmester et al., Phys.Lett. 66B, 395 (1977)
DASP Collaboration, R.Brandelik et al., Phys.Lett. 76B, 361 (1978)
116. J.Siegrist, Report No. SLAC-225 (1979)
117. R.M.Barnett, M.Dine and J.McLerran, Phys.Rev. D 22, 594 (1980)
118. D.Pandoulas, Proceedings of the XX International Conference on High Energy Physics, Madison, Wisconsin, July 1980
119. TASSO Collaboration, R.Brandelik et al., Phys.Lett.89B,418 (1980)
120. JADE Collaboration, W.Bartel et al., Phys.Lett. 88B, 171 (1979)
121. PLUTO Collaboration, Ch.Berger et al., DESY Report 80/69 (1980)
122. C.Bacci et al., Phys.Lett. 86B, 234 (1979)
SLAC-LBL Collaboration, G.G.Hanson, 13th Rencontre de Moriond (1978) ed.by J.Tran Than Van, Vol. III - 1978
PLUTO Collaboration, Ch.Berger et al., Phys.Lett.81B, 410 (1979) and V.Blobel private communication

122. continued
DASP Collaboration, R.Brandelik et al., Nucl.Phys.B 148, 189 (1979)
123. W.Thomé et al., Nucl.Phys.B 129, 365 (1977)
See also review by E.Albini, P.Capiluppi, G.Giacomelli, and A.M.Rossi, Nuovo Cimento 32A, 101 (1976)
W.Thomé, Aachen preprint PITHA 80/4 (1980)
124. R.Stenbacka et al., Nuovo Cimento 51A, 63 (1979)
125. W.Furmanski, R.Petronzio and S.Pokorski, Nucl.Phys.B155, 253 (1979)
A.Bassetto, M.Ciafaloni and G.Marchesini, Phys.Lett.83B, 207 (1978)
126. K.Konishi, Rutherford Preprint RL 79-035 T 241 (1979)
127. G.J.Feldman and M.L.Perl, Phys.Reports 33, 285 (1977)
128. TASSO Collaboration, R.Brandelik et al., Phys.Lett. 89B, 418 (1980)
129. TASSO Collaboration, R.Brandelik et al., Phys.Lett. 94B, 444 (1980)
130. TASSO Collaboration, R.Brandelik et al., Phys.Lett. 94B, 91 (1980)
131. V.Lüth et al., Phys.Lett. 70 B, 120 (1977)
132. T.F.Walsh and P.Zerwas, Nucl.Phys. B 77, 494 (1974)
133. S.L.Wu, Proceedings of the XX International Conference on High Energy Physics, Madison, Wisconsin, July 1980
134. P.Hoyer, P.Osland, H.G.Sander, T.F.Walsh and P.M.Zerwas, Nucl.Phys. 161, 349 (1979)
135. A.Ali, E.Pietarinen, G.Kramer and J.Willrodt, Phys.Lett.93B,155(1980)
136. R.D.Field and R.P.Feynman, Nucl.Phys. B 136, 1 (1978)
137. The Lund Monte Carlo, T.Sjöstrand, B.Södenberg, Lund Report LU TP 78-18 (1978)
T.Sjöstrand, Lund Report LU TP 79-8 (1979)
138. G.Altarelli and G.Parisi, Nucl.Phys. B 126, 298 (1977)
JADE Collaboration, W.Bartel et al., Phys.Lett. 91B, 142 (1980)
139. Physics with High Energy, Electron-Positron Colliding Beams with MARK J Detector, Physics Report 63, 340 (1980)
H.Newmann, Proceedings of the XX International Conference on High Energy Physics, Madison, Wisconsin, July 1980
140. PLUTO Collaboration, Ch.Berger et al., DESY Report 80/93
H.J.Daum, H.Meyer and J.Bürger, DESY Report 80/101
141. D.Cords, Proceedings of the XX International Conference on High Energy Physics, Madison, Wisconsin, July 1980
142. S.L.Wu and G.Zobernig, Z.für Physik C2, 107 (1979)

e^+e^- COLLIDING BEAM EXPERIMENTS

143. JADE Collaboration, W.Bartel and A.Petersen, Talks given at the XV Rencontre de Moriond, Les Arcs, March 9-21, 1980
144. J.Ellis and I.Karliner, Nucl.Phys. B 148, 141 (1979)
145. V.Hepp, Proceedings of the XX International Conference on High Energy Physics, Madison, Wisconsin, July 1980
146. TASSO Collaboration, R.Brandelik et al., Phys.Lett. 97B, 453 (1980)
147. F.A.Berends and R.Kleiss - to be published
148. MARK J Collaboration, D.P.Barber et al., Phys.Lett. 89B, 139 (1979)
149. TASSO Collaboration, R.Brandelik et al., Phys.Lett. 94B, 437 (1980)
150. R.K.Ellis, D.A.Ross and A.E.Terrano, Caltech.Report 68-785 (1980)
Z.Kunszt,DESY Report 80/79 (1980)
K.Fabricius, I.Schmitt, G.Schierholz and G.Kramer,
DESY Report 80/79 (1980)
151. S.Yamada, Proceedings of the XX International Conference on High Energy Interactions, Madison, Wisconsin, July 1980
152. Yu.L.Dokshitzer, D.I.D'yakonov and S.I.Troyan,
Phys.Lett. 78B, 290 (1978)
153. PLUTO Collaboration, Ch.Berger et al., Phys.Lett. 90B, 312 (1980)
154. R.Baier and K.Fey, Univ. of Bielefeld preprint BI-TP 80/10 (1980)
155. B.Anderson and G.Gustavson, Lund Preprint LU TP 79-2 (1979)
B.Anderson, and G.Gustafson, Z.für Physik C3, 223 (1980)
B.Anderson, G.Gustavson and T.Sjöstrand, Lund Report LU TP 80-1(1980)
B.Anderson, G.Gustafson and C.Peterson, Nucl.Phys.B135,273 (1978)
156. E.J.Williams, Kgl.Danske Videnskab.Seiskab, Mat.Fys.Medd.
13 No. 4 (1934)
L.Landau and E.Lifshitz, Physik Z, Sovjetunion 6, 244 (1934)
A.Jaccarini, N.Arteaga-Romero, J.Parisi and P.Kessler,
Compt.Rend. 269B, 153, 1129 (1969)
Nuovo Cimento 4, 933 (1970)
157. F.F.Low, Phys.Rev. 120, 582 (1960)
F.Calogero and C.Zemach, Phys.Rev. 120, 1860 (1960)
158. G.S.Abrams et al., Phys.Rev.Lett. 43, 477 (1979)
159. D.M.Binnie et al., Imperial College London, NO IC/HENP/79/2 (1979)
160. PLUTO Collaboration, Ch.Berger et al.,Phys.Lett.94B, 254 (1980)
161. J.A.M.Vermaseren, private communication
R.Bhattacharya, J.Smith and G.Grammer, Phys.Rev.D15, 3267 (1977)

162. W.Wagner, Proceedings of the XX International Conference on High Energy Physics, Madison, Wisconsin, July 1980

163. A.Roussairie, Proceedings of the XX International Conference on High Energy Physics, Madison, Wisconsin, July 1980

164. TASSO Collaboration, R.Brandelik et al, DESY Report 80/77

165. J.J.Sakurai, Ann.Phys. 11, 1 (1960)

166. S.M.Berman, J.D.Bjorken and J.B.Kogut, Phys.Rev.D4, 3388 (1971)

167. H.Spitzer, talk given at the XV Rencontre de Moriond, Les Arcs, France, March 15-21, 1980

168. T.F.Walsh, Phys.Lett. 36B, 121 (1971)
S.B.Brodsky, T.Konoshita, and H.Terazawa, Phys.Rev.Lett.27,280(1971)
T.F.Walsh and P.Zerwas, Phys.Lett. 44B, 198 (1973)
E.Witten, Nucl.Phys. B 120, 189 (1977)
C.H.Llewellyn-Smith, Phys.Lett. 79B, 83 (1979)